A structural and geochemical traverse across the NW outcrop of the Colenso Fault Zone, Saldanha, South Africa.

By Kaylan Hamel

Dissertation presented for the degree of Master of Science

Department of Geological Sciences

University of Cape Town

December 2015

Declaration

I hereby declare that all the work presented in this thesis is my own, except where stated otherwise in the text.

K. Hamel

Table of Contents

Abstract

The Colenso Fault Zone marks the boundary between the Tygerberg and Swartland Terranes in the Pan-African Saldania Orogenic Belt. The fault zone comprises several discrete shear discontinuities that in places cross-cut relatively undeformed granites of the Cape Granite Suite. It is NW-SE striking, ~150 km long, and ~7km wide, but poorly exposed except in coastal exposures at the NW end. The deformation sequence can be divided into 2 sequences: The oldest deformation started with the emplacement of the G1, G2 and then the G3 of the Cape Granite Suite, followed by formation of aplite veins and strike-slip faulting generating cataclasites. The initial strike-slip sense of movement along the fault was sinistral, followed by dextral strike-slip shearing and finally late stage jointing.

The Colenso Fault Zone is host to 3 large zones of cataclasis that are in the order of up to a few hundred metres in exposed down-dip and along-strike lengths. The cataclasites are composed of quartz and plagioclase clasts, in a phyllosilicate matrix. Both the wide cataclasites (several metres) and small cataclasite zones (tens of centimeters) show a decrease in shear intensity away from the core of the fault zone. The cataclasites have the same bulk chemical composition as the surrounding granite.

The average whole rock (WR) $\delta^{18}O$ for the G1, G2 and G3 granites associated with the fault zone are 7.8, 7.7 and 10.3 ‰ respectively. The cataclasite WR $\delta^{18}O$ value increases from 5.9 to 7.1 ‰ away from the fault zone. The WR and quartz $\delta^{18}O$ values of the granites and cataclasites increase away from the fault zone towards the average $\delta^{18}O$ for the G1, G2 and G3 granites of 9.5, 9.8 and 12.1 ‰, respectively. The increase in WR $\delta^{18}O$ value away from the fault is consistent with enhanced fluid-rock interaction in the fault zone. The lowest $\delta^{18}O$ value was found in the cataclasites, which is consistent with the fluid flow being localised along discrete faults with a high permeability. The phyllosilicates within the cataclasites imply alteration related to the hydration of feldspars of the granites during deformation. The δD values of the cataclasites range from -130 to -80 ‰, with an average δD value of -105 ‰. Assuming greenschist facies temperatures, the mineral-water fractionation factor would be approximately -30 ‰. The fluid therefore has an inferred (by the Global Meteoric Water Line) δD of -75 ‰, and $\delta^{18}O$ of -10.6 ‰. This negative meteoric value is typical of areas at high latitudes but might also reflect global glaciation at the time of deformation.

1. Introduction

The Colenso Fault Zone is one of two large terrane boundary faults of the Saldania Belt that formed during the Pan-African Adamastor Orogeny also known as the Brasiliano Orogeny (Frimmel and Folling, 2004, Cawood and Buchan, 2007, Goscombe and Gray, 2008). The closure of the Adamastor Ocean allowed the creation of the supercontinent Gondwana (Frimmel and Folling, 2004). The subgreenschist to lower greenschist facies strike-slip Colenso Fault Zone separates the Tygerberg and Swartland Terranes and is situated to the northeast of Cape Town, South Africa and runs between the towns of Saldanha and Stellenbosch (Figure 2.4). Due to the lack of exposure, the Saldania Belt and thus the Colenso fault structural history has not been researched in great detail (Kisters et al., 2002; Rowe *et al,* 2010).

The study of fluid interaction within fault zones is a well-studied occurrence and the involvement of fluids in fault zones and brittle-ductile shear zones. Studies by e.g.Kerrich *et al*, 1984 has proved the importance of these studies through the presence of mineralization in old fault zones exhumed by erosion. Hickman *et al* (1995) state the numerous ways in which fluids are involved during faulting; such as through chemical effects due to fluid presence or mechanical effects due to fluid pressure. Some examples include hydration reactions, mechanical weakening through fluid-assisted diffusion as well as reactions. Hickman *et al* (1995) also highlighted gaps within knowledge of how fluids flow through faults; through distributed or localised fluid flow. More work also needs to be done on where fluids are coming from at depths in faults; questions remain of meteoric water coming down or metamorphic water coming up. The Colenso Fault Zone is a perfect example of these fluid interactions in fault zones that can be used to further understand this interaction on a world class example of Brittle-Ductile Shear zones. We know the granite properties away from the fault so can track changes caused by the fluids.

This research aims to address the nature of the Colenso Fault Zone and its structural history and the nature of fluid-rock interaction, using a combination of geochemical analyses and geological mapping at a range of scales. Geological maps have been made over the whole fault zone (5.5 km) as well as through form surface grid mapping of areas of particular interest. These maps allow for determination of the deformation sequence, interpretation of deformation mechanisms and evaluating the relative ages of granite intrusions. Petrography of the three

granite phases exposed in the study area, as well as late stage aplite veins has been undertaken using both hand samples and thin section descriptions. Microstructures of sheared granites have also been done using thin section petrography. The fluid-rock interaction study involved the identification of fluid flow pathways either along, or through, the fault zone using oxygen and hydrogen isotope data on whole rock and quartz, as well as bulk-rock composition (XRF) and mineralogical studies (XRD).

2. Regional Geology

2.1 The Malmesbury Supergroup

The Saldania Belt is one of the internal suture zones of the Late-Neoproterozoic to Early Palaozoic Pan-African Orogeny, during the event continental fragments were amalgamated to form the Gondwana supercontinent (Miller, 1983; Hartnady *et al,* 1985, Gresse and Scheepers, 1993; Frimmel *et al,* 1996; Frimmel and Frank, 1998; Rozendaal *et al,* 1999). The Pan-African orogenic belts formed part of a global event, which took place during the formation of Gondwana (Figure 2.1) (Rozendaal *et al,* 1999). It is represented in South America by the Brasiliano Belt and in southern Africa by the Damara, Gariep and Saldania Belts (Rozendaal *et al,* 1999). These orogenic belts are generally composed of low-grade metamorphic volcanosedimentary rocks and are intruded by syn-, late- and post-tectonic granitoids (Rozendaal *et al,* 1999).

Of the southern African orogenic belts the Saldania Belt, situated along the southern and southwestern margins of the Kalahari Craton (Rozendaal *et al,* 1999, Gresse *et al,* 2006), is the least understood because of limited surface exposure, structural complexity and low mineral exploration potential. It is described by Rozendaal *et al* (1999) and Gresse *et al* (2006) as being composed of three main terranes as well as a number of inliers (Figure 2.2 and Figure 2.3), which are exposed within large unroofed anticlinal hinges of the Permo-Triassic Cape Fold Belt along the southern edge of South Africa. These inliers lie to the east of the main exposure of the Saldania Belt and include the Kango Group, Kaaimans Group and the Gamtoos Group (Rozendaal *et al,* 1999).

Gresse and Scheepers (1993), Frimmel and Frank (1998), Rozendaal *et al.* (1999) and Frimmel *et al.* (2001) have suggested that the Saldania Belt is a poorly exposed Pan-African low-grade, generally greenschist facies, orogenic belt and is a continuation of the northern Gariep Belt and Vanrhynsdorp basin. The Saldania Belt formed during predominantly sinistral transpressional tectonics and associated accretionary tectonics. However, there are great differences between the northern and southern belts that may indicate a different tectonic evolution for the Saldania Belt (Kisters *et al,* 2002). These differences include: (a) the lack of voluminous granites of the Cape Granite Suite (CGS) in the Gariep Belt, (b) the lack of a low-angle thrust faults in the southern Saldania Belt and (c) evidence in the Saldania Belt for a transition from collisional to extensional tectonics that is not described in the northern Gariep Belt (Kisters *et al,* 2002). The

sinistral transpression seen within the Saldania and the Gariep Belts can be ascribed to the reversal of spreading and closing of the Adamastor Ocean, which was possibly caused by the opening of the Iapetus Ocean between 600 – 570 Ma (Rozendaal *et al,* 1999).

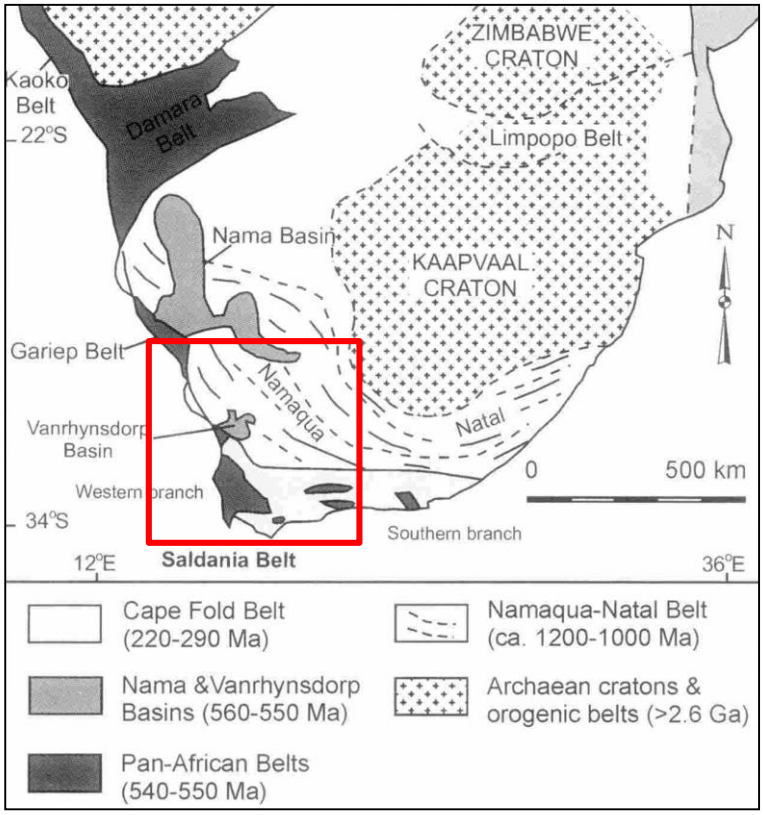

Figure 2.1: Regional Geological map showing the major tectonic provinces of Southern Africa. The Saldania belt is situated in the southwest corner of the continent and the other outliers to this belt belong to the group of Pan-African Belts (Kisters *et al*, 2002). The area of the Gariep and Saldania Belts covered in Figure 2.3, are indicated by the red square.

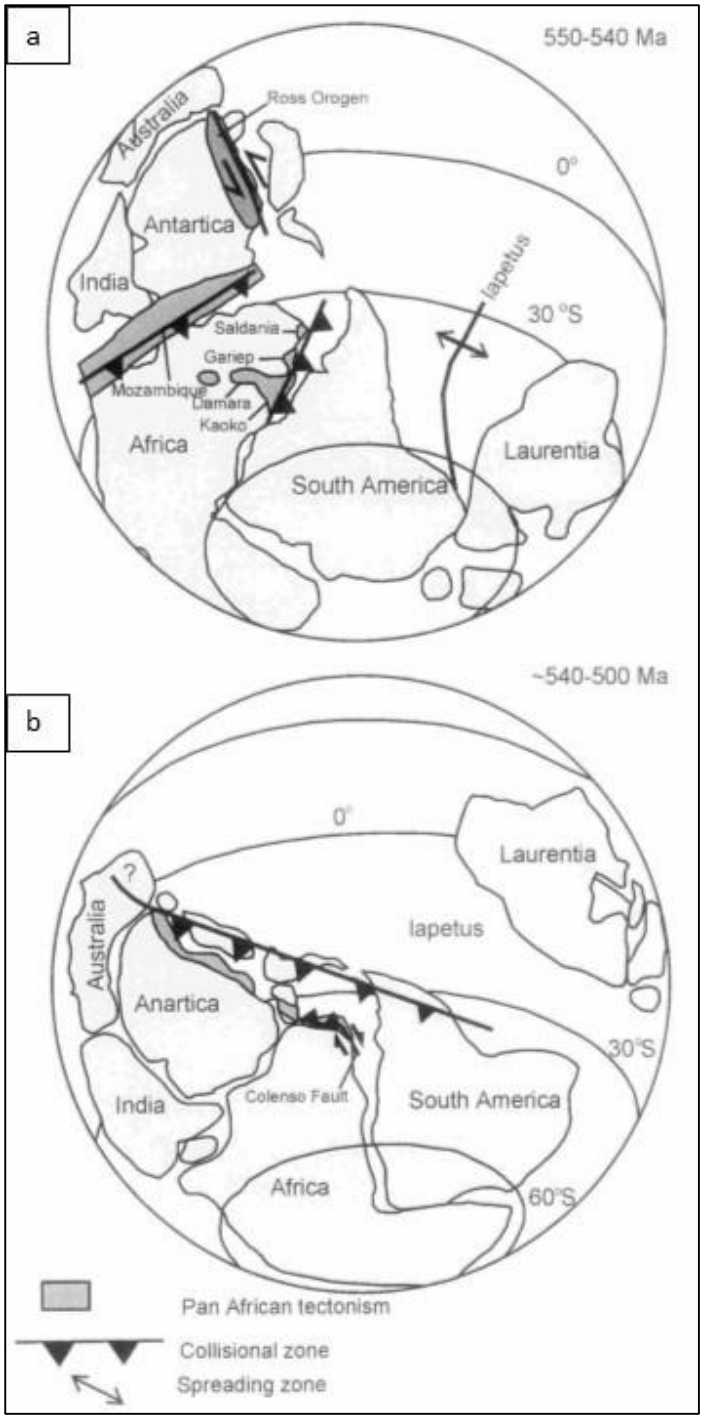

Figure 2.2: Plate reconstructions of Gondwana and Laurentia (a) after the closure of the Adamastor and Mozambique oceans outlining the position of the Saldania Belt in relation to collisional tectonics. (b) after the shift in the direction of subduction along the exterior margins of Gondwana outlining the spatial location of the Colenso fault zone after reactivation to be a dextral strike slip fault at that time (Kisters *et al*, 2002).

The main exposure of the Saldania Belt is to the north and northeast of Cape Town (Figure 2.4), and occur as large scale fault zones within Malmesbury Supergroup metasedimentary

rocks and Cape Granite Suite intrusions (Gresse *et al*, 2006). Hartnady *et al* (1974) divided the Malmesbury Group into three domains (north-eastern, central and south-western) separated by northwest trending strike-slip faults and shear zones (Rozendaal *et al*, 1999). The major differences of the tectonic styles between the three terranes of the Malmesbury Group are related to the different levels of exposure, the amount of strain partitioning, which is controlled by the faults and shear zones and by the difference in the competency of the basement rocks beneath each of the terranes (Rozendaal *et al*,1999). Von Veh (1983) later named these three domains the Boland, Swartland and Tygerberg Terranes for the north-eastern, central and south-western domains respectively. Terrane accretion has been thought to have occurred during the main episode of the Pan-African orogeny at ~545 Ma during a sinistral transpression forming these three terranes (Rozendaal *et al*, 1999).

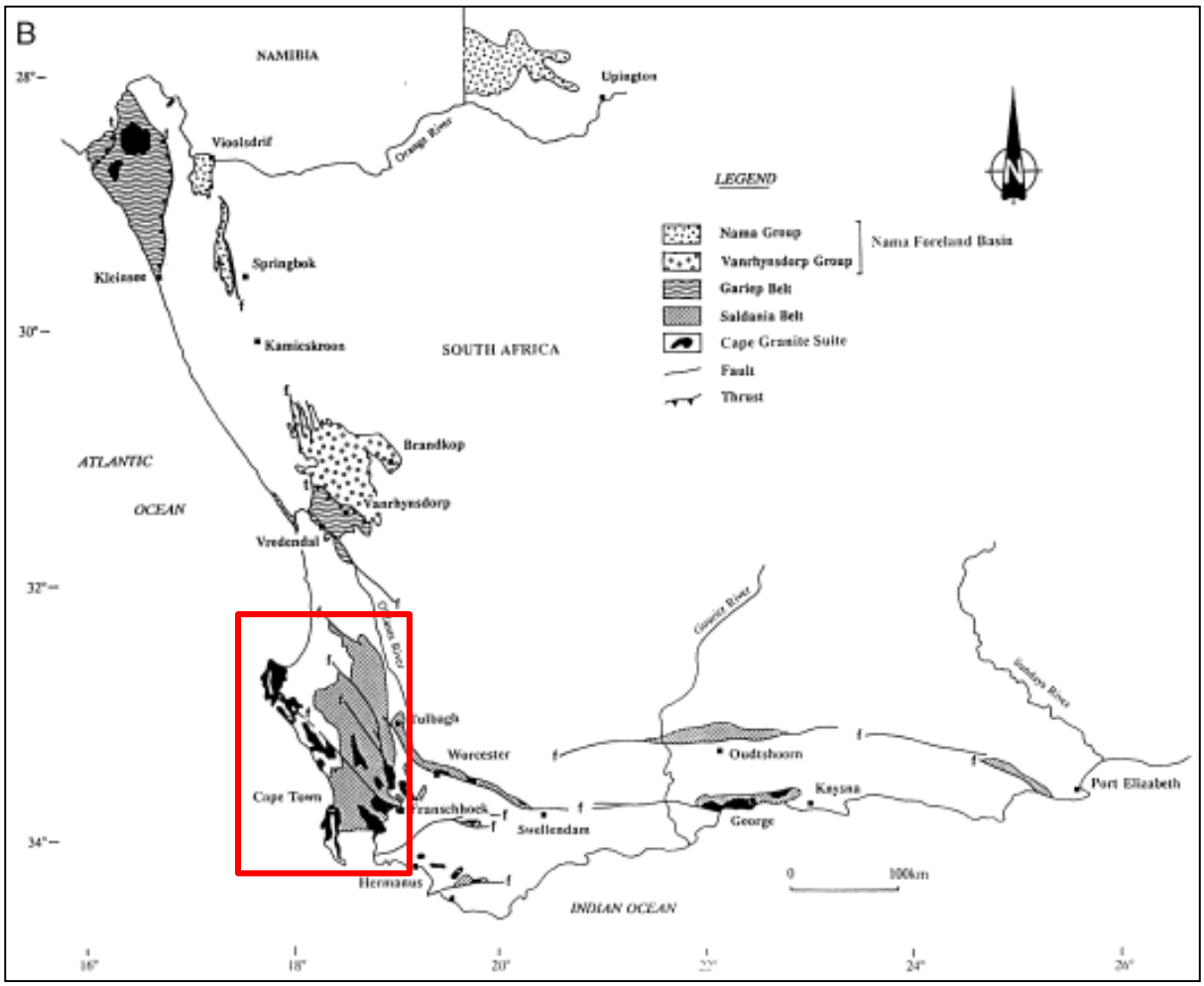

Figure 2.3: The distribution of the Gariep and Saldania Belts in southwest South Africa (Rozendaal *et al*, 1999). The area of the northern block of the Saldania Belt covered in Figure 2.4, are indicated by the red square.

Although the spatial occurrence of the terranes is poorly constrained both stratigraphically and tectonically it is known that the Boland and Swartland Terranes are separated from one another by the Piketberg-Wellington Fault Zone and the Swartland and Tygerberg terranes are separated by the Colenso Fault Zone (Rozendaal *et al* 1999, Gresse *et al,* 2006). Hartnady *et al,* (1974) suggested that these fault zones are terrane bounding faults caused by the oblique collision of the Kalahari Craton and the South American Craton, during the closure of the Adamastor Ocean. A later change in lateral strike-slip motion from sinistral to dextral, was likely caused by a change in direction of subduction around the southern tip of southern Africa (Grunow *et al,* 1996). Kisters *et al,* (2002) could neither rule out the idea that the Colenso fault is terrane bounding nor substantiate the idea after researching the areas the fault crops out, as there is no structural history preserved from before ~545 Ma. This may be due to the simple fact that exposures of the Colenso Fault are very poor and hidden within the sedimentary units of the Malmesbury Group (Kisters *et al,* 2002).

Rozendaal *et al,* (1999) described the Boland Terrane as having adjoined the Kalahari Craton, and displaying characteristics of a rifted margin succession, whereas the other terranes could belong to subsequently accreted para-auchtonous and allochtonous terranes. The Swartland-Boland Terrane boundary represents a suture similar to that of the South Atlantic suture that formed the Gariep Belt between 575 – 543 Ma (Frimmel *et al,* 1996). The Tygerberg Terrane deposits were described by Von Veh (1983) as having been of turbidite origin and accumulated either in a continent rise or ocean trench environment or even as submarine fans at the foot of the continental slope in a tectonically active environment.

2.1.1 Tygerberg Terrane

The south-western Tygerberg Terrane is characterised by alternating greywacke, phyllitic shale and siltstone, immature quartzite, a few thin impure limestones, conglomerate beds as well as volcanogenic sediments (Gresse *et al,* 2006). Sedimentary rocks within the Tygerberg Terrane reflect deep water facies such as turbidites and were deposited during the evolving stages of the ocean or continent margin during times of sea level rise (Rozendaal *et al*, 1999). Sedimentary structures seen within the sediments are cross-bedding, ripples, ripple cross-lamination, normal grading, slumping and channelling (Von Veh, 1983). The volcanic member of the Tygerberg Terrane is composed of volcanogenic mudstone, agglomerate and altered amygdaloidal, calc-alkaline andesite (Rozendaal *et al*, 1999). Gresse and Scheepers (1993) described the structural style of the Tygerberg Terrane as relatively simple with near upright

to slightly southwest verging tight folds that formed prior to the intrusion of granite. Intrusives of the Tygerberg Terrane are the older S-type granitoids of the CGS (Rozendaal *et al*, 1994).

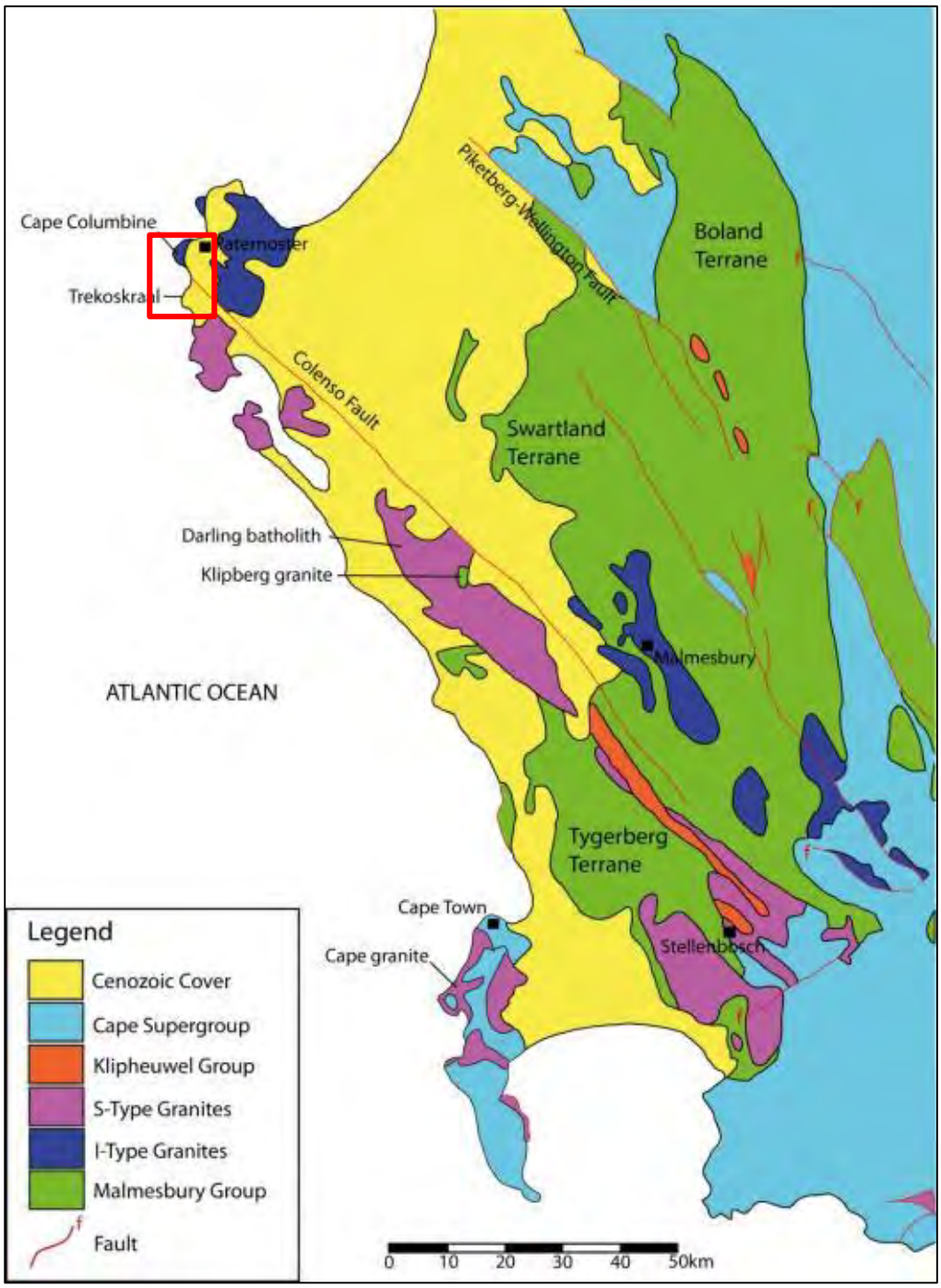

Figure 2.4: Simplified Geological map of the northern block of the Saldania Belt north of the City of Cape Town (modified after Kisters *et al*, 2002). Granites of the Cape Granite suite mentioned here are indicated along the Colenso Fault. Note the separation of the Cape Supergroup of the Boland Terrane from the I-Type Granites of the Swartland Terrane by the Piketberg-Wellington Fault. The Colenso Fault separates the I-Type granites of the Swartland

Terrane from the S-Type granites of the Tygerberg Terrane. The red square defines the study area of this thesis described in Figures 3.1 and 3.2 in more detail.

2.1.2 Swartland Terrane

The central Swartland Terrane is composed of the Swartland Subgroup of the Berg River, Klipplaat and Moorreesburg Formations. The terrane is both stratigraphically and structurally very complex in comparison to the Tygerberg Terrane (Gresse *et al,* 2006). Rozendaal *et al*, (1999) described the sediments of the Swartland Terrane as being deposited at times of sea level rise and thus decreasing continental exposure.

Sedimentary rocks of the Berg River Formation are composed of chlorite schist, greywacke and impure cherty limestone lenses with quartz schist closer to the top of the formation (Rozendaal *et al*, 1999). The overlying Klipplaat Formation of quartz-sericite-chlorite schist tends to be tectonically interfingered with the Mooreesburg Formation basal arenites and chlorite-muscovite schist above which are interlayered greywacke and phyllite units (Theron *et al,* 1992, Rozendaal *et al*, 1999). The Franschoek Formation is composed of a feldspathic conglomerate and quartzite, grit, slate and phyllite. The Franschoek Formation is intruded by quartz porphyry dykes and sills, which are related to the last phase of the Cape Granite Suite magmatism at ~ 510 Ma (Scheepers and Nortje, 2000). The suture between the Kalahari Craton's southern rifted margin Boland Terrane and the poorly exposed southern orogenic belts of the Swartland and Tygerberg Terranes (in part) is represented by the Bridgetown Formation (Rozendaal *et al*, 1999). The Bridgetown Formation is a metavolcanic sequence which follows the border of the Swartland and Boland Terranes (Slabber and Scheepers, 1994). It comprises a complex series of metamorphosed mafic and ultramafic igneous rocks along with, dolomites, chert and graphitic schists (Slabber and Scheepers, 1994). The oceanic metavolcanics and metasedimentary rocks are considered to represent a dismembered ophiolite complex with seamount capping of dolomite and jaspilitic chert bodies (Slabber, 1995).

Deformation of the Swartland group is described by Rozendaal *et al,* (1999) as being dependent on the level of exposure of the rock units and is defined as polyphase deformation, where the upper levels of the terrane are similar to that of the deformation of the Tygerberg Terrane. In the core of the Swartland Terrane the bedding is obliterated and is dominated by multiple planar tectonic fabrics (Rozendaal *et al,* 1999). The Swartland Terrane is intruded by younger I-type

granites, whereas the Tygerberg Terrane is intruded by older S-type granitoids (Rozendaal *et al*, 1994).

2.1.3 Boland Terrane

The most north-eastern terrane is the Boland Terrane, characterised by the rocks of the Boland Subgroup (Gresse *et al,* 2006), and considered by Rozendaal *et al,* (1999) to be sedimentary and volcanic rocks deposited in a rift succession distal facies, which overlie the south-western edge basement rocks of the Kalahari Craton. The rifting was caused by the opening of the Adamastor Ocean during the break-up of the supercontinent Rodinia between 780 – 750 Ma (Rozendaal *et al*, 1999). Rozendaal *et al*, (1999) highlighted that the Boland Terrane is sub-divided into the lowermost exposed Porterville Formation, Norree Formation, Picketberg Formation above which is the Brandwacht Formation.

The Porterville Formation comprises limestone, chert and quartzite and is dominated by phyllitic shales and greywacke, in some areas the Voëlvlei metavolcanic greenstones (altered pillow lavas and volcaniclastics and polymictic conglomerates) are exposed. These metavolcanic rocks are related to the Bridgetown Formation (Rozendaal *et al*, 1999). Similar rocks to that of the Porterville Formation of clastic lithologies are found near the Swellendam area and are called the Norree Formation (Rozendaal *et al*, 1999). The Picketberg Formation is composed of both foliated and lineated feldspathic quartzites, greywackes, sericite schist, banded iron formation, feldspathic grits, feldspathic conglomerates, and impure marly limestones (Rozendaal *et al*, 1999). The Brandwacht Formation is comprised of poorly sorted conglomerates in lenses with quartz, greywacke and phyllite clasts, which may possibly represent a tectonic mélange (Hartnady, 1969, Rozendaal *et al*, 1999).

The Boland Terrane has an even less complex structural history than that of the Tygerberg and Swartland Terranes, with north to northwesterly trending, near upright tight folds with an axial planar cleavage (Rozendaal *et al*, 1999). However, the eastern parts of the Boland Terrane have a complex polyphase deformation, which is a result of the superimposed Permo-Triassic Cape Orogeny (Gresse *et al,* 1992, Barnett *et al,* 1997).

The Boland, Tygerberg and the Swartland Terranes are all separated by faults and shear zones (Figure 2.4). These include the Colenso fault and the Picketberg-Wellington Fault. The Colenso Fault is a northwest-southeast trending fault zone in the Saldania Belt (Kisters *et al,* 2002). The

Colenso fault not only is the terrane boundary between the Tygerberg and Swartland Terranes but also separates the older S-type granitoids in the Tygerberg Terrane from the younger I-type granitoids in the Swartland Terrane (Gresse *et al,* 2006). It was therefore suggested by Gresse *et al,* (2006) as a significant crustal-scale feature. A reversal of strike-slip motion on the Colenso Fault is recorded at ~540 Ma which coincides with the uplift of the rocks of the Saldania Belt (Kisters *et al,* 2002). The Piketberg-Wellington Fault is a northwest-southeast trending fault zone that separates the Boland Terrane from the Swartland Terrane which contains younger I-type granitoids.

2.2 Colenso Fault

The Colenso Fault is a sub-vertical, northwest-southeast trending terrane boundary fault, which is poorly exposed but has a continuous strike extent, from Saldanha Bay to Stellenbosch and can be traced for ~150 km (Schoch, 1975; Theron *et al*, 1992; Gresse *et al*, 2006). Exposure is poor due to the fact that it is only well defined by mylonitized and brecciated rocks that outcrop along its strike extent as well as being marked by a magnetic anomaly (Schoch, 1975; Theron *et al*, 1992; Kisters *et al*, 2002). The Colenso Fault has an aerial extent of ~7 km width and consists of a number of sub-parallel to anastomising fault strains (Kisters *et al*, 2002). It defines the boundary between the Tygerberg Terrane and the Swartland Terrane of the Malmesbury Group of the Pan-African Saldania orogenic belt along the southern and south-western edges of South Africa (Gresse *et al*, 2006).

Kisters *et al*, (2002) described the kinematics of the area as initially have being sinistral strike-slip motion starting at 547 ± 6 Ma and having changed around ~540 Ma to a dextral sense of strike-slip motion along the Colenso Fault. This change in strike slip motion has been attributed to the uplift of the rocks of the Saldania Belt due to the closure of the Adamastor Ocean. Dextral strike-slip faulting is shown to have continued all the way up until the emplacement of the late-kinematic Cape Columbine granite at ~520 Ma.

2.3 Granites

Magmatism in the Saldania Belt is widespread, and post-dates sedimentation and volcanism (Rozendaal *et al,* 1999). Intruding the Malmesbury Supergroup are the Cape Granite Suite granitoids of ~560 - ~510 Ma age during and after the Saldanian orogeny at around 580 – 545 Ma (Scheepers, 1995; Da Silva *et al,* 1997, Villaros *et al,* 2006). These multiphase intrusions into the Saldania Belt were emplaced into a pervasive transpressive regime and with the

absence of a proper collisional orogen in the belt and the prominent north-westerly developed structural grain of the belt suggests that the Cape Granite Suite were generated in a strike-slip fault regime very similar to that of the granites of Brittany, western France (Hutton, 1982, Vigneresse, 1995, Rozendaal *et al,* 1999). The association between strike-slip faults and granite emplacement may explain the distribution of the Cape Granite Suite and the extensive strike-slip faults such as the Colenso Fault Zone (Rozendaal *et al,* 1999). The Cape Granite Suite had a sequential intrusive history of earlier S-type granites, after which the intrusion of the I- and A-type granites followed, with an increase in juvenile mixing, which Rozendaal *et al,* (1999) inferred as indicating tectonic evolution of the strike-slip zones.

The Cape Granite Suite has been divided into A-, I- and S- type granites on the basis of geochemistry and petrography by Scheepers (1995). The granite bodies are generally elongated in shape and trend in the same direction as that of the structural features of the Saldania Belt; towards the northwest (Kisters *et al,* 2002). The Cape Granite Suite dominates the Atlantic coastline and is best exposed in the terranes, underlain by the Malmesbury Supergroup (Rozendaal *et al,* 1999). There are 3 major phases of granitoids magmatism associated with the Saldania Belt and are described in Figure 2.5.

2.3.1 Phase 1: S-type

These granites occur southwest of the Colenso Fault Zone in the Tygerberg Terrane and were generally derived from the partial melting of sedimentary rocks containing clay minerals (Hartnady *et al,* 1974; Best and Christiansen, 2001). The S-Type granites are syn- to late-tectonic granites dominated by a peraluminous chemistry; with Al-rich minerals such as cordierite and muscovite and accessory amounts of biotite and garnet (Villaros *et al,* 2006). The initial Nd and Sr isotope composition of these granites suggest their origin to have been purely crustal and the source is inferred to be the Malmesbury Group, and similar to the metasediments along a convergent continental margin (Harris *et al*, 1997, Villaros *et al,* 2006). These granites intruded between ~560 – 540 Ma and include the Darling, Peninsula, Stellenbosch and Saldania plutons (Villaros *et al,* 2006).

Scheepers and Nortje (2000) described the existence of a group of felsic ignimbrites and rhyolites that extruded at around 515 ± 3 Ma (Scheepers and Poujol, 2002). These extrusives have been described as being associated with the Cape Granite Suite and occur in the western

Tygerberg Terrane (Scheepers and Nortje, 2000). They occur on the Potberg peninsula opposite Langebaan.

2.3.2 Phase 2: I-type

Occur only in the Boland and Swartland Terranes north of the Colenso Fault and represent Phase 2 of the Cape Granite Suite between ~540 - 515 Ma (Da Silva *et al,* 1997, Villaros *et al,* 2006). I-type granites are generally derived from magmas generated by the partial melting of mafic and intermediate igneous rocks (Best and Christiansen, 2001). There are 2 types; the Ia and Ib-types, both of which are metaluminous and contain no other minerals other than biotite and horneblende (Scheepers, 1995). The Ia type is pre-dominant and is represented by the Paarl, Malmesbury and Vredenburg plutons (Scheepers, 1995). They are generally non-deformed and may be either fine- or coarse-grained and range from granite, quartz-monozite to alkali-feldspar granite which often contain country rock xenoliths (Scheepers, 1995). The Ib type is minor and only found within the granitoids of Phase 2 (Scheepers, 1995).

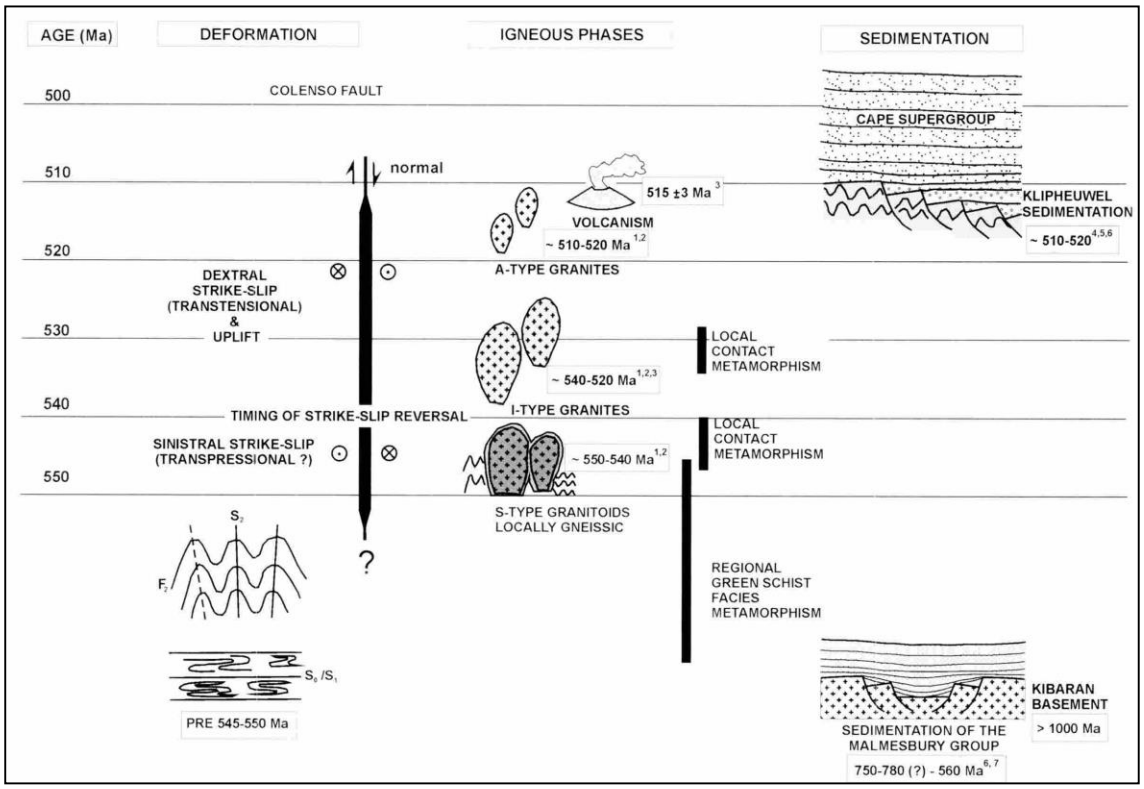

Figure 2.5: The 3 main phases of magmatism associated with the Saldania Belt in relation to the age of occurrence as well as proposed tectonic activities, the earlier S-Type granitoids, the I-Type granitoids and the A-Type granitoids (Scheepers, 1995, Kisters *et al*, 2002).

2.3.3 Phase 3: A-type

A-type granites are a group of diverse felsic rocks typically formed in anorogenic settings having diverse sources and origins (Best and Christiansen, 2001, Frost, 2010). In the case of the Cape Granite Suite the corresponding A-type granites are post-kinematic ~515 – 510 Ma (Villaros *et al,* 2006). These include small intrusions such as the Cape Columbine and Riviera granites as well as the Yzerfontein granite (Scheepers and Rozendaal, 1992). There are 2 types of A-type granitoids in the area those being the Aa- and Ab-types, both are metaluminous and sometimes evolving towards peralkaline compositions containing both amphibole and biotite (Scheepers and Rozendaal, 1992). The Aa-type range from amphibole-bearing quartz syenite to alkali granite and biotite quartz syenite, dominate in the Tygerberg Terrane such as the Klipberg pluton (Scheepers and Rozendaal, 1992). The Ab-type intrudes the Swartberg Terrane such as the Cape Columbine granite and range from alkali feldspar granite, quartz syenite, and syenite (Scheepers and Rozendaal, 1992). The Yzerfontein intrusive rocks represent the high-K calc-alkali series and is defined by olivine gabbro, gabbro, monzogabbro, monzonite and syenite and is intrusive into the Tygerberg Terrane (Scheepers and Rozendaal, 1992).

Nomenclature later refered to in the text refers to the following relationship:

Classification and naming of granites in the thesis	
Scheepers (1995) Classification	Nomenclature used in thesis
S-Type granites	G1
	G2
I-Type granites	G3
	G4

2.4 Petrogenetic model for the Saldania magmatism

Scheepers and Rozendaal, (1992) imply that the syn- to post- orogenic, S-Type granites were the first to intrude the folded Malmesbury lithologies. The granitoids originated from primary peraluminous melts presumably derived from the Namaqua-Natal crustal basement aged 1.5 and 1.9 Ga (Scheepers and Nortje, 2000).

Later phases of the S-Type suite crystallized from metaluminous magmas and mark the transition to the younger post-tectonic I-Type granites (Rozendaal *et al,* 1999). Large shear zones such as the Colenso Fault Zone, displaying successive sinistral and dextral movement

episodes, influenced localization of the S-Type granites, whereas the I-Type plutons intruded into large periclinal structures in the Swartland and Boland tectonic terranes (Rozendaal *et al,* 1999). The suite of I-Type plutons is related to shoshonitic or high-potassium calc-alkaline volcanism and is typical of magmatism in island arcs or active continental margins (Rozendaal *et al,* 1999). In the Cape Granite Suite, these late orogenic I-Type granitoids have an age of 539 ± 5 Ma (Scheepers and Nortje, 2000). Prior to the intrusion of the anorogenic A-Type granites, an episode of mafic to intermediate high-K calc-alkaline magmatism followed, at approximately 519 Ma (Rozendaal *et al,* 1999).

Magmatism in the Saldania Belt ended with the intrusion of minor plutons of anorogenic alkali granite (510 ± 4 Ma) into most of the tectonic terranes, these granites are fractional mantle-derived magmas (Rozendaal *et al,* 1999). The decrease of $\delta^{18}O$ values from 10.5 – 11.5 $^{0}/_{00}$ for the earliest S-Type granites, to 6.5 – 8.8 $^{0}/_{00}$ for the youngest A-Type phases, corresponds to a change in the nature of the source of magma with time (Harris *et al*, 1997, Rozendaal *et al,* 1999).

2.4.1 Saldanian orogenic cycle

In short there are 4 phases to the Saldanian orogenic belt, a rifting phase, a reversal or transpression, a subduction phase and then a foreland basin phase. Between 780 – 750 Ma break-up of supercontinent Rodinia forming rift basins that were the localities for the deposition of the Pan-African sedimentary lithologies including the Malmesbury, Kango, Kaaimans and Gamtoos Groups (Dalziel *et al,* 1994, Rozendaal *et al,* 1999). During the construction of the supercontinent Gondwana in the Late Neoproterozoic to early Cambrian, closure of the Pan-African ocean occurred to become orogenic mountain belts (Rozendaal *et al,* 1999).

Rifting south of the Damara, Kaoko and Gariep triple point off the west coast of Namibia formed stepped pull-apart basins, defined by northwest trending, dextral transpressional margins and north-northeast trending normal rift margins (Von Veh, 1992, Gresse, 1995). Transtensional north-westerly trending basin margins coincide with transform faults that offset the northerly trending proto-Atlantic (Adamastor) spreading ridge (Rozendaal *et al,* 1999). Ocean floor spreading occurred between 700 – 600 Ma in the continuing transtensional tectonic regime, the basin type during this time was that of an evolving ocean or continental margin

forming the Swartland Terrane, Goegamma Subgroup, Kaaimans and Gamtoos Groups (Rozendaal *et al,* 1999).

Reversal of spreading in the Adamastor Ocean, which may have been initiated by the opening of the Iapetus between 600 and 570 Ma (Grunow *et al,* 1996). Northwest trending transforms of the spreading area, including the north-eastern Saldanian margin, were reactivated in the same direction by the same forces. The boundary between the Swartland and Tygerberg Terrane; the Colenso Fault Zone, also exhibits evidence of early sinistral (ductile) shearing followed by later dextral and repeated sinistral movement (Gresse and Scheepers, 1993).

Intrusion of the multi-phase S-, I- and A-type granites of the Cape Granite Suite into the Saldania Belt in a pervasive transpressive regime, which resulted in prominent northwest elongated late- to post- orogenic plutons (Rozendaal *et al,* 1999). Magma emplacement was into openings of releasing bends along transcurrent fractures during reversal of the sense of motion as well as during the relaxation of stress after collision (Veevers, 2007). The Peninsula pluton, Darling batholith and Trekoskraal granite of the S-Type intrusions show syn-intrusive ductile shearing and foliation development, which formed between 550- - 510 Ma and post-dates peak metamorphism (Da Silva *et al,* 1997, Rozendaal *et al,* 1999, Scheepers and Nortje, 2000).

Foreland basin development occurred between 570 – 560 Ma (Rozendaal *et al,* 1999). With the final stages of the Saldania Orogenic cycle ending at 510 Ma and marked by the upper Kango and Franschoek deposits (Rozendaal *et al,* 1999). Below (Table 2.3) the events of the Saldanian Orogenic cycle are summarized and the different intrusive rocks and sedimentary sequences that are associated with each of the above stages of the evolution are shown.

Table 2.3: Summary table from Rozendaal *et al,* (1999) defining the evolution of the Saldania Belt highlighting the relative events during the formation of the belt and the associated ages, tectonic regime, basin type, sedimentation and plutonism.

Table 3
Summary of the evolution of the Saldania Belt

Event	Age (Ma)	Tectonic Regime	Basin Type	Sedimentation	Plutonism
Rifting phase					
Break-up of supercontinent Rodinia and opening of proto-Atlantic ocean	780-750	Transtentional, rifted margin	Stepped pullapart basins	Rift-related diamictite, arkosic quartzites, distal facies conglomerate quartzite and limestone (Goegamma Subgroup, Boland Terrane, Gamtoos Group)	Rift volcanics/ intrusives andesite, dolerite/diabase (Brewelskloof, Tulbagh, Kango)
Ocean floor spreading	700-600	Trantensional	Evolving ocean/continental margin basins	Deep water thick turbidite successions (Swartland Terrane, Goegamma Subgroup, Kaaimans and Gamtoos Groups)	Basaltic, WPB-MORB (Bridgetown Formation)
Reversal/transpression and subduction phase					
Reversal of spreading and closure of proto-Atlantic ocean	600-570	Sinistral transpressional			
Subduction/obliqu e collision	570-545	Poorly developed collision orogen			Syn- and post-tectonic S-, I- and A-type granites (Cape Granite Suite)
(Cape Granite Suite)	(550-510)				
Foreland Basin Phase					
Development of syn- to post-orogenic basins	570-510	Syn- to post-orogenic	Foreland, intra-orogen and marginal pull-apart basins	Molassic and related deposits (Kansa Subgroup, Franschhoek Formation)	

The link between the Delamarian, Ross and Saldania orogenic areas during the reversal or transpression and subduction phase has been outlined in Rozendaal *et al,* (1999) as the orogenic chain shares a common history of sinistral transpressive deformation with corresponding structural styles and orientations. Granite emplacement occurred along the extensive palaeo-Pacific active margin stretching over 60° of latitude. The common history continues with the fact that the orogenic granites intrude non-fossiliferous deposits of the Late Neoproterozoic age, and occurred coevally with the closure of the Gariep-Damara-Dom Feliciano Belts, which corresponds to a common plate tectonic model for the simultaneous sinistral transpressive subduction in both belts. The plate tectonic model for this area was initiated by the rifting of Laurentia from South America and the opening of the Iapetus Ocean, which suggests that the Swartland and Tygerberg Terranes form both part of the series of plates that were accreted to the central Australian-Antarctic-Kalahari string of cratons along the palaeo-Pacific margin of

western Gondwana during the Late Vendian and Cambrian eras. Notwithstanding the above, the plate tectonic model is still to be contested and its validity tested.

2.5 Geochemistry in literature of Cape Granites and Colenso Fault Zone

There is a complex compositional variation for the Cape Granite Suite as a whole (Scheepers, 1995). Scheepers (1995) highlight that P_2O_5 and Th can be used as discriminating elements followed by elements Na_2O, K_2O, Zr, Nb, Y and REE with a 90 % certainty. Isotopes in the Cape Granites can also be used as discriminating criteria between the different types of granites (S and I), as $\delta^{18}O$ is a good covariate with P_2O_5 (Harris *et al*, 1997). The fresh rock $\delta^{18}O$ value of feldspar ranges from 5 to 13.6 ‰ and the $\delta^{18}O$ of quartz ranges from 8.6 to 13.4 ‰ with the average $\Delta_{quartz\text{-}feldspar}$ is +2.1 ‰ (Harris *et al*, 1997). All the granites in the area have a low LOI between 0.42 and 1.41 which means there is extensive degassing of water during crystallization with resulting shifts to lower magma δD values as crystallization proceeded (Harris *et al*, 1997). The A-type granites have a low P_2O_5 (<0.1 wt%) and high Th content (>40ppm), the S-type granites have a low Th (<40 ppm) content with a high P_2O_5 (>0.1 wt%) content (Scheepers, 1995; Harris *et al*, 1997). The I-Type granites are an intermediatary body of composition between A- and S-type granites. One can also use P_2O_5, CaO and (Na+K)/Al to distinguish between the A-, I- and S-type granites; S-types granites are enriched in P_2O_5, I-type granites enriched in CaO and the S-type granites enriched in the alkalis (Scheepers, 1995).

The S-Type granites can be sub-divided into 2 groups, the Sa and Sb granites with the Sa granites being further divided into Sa1 and Sa2 granites (Scheepers, 1995). The S-type granites outcrop to the South West of the Colenso Fault Zone in the Tygerberg Terrane and their K/Na ratio is higher than those of the I- or A-Type granites (Scheepers, 1995). S-types granites have crystallized from magma with a $\delta^{18}O$ value of 9.5 to 11.4 ‰ (mean of 10.6 ‰), this is higher than that of the I- and A-type granites with a boundary between these at 9.3 ‰ (Harris *et al*, 1997). The $\delta^{18}O$ values for Sa granites is relatively greater than that of the Sb granites (Harris *et al*, 1997). The Sb granites are those represented by the Trekoskraal, Karnberg and Olifantskop granites and represent the end of the first phase of Plutonism (Scheepers, 1995). They in general intrude along or in the vicinity of large shear zones such as the Colenso Fault Zone (Scheepers, 1995). The Sa1 and Sb granites are enriched in K_2O, Rb Th and selectively enriched in Ce and Sm relative to adjacent elements and have lower values of Y and Yb (Scheepers, 1995). The Sa1 and Sb granites are also enriched in Nb and have minor Zr which is indicative of crustal contamination (Scheepers, 1995). The Sa2 granites are depleted in Sm

and especially in Y and Yb (Scheepers, 1995). These granites represent the younger phases of S-type granites and show high levels of depletion in Y, Yb and other HREE elements; indicative if melting of a garnet-rich source (Scheepers, 1995).

The I-type granites can be sub-divided into 2 groups as with the S-type granites. These are called the Ia and Ib sub classifications according to Scheepers (1995). These units are the Malmesbury plutons and trend on AFM diagrams in the Tholeiitic area and on TAS (total alkali vs silica) diagram on the boundary between K and Na series (Middlemost, 1991). The I-type granites contain high Sr due to their very high plagioclase content (Scheepers, 1995). The Fe_2O_3/FeO ratios vary from 0.5 – 0.8, suggesting a magmatic series granitoids affinity (Scheepers, 1995). The high K_2O, Rb and Th content is characteristic of I-type granites, they also show an enrichment in Ce (Scheepers, 1995). In comparison to the S-type granites they contain lower concentrations of Zr, Nb and Sm with higher Y and Yb contents (Scheepers, 1995). In general the Ib granites are CaO poor, Nb enriched and the Ia granites are CaO, Th, Zr and K_2O rich (Scheepers, 1995).

The A-type granite can be also sub-divided into 2 sub classifications Aa and Ab types, Aa types are expressed on surface in the Tygerberg Terrane as the Klipberg granite and the Ab types as the Cape Columbine, Yzerfontein, Mud River and Botterberg granites (Scheepers, 1995). The Aa and Ab granites are both highly enriched in K_2O, Rb, Th, Nb, Ce and the Ab granites enriched in Y as well (Scheepers, 1995). Ab granites are defined as calc-alkaline series on AFM diagrams, and on TAS graphs fall within the typical composition of transalkali granite suites (Middlemost, 1991). The Ab granites have compositions of upper continental crust in terms of their Y content, enriched in La and very poor in Nb (Scheepers, 1995).

In summary, the magmas that created the continental crust of the Saldania Belt started with older peraluminous S-type granites increasing in alkalinity with increasing differentiation (Scheepers, 1995). Followed by a phase of alkaline basaltic magma emplaced into the lower crust and the creation of metaluminous, alkaline I-type granites during differentiation (Scheepers, 1995). Magmatism was concluded by the intrusion of alkaline magmas of the A-type granites (Scheepers, 1995). Isotopically as the intrusion if the CGS proceeded from SW (S-type granites) to NE (I-type granites) with time the $\delta^{18}O$ value of the intruding magma decreased. Following the sequence of intrusion Sa1, Sa2 then Ia, Ib then Aa, Ab corresponds

to magmas of $\delta^{18}O$ 10.5 to 11.5 ‰ to 9.5 ‰, then 7.5 to 9.0 ‰ and then 6.5 to 8.8 ‰ (Harris *et al*, 1997).

3. Methodology

A total of 64 samples were used for this research. 16 samples from a project in the study area previously performed in a BSc (Hons) project by Simon Baer, 7 samples used for a paper previously done on the Colenso Fault Zone area and 42 samples that were collected during the field work for the current study. Of the current samples 17 are relatively undeformed granites from across the study area representing I-, S- and A-type granites. One sample is a xenolith, 3 samples are of different large cataclasites, there are 7 vein samples and 14 smaller cataclasites. The sample localities are listed in Table 3.1.

3.1 Sampling

Samples of the Colenso Fault zone and the associated Cape Granite Suite units within the study area were selected to appropriately represent the different granites in the area: the S-, I- and A-type granites; G1, G2 and G3 intrusive rocks respectively, as well as the large and small cataclasitic shear zones along the traverse across the outcropping fault zone, and the late stage aplite veins. Each sample collected was roughly 0.3 m^3, large enough to be representative of the outcrop. All samples were prepared and analysed at the Department of Geological Sciences, University of Cape Town, South Africa. Samples were analysed by X-Ray Fluorescence (XRF) Spectrometry, and for $\delta^{18}O$ of both whole rock and quartz.

3.1.1 Location and GPS co-ordinates of the samples

Figures 3.1 and 3.2 are google earth images of the study area indicating the sample area in relation to the town of Vredenburg and the sample sites selected for this research, the exact GPS co-ordinates for which can be found in Table 3.1.

Figure 3.1: Google Earth image of the sampling area to the west north west of the town Vredenburg on the West Coast Peninsula of South Africa.

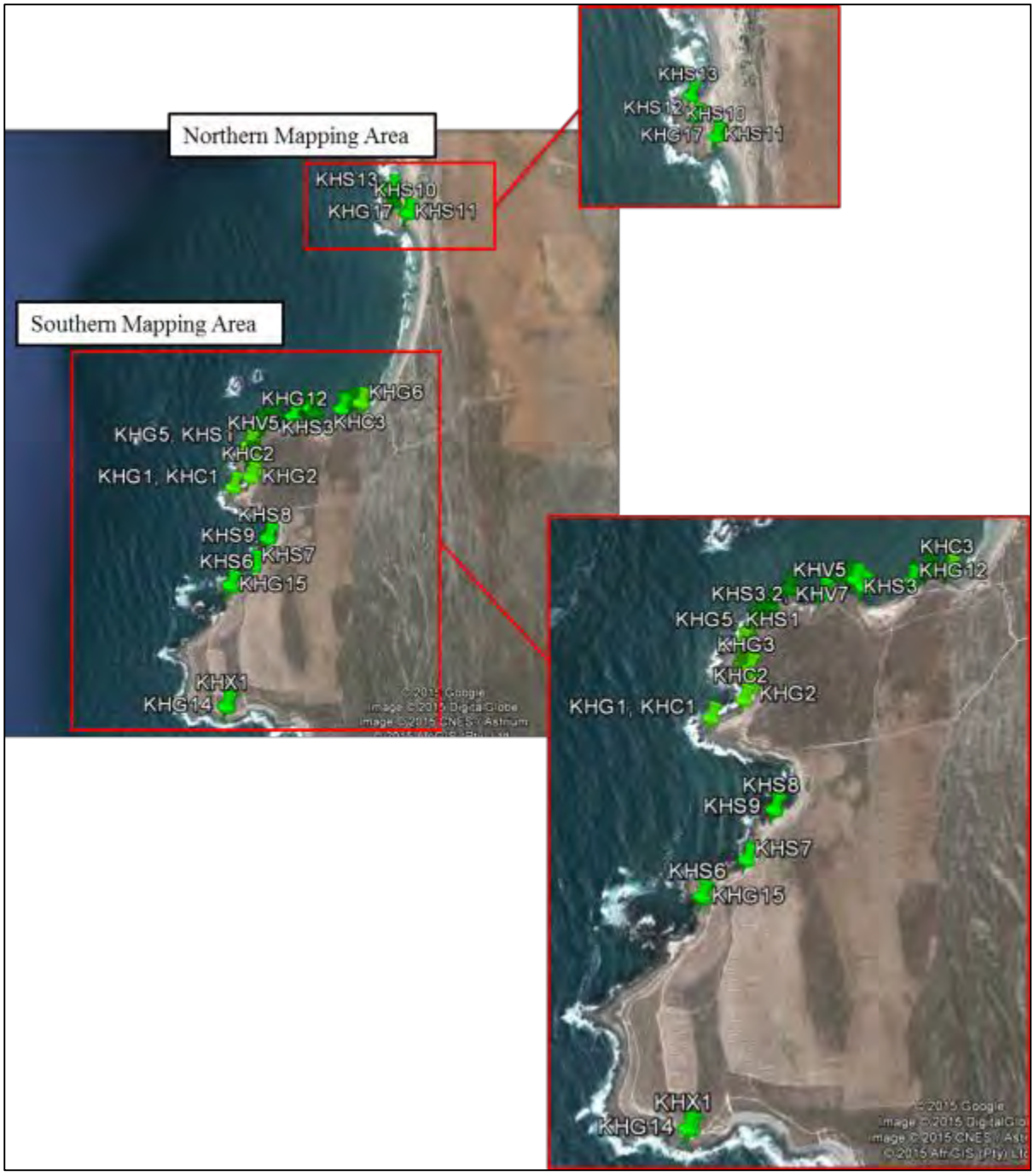

Figure 3.2: Google Earth image of the sampling sites along the West Coast of South Africa.

Table 3.1: Table of WGS 33 South UTM co-ordinates for each sample site.

Sample_ID	Basic Rock Type	Easting (UTM)	Northing (UTM)
KHC1	cataclasite	767863	6356981
KHC2	cataclasite	768040	6357060
KHC3	cataclasite	769172	6357711
KHG1	granite	767863	6356981
KHG10	granite	768302	6357671
KHG11	granite	768581	6357719
KHG12	granite	768959	6357666
KHG13	granite	769058	6357722
KHG14	granite	767713	6354914
KHG15	granite	767801	6356036
KHG16	granite	768974	6357689
KHG17	granite	769731	6359596
KHG2	red granite	768083	6357132
KHG3	granite	768073	6357235
KHG4	granite	768031	6357264
KHG5	granite	768035	6357379
KHG6	granite	769154	6357714
KHG7	granite	230463	6340366
KHG8	granite	768136	6357553
KHG9	granite	768202	6357579
KHS1	shear	768035	6357379
KHS10	shear	769747	6359602
KHS11	shear	769740	6359600
KHS12	shear	769621	6359722
KHS13	shear	769597	6359855
KHS2	shear	768302	6357671
KHS3	shear	768660	6357697
KHS3.2	shear	768698	6357650
KHS4	shear	769058	6357722
KHS5	shear	254907	6304912
KHS6	shear	767792	6356043
KHS7	shear	768026	6356213
KHS8	shear	768175	6356463
KHS9	shear	768181	6356473
KHV1	vein	768076	6357447
KHV2	vein	230463	6340366
KHV3	vein	768129	6357526
KHV4	vein	768202	6357579
KHV5	vein	768481	6357627
KHV6	vein	768628	6357711
KHV7	vein	768698	6357650
KHX1	xenolith	767694	6354915

3.2 Analytical Techniques

3.2.1 Sample preparation

The samples were individually split into smaller pieces that were 3-6 cm in length with a hydraulic splitter. Weathered edges of these pieces were discarded so as to prevent contamination. The pieces were then placed into a jaw crusher to crush them by a factor of ~25. The samples were then separated into 2 groups: one to go into the rotary swing-mill and the other to be sieved to select grains for isotope quartz grain selection. The one set of crushed sample was placed into a carbon-steel rotary swing-mill for 2 minutes, so as to grind it to a very fine grained powder. The other crushed sample was sieved to between 20 and 60 mesh size, which was then washed with water and ethanol. They were then dried overnight at 110 °C, after which clean quartz grains were handpicked using a binocular microscope and tweezers. The grains selected were then cleaned again with ethanol and crushed using a hand grinder and placed within a glass vial. The glass powder sample vials were left to dry overnight in the oven at 50 °C.

3.2.2 Major element and selected trace element analysis by XRF

Major elements and selected trace elements were analysed using wavelength dispersive X-Ray Fluorescence Spectrometry (XRF). The analyses were carried out using a Phillips X'Unique wavelength spectrometer at the Department of Geological Sciences, University of Cape Town, South Africa. Both powder briquettes and fusion discs were prepared for analysis. Approximately 6 g of powdered sample with a coating of 4 g boric acid were compressed under 10 tonnes of pressure to make the powder briquettes. The fusion discs were made using 2 g of powdered sample placed into a crucible, which was placed into the oven at 110 °C for 4 hours and then roasted overnight at 850 °C so as to determine the loss of ignition (LOI) and so as to oxidise the Fe to Fe^{3+}. After taking the crucibles out of the oven, 0.7 g of the sample was added to 6 g of LiT - LiM flux in the proportion 57 : 43, with LiBr as the releasing agent, this mixture was then used to form a fusion disc. Analytical errors and detection limits are given by le Roex *et al*, (1981), Duncan *et al*, (1984) and le Roex, (1985), of 95 % (ppm) for major elements and 99 % (ppm) confidence levels for trace elements.

3.2.3 Stable isotopes

3.2.3.1 Oxygen

Oxygen isotope ratios for whole rock and quartz grains were determined on the conventional silicate line. Roughly 10 mg were then transferred into Ni reaction vessels where 8 samples

and 2 standards were run at the same time. The standard used for both the quartz and whole rock oxygen isotopes was the MQ (Murchison Quartz) standard. The samples were degassed under a vacuum at 200 °C for 2 hours.

All stable isotope analyses were conducted at The University of Cape Town, Geological Department. Oxygen isotope data were obtained by conventional methods using CIF3 as the fluorinating reagent (Borthwick and Harmon, 1982). The data are reported in the familiar δ notation where $\delta^{18}O = (R_{sample}/R_{standard} - 1)$ x 1000 and $R = {}^{18}O/{}^{16}O$. Further details of methods used at UCT for extraction of Oxygen given by Vennemann and Smith (1990) and Harris and Erlank (1992).

Fourie and Harris described how isotopes were measured and stated; all isotope ratios were measured off-line using a Finnigan Delta XP mass spectrometer in dual-inlet mode. Duplicate splits of the quartz standard (NBS28) run with each batch of eight samples were used to convert the raw data to the SMOWscale using the $\delta^{18}O$ value of 9·64‰ for NBS28 recommended by Coplen *et al*. (1983). During the course of this work, eight analyses of NBS28 gave a 2σ error of 0.16 ‰. The O-isotope ratios of samples analysed using laser fluorination were measured on O2 gas. Measured values of our internal standard MON GT (Harris et al., 2000) were used to normalize the raw data and correct for drift in the reference gas. The average difference in $\delta^{18}O$ values of duplicates of MON GTanalysed during this study was 0·14 ‰, and corresponds to a 2 σ value of 0.19 ‰. MON GTwas recalibrated against the UWG-2 garnet standard of Valley et al. (1995) using the current laser system, and has a revised $\delta^{18}O$ value of 5.38 ‰, assuming a $\delta^{18}O$ value of 5.80 ‰ for UWG2.

Only WR $\delta^{18}O$ values were obtained for the cataclasite samples as one could not be entirely certain that the quartz grains sampled for Qtz $\delta^{18}O$ values would be that of the cataclasite itself but may have been of vein material that precipitated during cataclasis. Therefore only WR $\delta^{18}O$ isotopes were examined for the cataclasite zones.

3.2.3.2 Hydrogen

During hydrogen analysis 50 – 200 mg of powdered sample was weighed out according to loss of ignition values, in that high L.O.I. values allow for less sample to be required. Sample powder were loaded into 6 mm quartz tubes (oven dried at 800 °C). Decrepitated gravel-size

quartz chips and quartz wool was loaded on top of the sample so as to prevent the neck of the tube from collapsing during pyrolysis, and to prevent the sample powder from being pumped into the vacuum line. The quartz tube filled with the sample was oven-dried overnight at 110 °C and was afterwards placed on a hot plate at 190 °C for an hour. The quartz tube was attached to the vacuum line and degassed for 15 minutes at 190 °C by using a heated aluminium block from a hot plate. The structural H_2O within the sample was released by heat (pyrolysis) using a propane-oxygen torch (>1200 °C) for 3 – 5 minutes until the whole sample had fused.

The released H_2O was collected in a liquid nitrogen trap and any organic or molecular hydrogen was oxidised to H_2O using a copper-oxide furnace at 700 °C. After which the liquid nitrogen trap was replaced by an alcohol trap (isopropanol mixed with liquid nitrogen) and all the non-condensable gasses were pumped out. The H_2O from the sample was then trapped in a glass 'break-seal' tube containing zinc shavings (low blank 'Indiana Zinc' 569B) using liquid nitrogen. Excess Zn was used to prevent poisoning from fluorine present in the samples. The glass break seal tube was then placed in a furnace for 30 minutes at 450 °C to reduce the H_2O to elemental hydrogen.

The hydrogen isotope composition of the sample was measured using a Finnigan MAT-252 mass spectrometer at the University of Cape Town. The instrumental hydrogen isotope ratios were normalised and standardised relative to SMOW using the equations of Coplen (1988). The analytical errors (1σ) for δD and H_2O are ± 2 $^0/_{00}$ and 0.10 wt %, respectively. The error of δD increases as the amount of water extracted decreases as there is insufficient gas to measure δD accurately.

4. Field Observations

As described previously the study area is a coastal outcrop of the Colenso Fault on the west coast of the Western Cape Province at West Coast Bay, which is situated ~12 km west of the town Vredenburg (Figure 3.1). The Colenso Fault in this area is situated between the Saldanha Batholith of the Tygerberg Terrane and the Vredenburg batholith of the Swartland Terrane (Figure 2.4). The rocks that occur in the study area are the Trekoskraal-, Cape Columbine- and Vredenburg-granites, with an approximately 3 km wide fault damage zone defining the Colenso Fault; the area is composed of Cape Granite Suite rocks with areas of 121 - 300 m in width which have been cataclastically deformed.

4.1 Granite

On the southern side of the beach in Appendix 2, shows the outcrops of G1 and G2 intrusion of the Cape Granite Suite (CGS). The G1 and G2 granites are increasingly inter-fingered the further north one moves along the coast line. The G2 is the first 'granite' that crops out in the south of the study area. The G2 granite is actually a quartz porphyry with minor granite porphyry and quartz felsites (Theron, 1970). In the southern-most region of the study area the G2 granite is cataclastic porphyritic granite with xenoliths of the medium-grained plagioclase G1 granite. These xenoliths are also visible on aerial photos as they can be up to 6 m in length. The G2 granite is ~1.8 km away from the inferred fault core and contains xenoliths of G1 granites. The xenoliths can only be found in the most south of the study area and are not visible where the G2 is inter-fingered with the G1 granite to the north. The G1 outcrops increase in width with proximity to the inferred fault core further to the north.

From the most southern area the G1 granite shows zones of cataclasis and areas of deformation increase northward from 1 cm to up to 80 cm. The G1 granite is medium- to coarse-grained and composed primarily of quartz, K-feldspar and biotite with accessory phases of chlorite and muscovite. Variation in this granite is within the grain size and feldspar content. In places the G1 granite is medium-grained K-feldspar granite, containing coarse-grained, rounded K-feldspar, but in general the G1 granite is a coarse-grained granite with K-feldspar grains varying from euhedral to rounded. The contact between the medium- and coarse-grained granite are cataclastically faulted and sheared.

There are 3 large fault strains that are brittlely deformed; cataclasites are sampled as KHC1,

KHC2 and KHC3. These cataclasites are 3 – 7 m wide fault zones and comprise finer grained ground up material of the granites as evidenced by whole-rock major and trace element data analyses (refer to geochemistry section). Large cataclasite volumes only occur in the southern part of the study area.

4.2 Study Site Large Map (South of fault)

The geological map for which the description below belongs is available in Appendix 2. From south to north on this attached map samples of the G1 granite include; KHG15, KHG1, KHG2, KHG3, KHG4, KHG5, KHG8, KHG9, KHG10, KHG11 and KHG6. Then from south to north on the same attachment we have cataclasites sampled respectively as KHS6, KHS7, KHS8, KHS1, KHS2, and KHS3.2.

The southernmost granite mapped to the south of the fault zone is a dark coarse-grained porphyritic G2 granite (KHG14) with xenoliths of the G1 granite (KHX1) rich in K-feldspar, plagioclase and surrounded by fine-grained matrix. This granite has no deformation fabric visible. The G1 granite just to the north (KHG15) is very coarse-grained with thin cataclasites that run through it such as KHS6, KHS7 and KHS8, with deformation intensity increasing closer to the fault. Further north is the intersection of the first finger of the inter-fingering granites of the G1 and G2 granites, this finger is relatively thin and is of the G2 granites. Within this G2 granite are thin cataclasites that again increase with intensity with proximity to the fault (KHS9).

Continuing the south to north traverse across the southern mapping area, after the intersection of the G2 granite after a break in outcrop the G1 granite is intersected, followed by the intersection with the first of the large cataclasites (KHC1 and KHC2) with an irregularly shaped contact to the G1 granite (KHG1 and KHG2). The granites in contact with the cataclasite are intensely sheared and show evidence of cataclasis away from the boundary with the cataclasite. In this area is were Grid Map 1 (Figure 4.1) below was taken.

Just to the north of the above is the continuation of the G1 granite that changes in texture from area to area, changes in shear intensity and width. Moving from south to north in this section, samples of the contacts of different deformation intensity granites, aplite veins, as well as samples of undeformed granites were taken. KHG3 is the contact between a fine grained red granite and porphyritic red granite with a shear between the two. KHG4 is an un-deformed

white porphyritic granite with rounded porphyroblasts of feldspar. KHG5 is a fine-grained granite that alternates with the porphyritic granite with evidence of shearing. KHV1 is an aplite vein within the fine-grained granite between KHG5 and KHG8. KHG9, is a highly sheared porphyritic granite with large ~1 m wide aplite veins which have a light brown weathering colour. KHG10 is even coarser grained than KHG9, with aplite vein material cutting across the granite in areas such as KHV5.

Moving in an east-north-easterly direction to the last outcrops before the inferred fault zone one can find KHG11 a sheared granite with wavy plagioclase, intruded by an aplite vein striking SW. The shear zone represented by sample KHS3 within a granite, is a large cataclasite on the basis that it is larger than 1 m in width and its deformation style in thin section matches that of the other large cataclasites that are defined below. After the intersection with a second large cataclasite further east is an intersection with a fine-grained G2 granite that has K-feldspar and is highly jointed (KHG12). This granite changes to a dark coarse-grained porphyritic granite similar to KHG14 to the south (KHG16). KHG13 and KHS4 is a sheared coarser grained porphyritic granite than that of KHG16.

After this finger of G2 granite, the G1 granite is again intersected as very coarse grained porphyritic 'white' granite (KHG6). KHC3 is a sample of the closest cataclasite to the fault zone and is in contact to the east of KHG6. This area was also mapped in greater detail in Grid Map 3 discussed below (Figure 4.3). The shear intensity of the entire area discussed above decreases away from the cataclasite zones.

4.3 Study Site Medium Map (North of fault)

The granite outcrops to the north of the Colenso Fault zone (Appendix 1) comprise G3 granite of the CGS, this is a coarsely porphyritic granite and tends to be much finer grained and more sheared towards the south. As one moves further away from the fault zone the granite becomes more coarsely grained and the deformation intensity decreases. The G3 is described by Theron, (1970) as a coarsely porphyritic granite. It is a coarse- to very coarse-grained granite composed of porphyritic K-feldspar and plagioclase with smaller phases of quartz and biotite. It is a different granite in comparison to the G1 and G2 granites, as there are no large feldspar grains in the areas closest to the fault zone, however the size of the feldspar grains increase northwards away from the fault zone. The granite has been sheared but to a lesser degree than the granite on the southern beach and lacks any large scale cataclastic veins.

There are zones through the granite which look like a fine-grained black fault rock such as in KHS13 and strike 050 °. Aplite veins in the area are petrographically similar to those to the south of the Colenso Fault. There are fewer joints north of the Colenso Fault zone than the area to the south of the fault zone.

4.4 Aplite Veins

Aplite veins throughout both areas range from 0.5 m to 1.5 m in width, and are composed of primarily quartz and plagioclase with accesory biotite. Aplite veins tend to not show evidence of deformation. The aplites are syn-kinematic with the cataclasites as their contacts are not fragmented nor en enchelon. Some shear fractures are visible in some of the aplites, but this must be due to very late stage deformation as these fractures cross cut both the cataclasite and the aplite veins. The fine-grained aplite veins in this area have a sharp contact to the granite. The close spatial association of the aplites and the cataclasites also show the syn-kinematic relationship during deformation of the Colenso Fault.

4.5 Cataclasites

KHC1 is re-cemented by a quartz breccia, with undulose extinction of the quartz, it has no carbonates within it and is mostly composed of quartz with very little to no feldspar. The feldspar has been altered to sericite. It contains micro-breccia of chlorite, clay and quartz, with deformed grains from the granite where the feldspar has already been removed from alteration and not from the cataclasis. Evidence of grain boundary migration in the fine grained quartz. There are numerous fluid inclusions in the quartz.

KHC2 has multiple fabrics and is very fine grained, thus XRD analysis was done on a powdered sample so as to identify the minerals that one cannot identify through thin section studies and the brown, very fine grained material is biotite. This sample has a high quantity of opaques and is altered to chlorite and biotite in areas.

KHC3 is a re-crystalised rock with a granitic texture. The very fine grained quartz has inter-fingering boundaries, and has no visible fluid inclusions but has lots of solid inclusions which are not fragmented. Just like the KHC1 sample, this rock has very little to no feldspar grains.

4.6 Geological map of Area 1 (Grid Map 1)

The most southern geological map; Grid Map 1 (Figure 4.1) represents the contact between the most southern cataclastic zone and the G1 granite and is represented in the geochemistry data by the samples KHC1 and KHG1 respectively. Figure 4.1 also represents the presence of a late stage medium- to fine-grained aplite vein series. The deformation events described for the Colenso Fault and surrounding areas include an initial sinistral strike-slip sense of movement with a reactivation stage at around 539±4 Ma to a dextral strike-slip sense of movement (Kisters *et al*, 2002). The 14 x 10 m grid map of Figure 4.1 only shows dextral sense of shear along the shear zones, which represent the later stage kinematics of the Colenso Fault Zone. The deformation events that are represented on the map include 2 generations of cataclastic shearing of the G1 Cape Granite, a generation of the large cataclasite as well as jointing. The area is highly jointed as well as intensely sheared, with mean joint strikes of 083° and 133°.

Table 4.1: Relative sequence of deformation in Area 1

	Deformation events
1	G1 Granite emplacement
2	Syn-tectonic development of the aplite vein
3	Dextral strike-slip motion shearing
4	Jointing
5	Sinistral strike-slip motion shearing

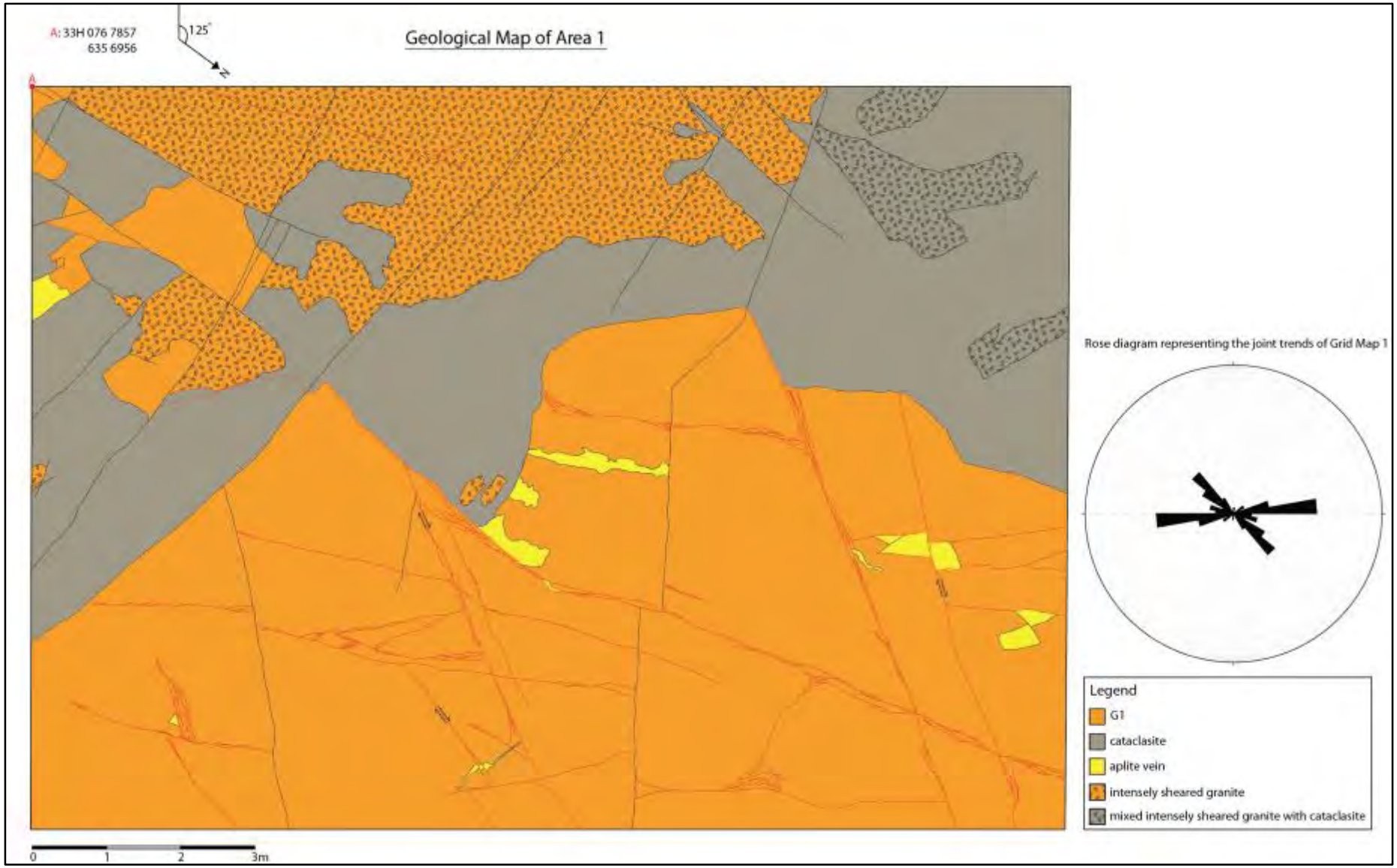
A: 33H 076 7857
635 6956
125°
N
Geological Map of Area 1
Rose diagram representing the joint trends of Grid Map 1
Legend
G1
cataclasite
aplite vein
intensely sheared granite
mixed intensely sheared granite with cataclasite
0
1
2
3m

Figure 4.1: Geological Map of Area 1, Grid Map 1 showing the relationships between the G1 CGS coarse porphyritic granite and the most southern large cataclasite zone. The included rose diagram represents the major strike directions of the joints (black lines) found in this area with a mean conjugate set of 083.4° and 132.6°. The red lines represent shears.

4.7 Geological Map of Area 2 (Grid Map 2)

The Geological Map of Area 2 (Figure 4.2) represents the contact between the third large cataclasite and late stage aplite veins. This large scale cataclasite just like that of Grid Map 1 sits within the G1 granite of the CGS. In the sample suite, KHS3.2 and KHV7 are the samples that belong to the geology below in the Grid Map 2 (Figure 4.2). The area mapped is 10 x 10 m in size and shows both the sinistral and dextral sense of shear phases of the Colenso Fault. The large shear zone that crosses the top of the grid map shows a sinistral sense of shear in the aplite veins that it crosses. The smaller offsets in the aplite vein in the bottom right hand corner of the map shows the dextral sense of shear. The area has both joint surfaces as well as shears of which are just small cataclastic deformation style shears. The joints strike predominantly at 015°, with the shear zones striking 048°. The trace of the contact between the aplite vein and the large cataclasite zone strikes ~052°. The contacts between the cataclasite and aplite veins are irregular; such that they are not straight and have no regular pattern.

Table 4.2: Relative sequence of deformation in Area 2

	Deformation events
1	G1 Granite emplacement
2	Syn-tectonic development of the aplite vein and large cataclasite as there is evidence of xenoliths of aplite vein within the cataclasite, that is within a larger aplite vein
3	Sinistral strike-slip motion shearing and associated jointing with syn-tectonic quartz vein development
4	Dextral strike-slip motion shearing

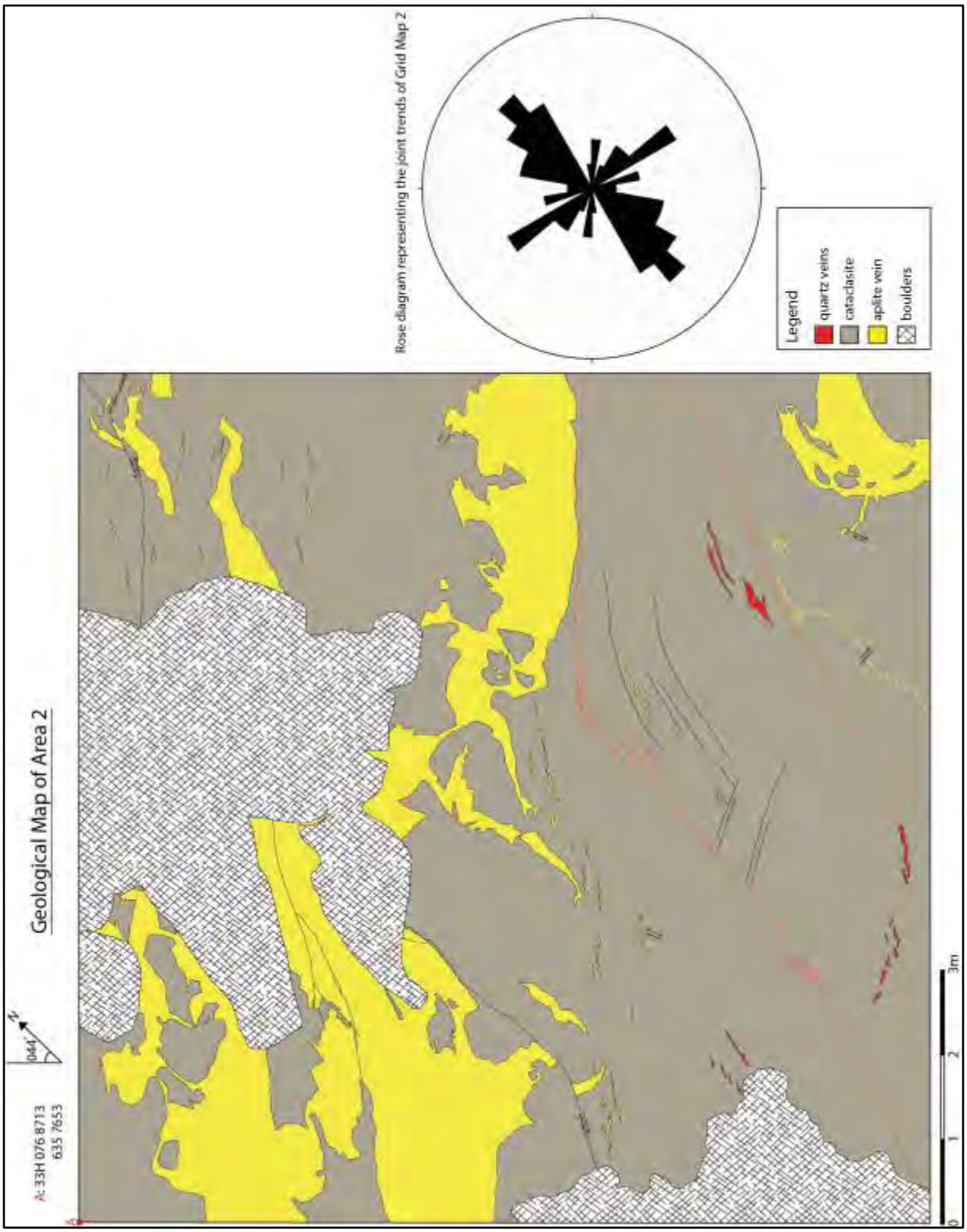

Figure 4.2: Geological Map of Area 2, Grid Map 2 showing the relationships between the late stage aplite veins and the second nearest cataclasite zone to the Colenso Fault. The included rose diagram represents the major strike directions of the joints (black lines) found in this area with a mean strike of 015°. The red lines represent shears.

4.8 Geological Map of Area 3 (Grid Map 3)

The area closest to that of the Colenso Fault Zone, which is inferred to have formed the large bay area at the West Coast near Trekoskraal. The map below (Figure 4.3) represents the contact between the G1 granite of the CGS and the third large cataclasite area to the south of the Colenso Fault. In the sample suites the rocks mapped in this grid map are represented by KHG6 and KHC3. The grid map was made in this area as it was the largest pavement showing good relational deformation events otherwise there are only bits and pieces of outcrop in between boulders. The area mapped is 6 x 6 m in size but still shows again as in area 2 both the deformation events associated with the Colenso Fault; sinistral as well as dextral strike-slip motion. The cataclasites are syn-kinematic with a sinistral sense of strike-slip as the contacts between the cataclasite and these shears are not fragmented and are essentially continuations of one another. The cataclasites that formed during the initial sinistral and then dextral sense of shear are progressive in formation. The jointing in this area is less intense than in the other areas investigated thus far, and interpreted as late-stage as the joints cross cut shear zones without being displaced themselves. The average strike of the joints is 095° and the average shear strike is 355°.

Table 4.3: Relative sequence of deformation in Area 3

	Deformation events
1	G1 Granite emplacement
2	Sinistral shearing with cataclasite development
3	Dextral shearing with cataclasite development
4	Late stage jointing

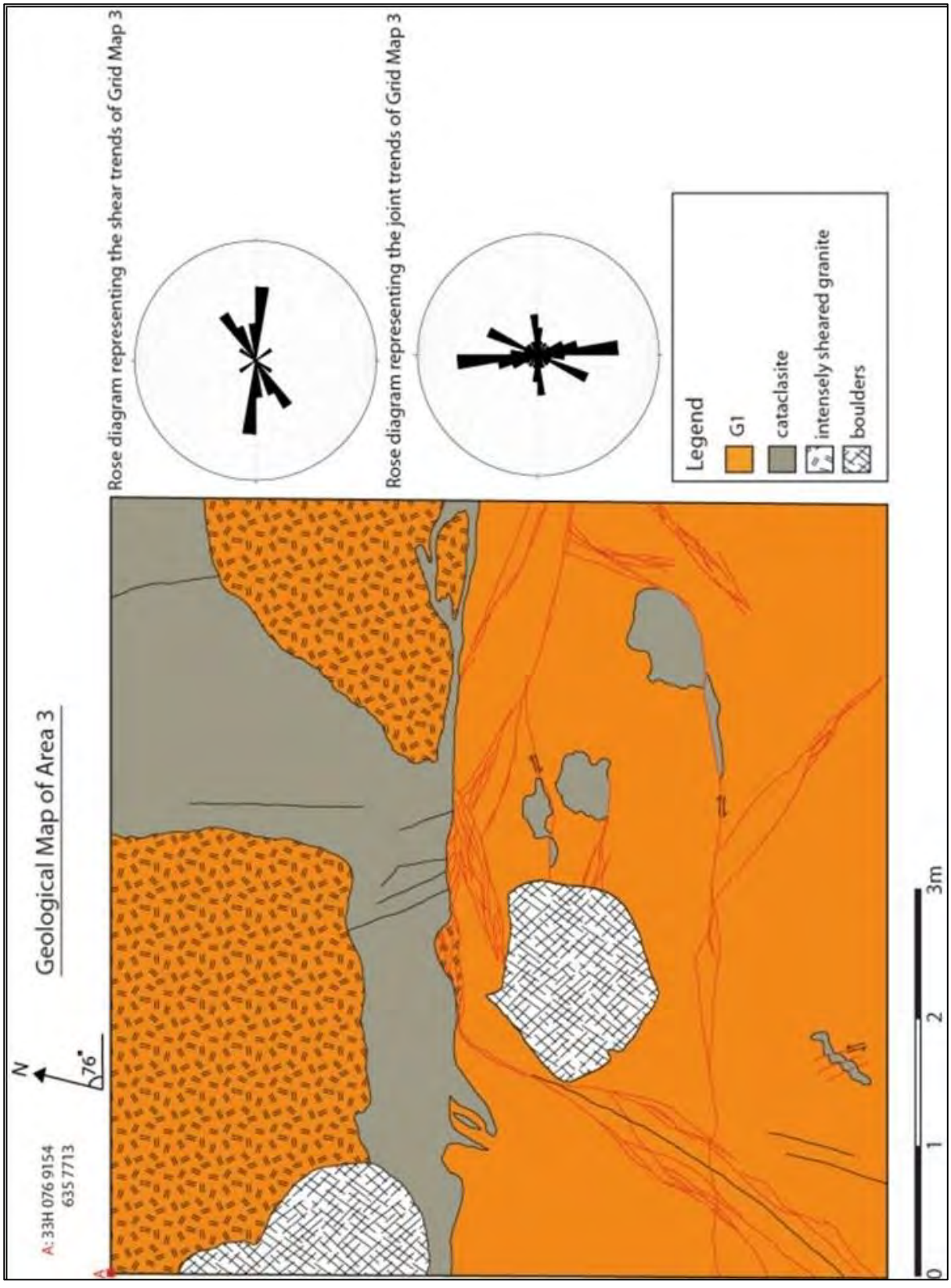

Figure 4.3: Geological Map of Area 3, Grid Map 3 showing the relationships between the G1 CGS coarse porphyritic granite and the most northern large cataclasite zone. The rose diagram represents the major strikes of the joints (black lines) found in this area with a mean strike of 095° and strike of the main shears (red lines) found in this area with a mean of 355°.

4.9 Geological map of Most North Area (Grid Map 4)

The geological map of the area to the north represents to most northern contact to the inferred Colenso Fault Zone. The map below (Figure 4.4) represents the G3 granite of the Cape Granite Suite. In the sample suite the rocks mapped in this grid are represented by KHG17 and KHS12. The grid map was made in this area because it is most representative of the area to the north of the Colenso Fault Zone, which contains xenoliths of both the Malmesbury Group rocks and of granitic composition. The mapped area is 10 x 10 m in size as with the grids to the south of the Colenso Fault Zone, and contains both the deformation events associated with the fault; sinistral as well dextral strike-slip motion. There is very little jointing to the north of the Colenso Fault Zone and is represented in the Grid Map as one joint in the bottom left of the map. The joints associated with sinistral shearing in this area is a later deformation as it cross cuts shear zones without being displaced. The average strike of the shears is 141° and the joint strike 002°.

Table 4.4: Relative sequence of deformation in Area 4

	Deformation events
1	G3 granite emplacement with xenoliths included into the emplacement
2	Syn-tectonic development of the aplite vein with sinistral shearing
3	Dextral shearing
4	Late stage jointing

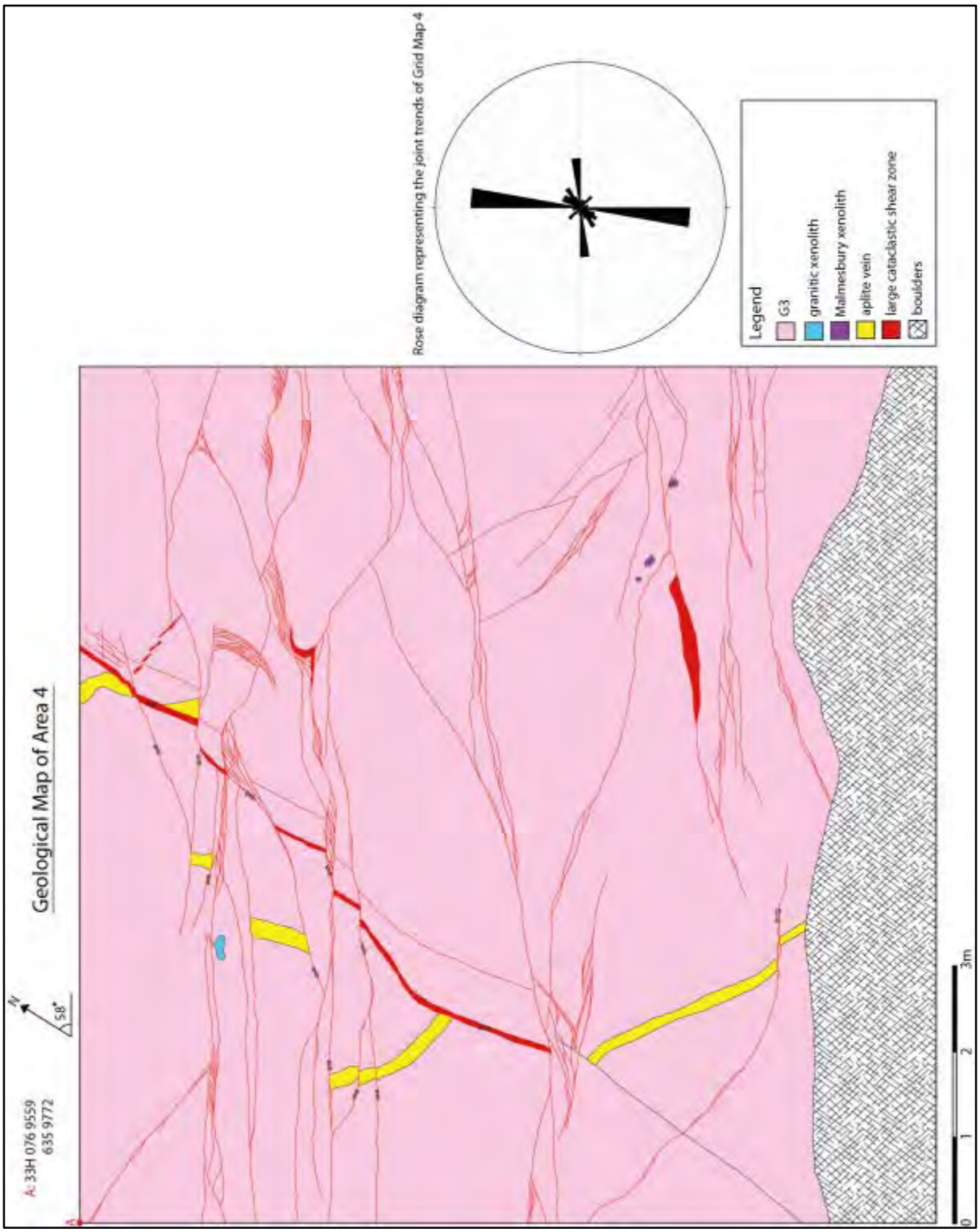

Figure 4.4: Geological Map of Area 4, Grid Map 4 showing the relationships between the G3 CGS coarse porphyritic granite with xenoliths of the G1 granite and Malmesbury Sedimentary rock. The major strike directions of the shears (red lines) found in this area with a mean strike of 141°. The included rose diagram represents the strike direction of the joints (black lines) found in this area with a strike of 002°.

4.10 Summary

In summary the rocks that occur in the study area are the G1, G2 and G3 granites (figure 2.4). The G1 and G2 granites interfinger with one another along the coastline to the south of the Colenso Fault Zone. The G3 granites occur to the north of the Colenso Fault Zone. Cataclasites in the area represent the large 3178 m fault damage zone and can be small shear zones of tens of centimetres with 3 areas of large cataclasites that are 121 - 300 m in width. The relative age of deformation sequence from the study can be divided into 2 sequences as the G3 is younger than the deformation of the G1 and G2 granites. The deformation that G3 exhibits must have also happened on the G1 and G2 granites. The first deformation sequence in age was the emplacement of the G1 and G2 granites of the Cape Granite Suite. The G2 granites came after that of the G1 granites as they contain xenoliths of the G1 granites in them. This was followed by syn-tectonic development of aplite veins and cataclasites. The initial strike-sense of movement along the fault was sinistral and created shearing and jointing of the granites, followed by dextral strike-slip shearing. The above was followed by dextral stike-slip jointing and another phase of shearing and late stage jointing. The second deformation sequence in age was the emplacement of the G3 granite of the Cape Granite Suite to the North of the Colenso Fault Zone. The relative deformation sequence follows from the granitic emplacement of the G3 granites with Xenolith of granitic material and Malmesbury Group sedimentary rocks to the syn-tectonic development of aplite veins. Then there was the sinistral shearing, followed by dextral shearing and finally late stage jointing.

5. Petrography

The following petrographic description of the rocks within the study area, describe the general textures evident from the outcrop scale down to the thin section scale. It is presented in age order for the Cape Granite Suite rocks and then the late stage aplite veins. A modal proportion table (Table 5.1) will be placed at the end of the chapter for easy reference and for correlation between the samples.

5.1 G1 Coarse porphyritic granite

The G1 S-type granite of the Cape Granite Suite is a medium to coarse grained, porphyritic granite (Figure 5.1a) composed of primarily quartz and plagioclase (Na-rich) with accessory biotite, muscovite, opaques and chlorite. The primary plagioclase and quartz grains have in places been altered to secondary phases of fine-grained chlorite, epidote, biotite and muscovite. Opaque minerals occur either within or adjacent to chlorite, muscovite and biotite grains (Figure 5.1b).

The granite is crossed by fracture networks that cross-cut the coarse-grained quartz-plagioclase matrix and earlier generations of fractures. These fractures are in-filled by muscovite that occurs as both laths and euhedral grains. Along the sharp boundaries of these fracture networks there is coarse igneous quartz (Figure 5.1c). Other fractures in the granites are filled with chlorite, muscovite, biotite and opaques. In some areas the fractures occur as conjugate sets infilled with chlorite and opaques, and small clusters of very fine-grained laths of muscovite and biotite that form at the boundaries of the vein.

The plagioclase in the G1 granite is deformed as is evident from the fine-grained, angular feldspar associated with of the coarse-grained igneous grains as well as the small laths of quartz with undulose extinction. The deformed and fractured plagioclase grains show displacement of the twins within them. Fractured plagioclase and quartz grains are in places in-filled with sericite (Figure 5.1d). The quartz grains also have recrystallised centres of fine-grained quartz (Figure 5.2b). Some samples of the granite are different in their petrography, relative to the majority of the samples, such as the KHG3 sample which contains a coarser-grained chlorite fraction which has a well-developed association with medium-grained muscovite and opaques (Figure 5.2a).

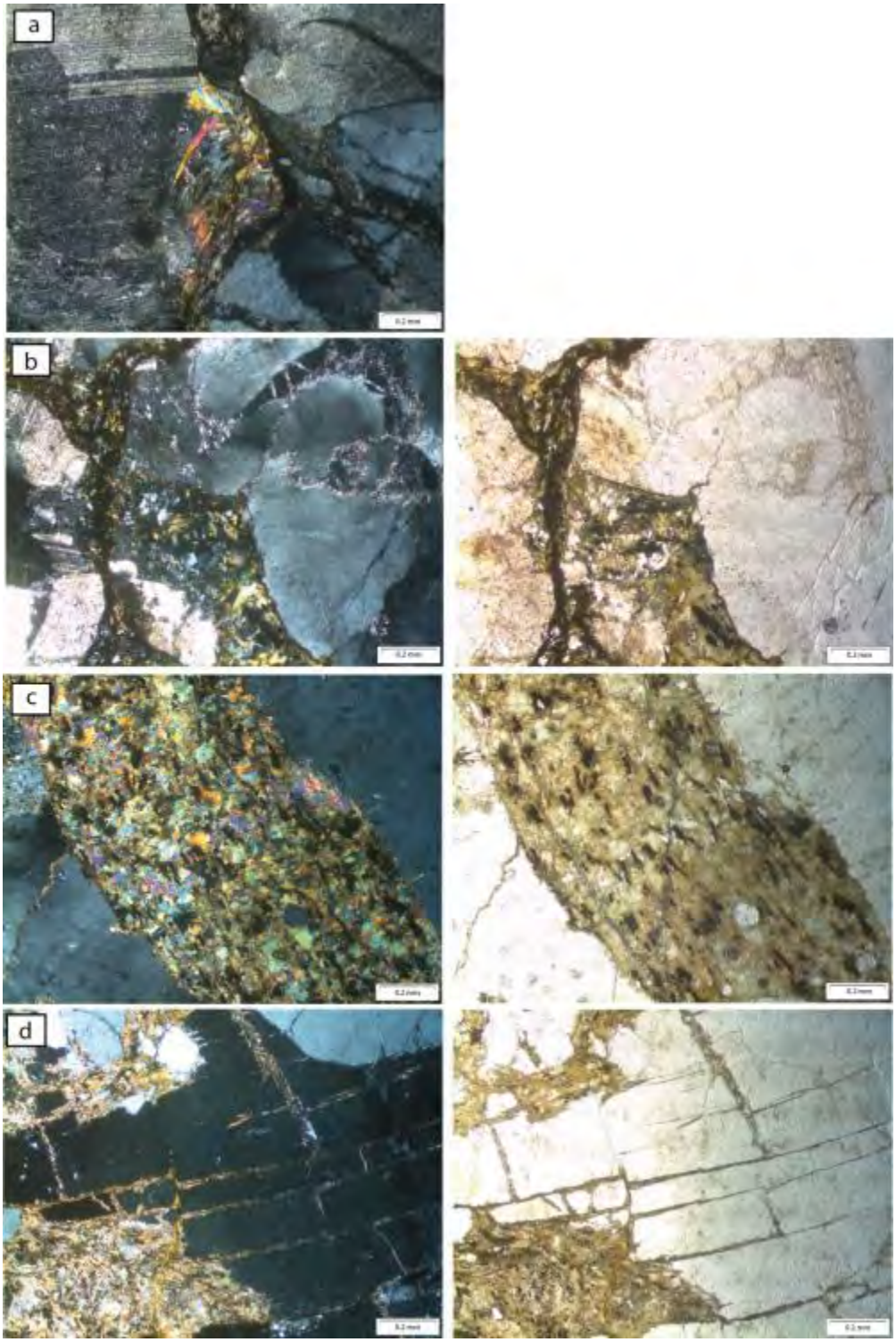

Figure 5.1: Photomicrographs of the G1 granite a) medium to coarse-grained granite composed of qtz, plag, bt, musc, opaques and chl b) association of opaques with chl, musc, bt and epidote c) boundaries of fractures have fine-grained quartz along them d) Sericitization, the alteration of feldspar to white mica by hydration along fractures.

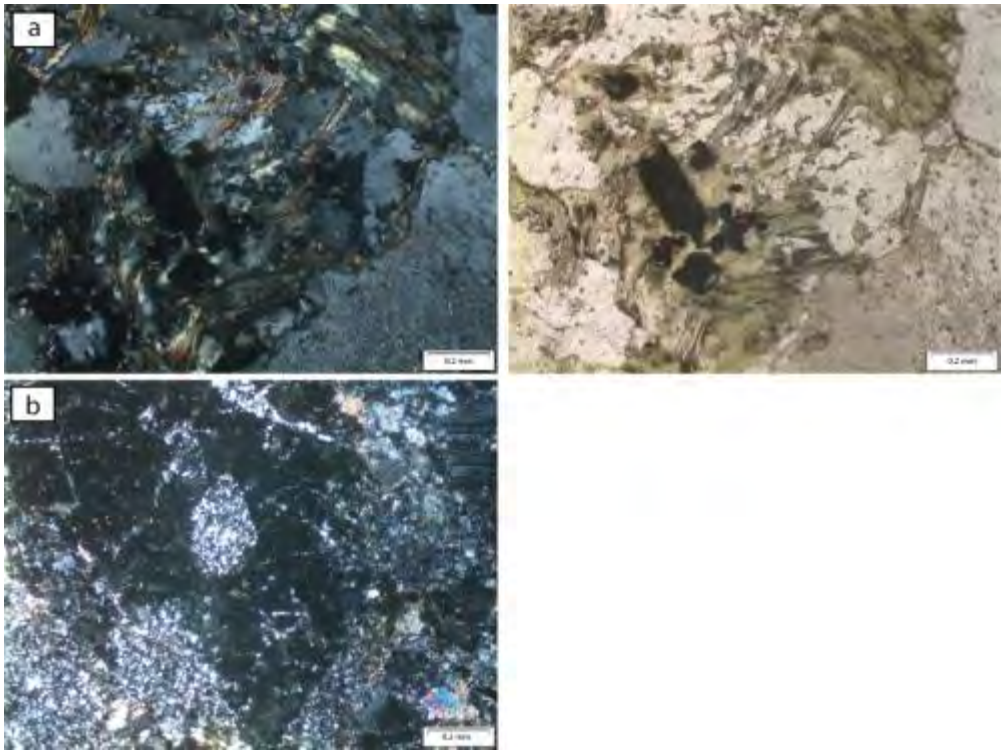

Figure 5.2: Photomicrographs of the G1 granite a) coarser chl of the KHG3 sample with the association with musc and opaques b) qtz grain with a recrystallised core.

5.2 G2 Quartz porphyry with minor granite porphyry and quartz felsites – Saldanha quartz porphyry

The G2 S-type granite is a coarse- to very coarse-grained quartz porphyry of the Cape Granite Suite and is composed of primary quartz, plagioclase, and biotite with accessory secondary phases of muscovite, opaques and chlorite. The matrix primarily comprises plagioclase, quartz, biotite and chlorite (Figure 5.3a). The clast to matrix ratio varies throughout the G2 granites, from being low (less than 30% clast) to moderate (between 30 and 70% clast) to high (greater than 70% clast). Alteration of the plagioclase, quartz and primary biotite to clusters of secondary sericite with minor biotite, opaques and chlorite (Figure 5.3c) is common, as well as the inferred re-crystallisation of quartz grains to a fine-grain matrix or the recrystallisation of the core of the quartz grains. The G2 granites in general within the fault damage zone tend to be highly fractured. The fractures throughout the G2 granite are in-filled with 2 main types of in-fill: one of chlorite and biotite and the other fine-grained quartz grains (Figure 5.3d).

In areas where the G2 granite is undeformed the granite has a typical granitic texture (Figure 5.3b). Deformation is expressed through strain in the form of dislocations in the crystal to give the quartz undulose extinction as well as localized shearing of the plagioclase evidenced by

displaced twins and quartz grains. Sheared grains have a contact of fine-grained material of the larger clast that is sheared, due to cataclasis, i.e. mechanical grain size reduction (Figure 5.3e) and show a dextral strike-slip motion (Figure 5.3f). Some of the quartz grains have clasts of muscovite within them and some of the plagioclase grains within the granite have biotite inclusions. Again some of the samples of the G2 granite; such as KHG13, has a higher proportion of biotite than in other samples. KHG14 has embayments of fine-grained quartz, plagioclase, biotite and muscovite within the coarse-grained quartz and plagioclase grains (Figure 5.3g).

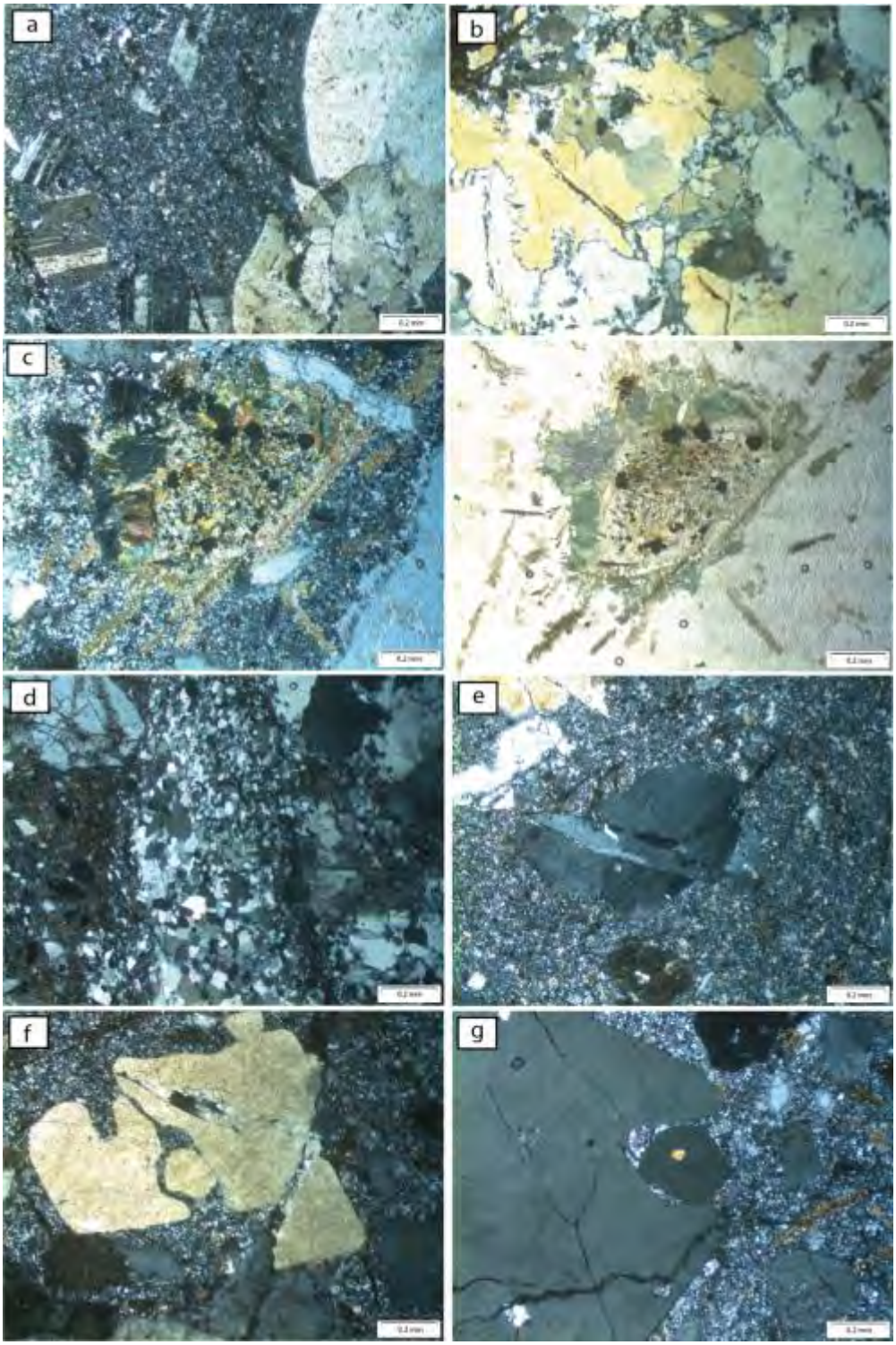

Figure 5.3: Photomicrographs of the G2 granite a) coarse- to very coarse-grained porphyritic granite composed of qtz and plag in a matrix of qtz, plag, bt, musc, opaques and chl b) in un-deformed areas of the granite this is the typical porphyritic granitic texture c) alteration of plag, qtz and bt to fine-grained sericite, bt, opaques and chl d) fracture in-fill of a vein now fine-grained qtz e) sheared qtz grain with mechanical grain size reduction at the shear contact f)

dextral sense of shear indicated in a qtz grain g) KHG14 with embayments in the quartz phenocryst filled with a groundmass of qtz, plag, bt and musc within a coarse-grained qtz grain.

5.2.1 Xenolith within the G2 granite

Within the G2 granite in the southernmost region of the study area there are xenoliths of a coarse-grained porphyritic granite. The xenoliths are composed of primarily plagioclase and quartz in a matrix of quartz, plagioclase and muscovite. The primary quartz and plagioclase are euhedral and are not altered other than minor areas of dynamic recrystallisation. Embayments within the quartz grains of the xenoliths have a groundmass of quartz and muscovite (Figure 5.4a). The clast to matrix ratio is greater than 30% clasts. Tabular grains of chlorite and biotite are randomly orientated throughout the rock (Figure 5.4b). Other features of alteration in this sample are clusters of coarse-grained chlorite, biotite and associated opaques. There is evidence of replacement of some plagioclase grains by muscovite and fine-grained biotite epidote (Figure 5.4c).

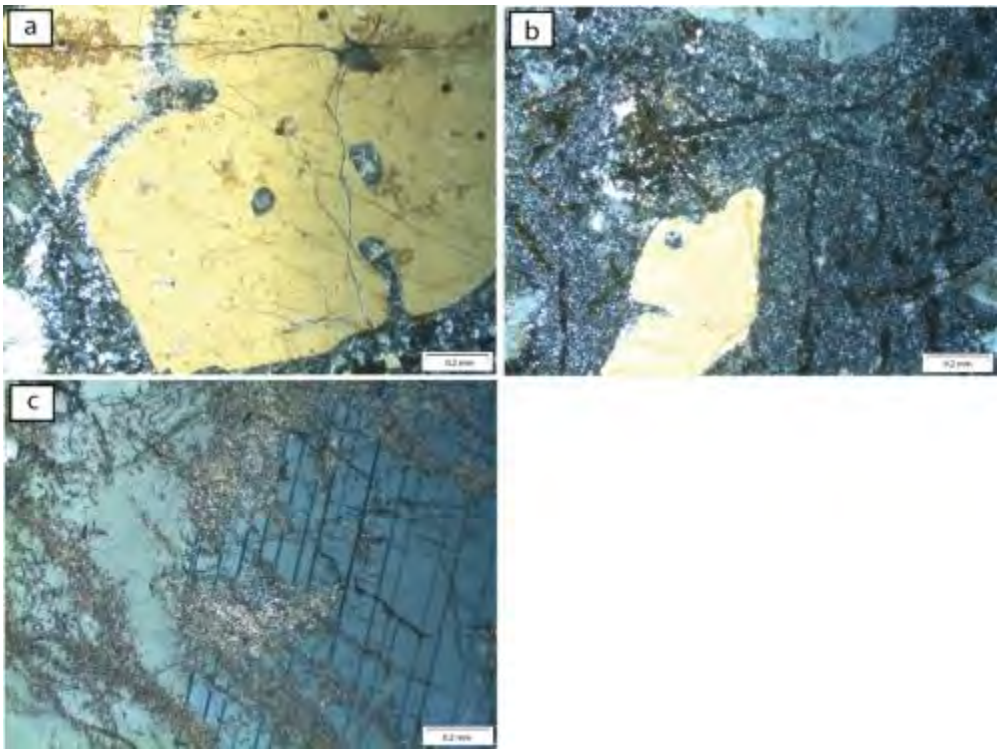

Figure 5.4: Photomicrographs of the xenolith within G2 granite a) embayments of a groundmass of qtz and musc within qtz grains b) Tabular grains of chl and bt that are randomly orientated throughout the xenolith c) resorbtion of plag by musc and fine-grained bt.

5.3 G3 Coarsely porphyritic granite - Saldanha granite

The G3 I-type granite of the Cape Granite Suite is a coarse-grained granite with primary phases of biotite, quartz, plagioclase, and perthite with alteration of the biotite to chlorite. The granite has a poikilitic texture with the quartz inter-grown within course-grained plagioclase (Figure 5.5a). There are small areas of dynamic re-crystallisation of quartz to a fine-grained cluster of grains (Figure 5.5b). Throughout the granite there are minor fracture networks that are in-filled with biotite (Figure 5.5c). The granite is brittlely deformed and this is indicated in the plagioclase grains, as the twining has been sheared and shows a sinistral sense of shear (Figure 5.5d).

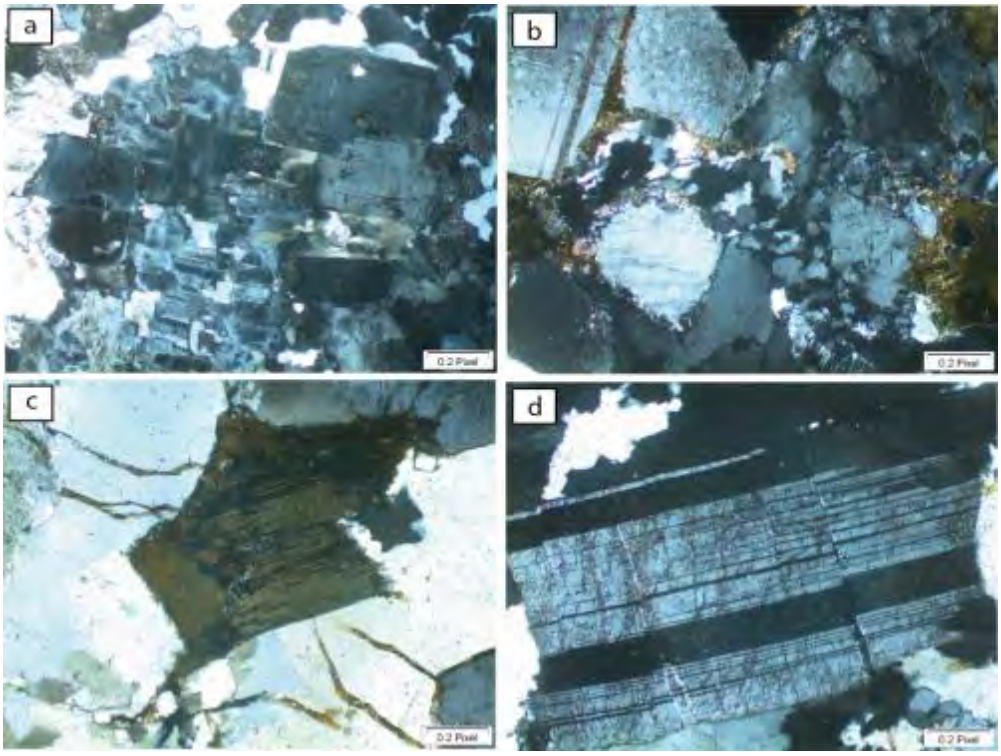

Figure 5.5: Photomicrographs of the G3 granite a) poikilitic texture with the qtz intergrown within the coarse-grained plag b) recrystallisation of qtz c) biotite in-filled fracture network across the granite d) brittle deformation of the plag twins to show sinistral sense of shear.

5.4 Aplite veins

Within the G1 granites there are fine- to medium-grained aplite veins composed of primarily quartz, plagioclase and biotite with a typical granitic texture (Figure 5.6a). In some areas there are fractures that cross-cut the whole aplite vein but otherwise the veins show little alteration or deformation. The fractures that are found are in-filled with cataclastic material of surrounding grains and biotite (Figure 5.6b). These veins are surrounded by fractured grains,

evidenced in Figure 5.6c by un-matching twins of the plagioclase. Some of the micas show evidence of ductile deformation seen by the undulose extinction in between the cleavage of the mineral.

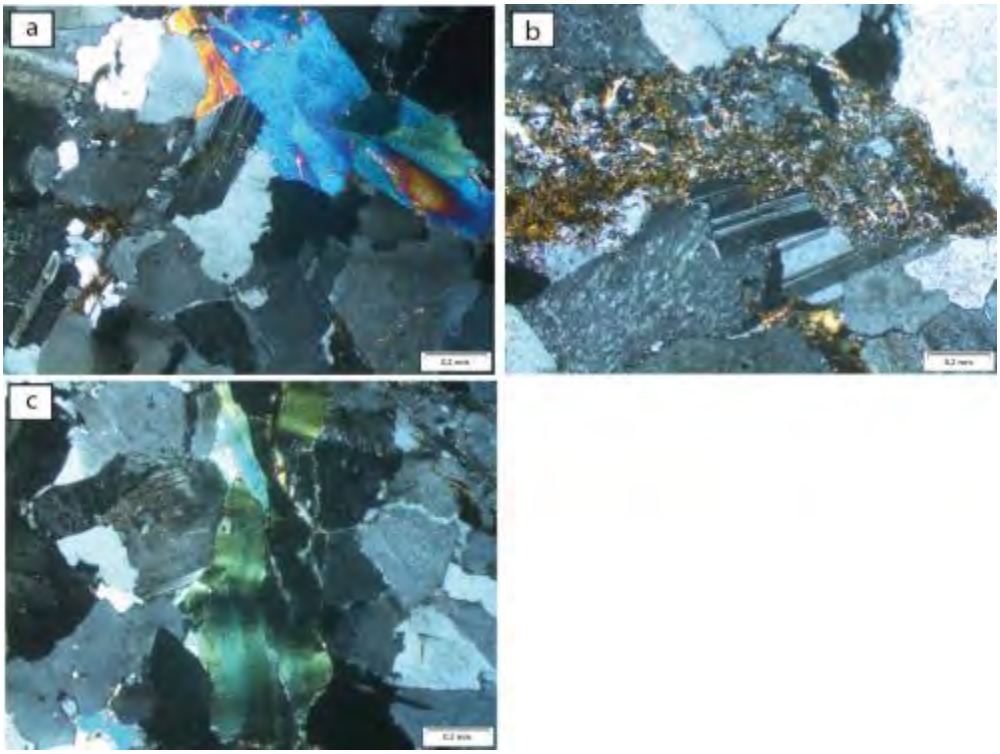

Figure 5.6: Photomicrographs of aplite vein a) fine to medium-grained aplite vein composed of qtz, plag and bt b) fractures in-filled with qtz, plag and bt c) some micas in the aplite vein exhibit ductile deformation through the undulose extinction of the birefringence.

Table 5.1: Modal proportions (all numbers are volume %) of the samples of the different rocks over the study area in the vicinity of the Colenso Fault Zone

Sample	Granite type/ in granite...	Qtz	Plag	Bt	Musc	Chl	Opaques	Perthite	Zircon	Total	Remarks
G1 granite of the Cape Granite Suite											
KHG1	G1	35	29	5	10	20	1			100	
KHG2	G1	39	35	4	8	10	4			100	
KHG3	G1	39	30	4	8	15	4			100	
KHG4	G1	42	37	10	4	6	1			100	
KHG6	G1	12	74	8	5		1			100	
KHC1	G1	42	12	20	8	6	12	12		100	
KHC2	G1	48	5	44	2		1			100	
KHC3	G1	45	10	39	5	1			1	100	
KHS1	G1	36	23	23	5	10	3			100	
KHS3.2	G1	32		30	12	20	6			100	
KHS3.3	G1	35		27	16	17	5			100	
KHV7	G1	40	30	10	20					100	
G2 granite of the Cape Granite Suite											
KHG12	G2	48	30	2	5	15				100	
KHG13	G2	40	30	15		15				100	
KHG14	G2	37	35	12	3	10	3			100	
KHG16	G2	48	37	5	2	8				100	
KHX1	G2	42	33	8	4	10	3			100	
KHS4	G2	36	27	30	5		2			100	
G3 granite of the Cape Granite Suite											
KHG17	G3	28	29	20	5	15	3	8		100	
KHS10	G3	73	2	15	1	8	1			100	
KHS12	G3	50		43			7			100	mylonite

5.5 Summary

In summary the study area sampled for this work represents both the S- and I-type granites of the Cape Granite Suite. The G1 (oldest) granite is an S-type granite of the CGS and is a medium- to coarse-grained porphyritic granite. It is composed of quartz and plagioclase with accessory phases of biotite, muscovite, opaques and chlorite. The G2 granite is an S-type granite as well and is coarse- to very coarse-grained quartz porphyry. Composed of quartz, plagioclase and biotite with accessory phases of muscovite, chlorite and opaques. This granite is the Saldanha quartz porphyry and contains xenoliths. The xenoliths are composed of plagioclase, quartz with accessory phases of muscovite, biotite and chlorite. The G3 granite is a I-type granite of the CGS, it is a poikilitic coarse-grained granite of biotite, quartz, plagioclase, perthite with accessory alteration phases of white mica, biotite and chlorite. The Aplite veins throughout the area are fine- to medium-grained composed of quartz, plagioclase, biotite with accessory phases of quartz, plagioclase and biotite. The aplite veins show little to no signs of deformation.

6. Micro-Structures

6.1 Cataclasites

6.1.1 Large 3-7 m wide

Cataclasites are brittlely deformed, cohesive rocks characterised by angular clasts in a range of sizes in a fine-grained matrix; in this cataclasite they are clasts of quartz and plagioclase (Figure 6.1a). The cataclasite matrix are phyllosilicates and are either sericite or biotite dominated, which has been surrounded by chlorite, biotite and muscovite laths (Figure 6.1c). The quartz-dominated matrix contains recrystallised quartz grains (Figure 6.1b) and the biotite dominated matrix is associated with the presence of opaques. There are networks of fractures that are filled with biotite, chlorite and muscovite (Figure 6.1c). There are ground up grains of quartz that occur alongside fracture networks that are in-filled by biotite and opaques, which have both rounded and angular clasts of fractured quartz grains on either side of the fractures (Figure 6.1d). Along some of the fractures in the cataclasite there are sheared grains of quartz (Figure 6.1d).

In areas where there is not a great amount of cataclasis the clasts are fine-grained rather than very fine-grained (Figure 6.2a). Throughout the cataclasite there is a prominent foliation that is defined by the biotite, muscovite and chlorite (Figure 6.2b). This foliation cross-cuts recrystallised quartz grains (Figure 6.2c). There are numerous types of veins within the cataclasite zones and these are conjugate sets of elongate blocky veins of fine- to medium-grained quartz that cross cut foliation (Figure 6.2d) (Oliver and Bons, 2001). Veins within the cataclasites are not the usual fracture filled by precipitate definitions they are cataclastic seams. Alongside some of these veins there are blocky quartz grains (Figure 6.2d). Other veins within the cataclasite are composed of biotite, chlorite and opaques with accessory muscovite (Figure 6.2e).

In KHS3.3 there is a micro-breccia of quartz fragments within a muscovite, chlorite anastomosing vein with accessory biotite (Figure 6.3b). At the contact with the undeformed granite, the vein keeps its shape but broadens and the clasts within the breccia are larger (Figure 6.3c). The vein can be traced further into the granite but then tends to “fizzle out” and not be visible amongst the primary muscovite (Figure 6.3d). At the boundary between the cataclasite and granite there is a conjugate vein to the afore mentioned vein.

At the contact between granite and cataclasite there are fractured grains of quartz and a few plagioclase grains, which are in-filled with very fine-grained chlorite within biotite, muscovite and quartz. Within this contact there are relict grains of quartz that are dynamically recrystallised (Figure 6.3e). The matrix close to the contact are phyllosilicates and are biotite dominated and one can find angular brecciated primary grains in the fractures and cataclastic quartz grains. The undeformed granitic areas are coarse-grained and composed of the G1 granite with primary muscovite, quartz and plagioclase with a matrix of quartz, plagioclase with accessory biotite and muscovite. The clast to matrix ratio is greater than 90% with very little to no matrix. Within the granite some of the quartz and plagioclase grains are cross-cut by fractures with a chlorite and muscovite infill, which are at 90° angles to one another (Figure 6.3f).

Some samples, for example KHC2, have a different texture than the other cataclasites, with hydrothermal quartz that has overprinted laths of biotite and opaques. In KHC3, we see quartz grains that have undulose extinction, with inclusions of muscovite and zircons (Figure 6.4a).

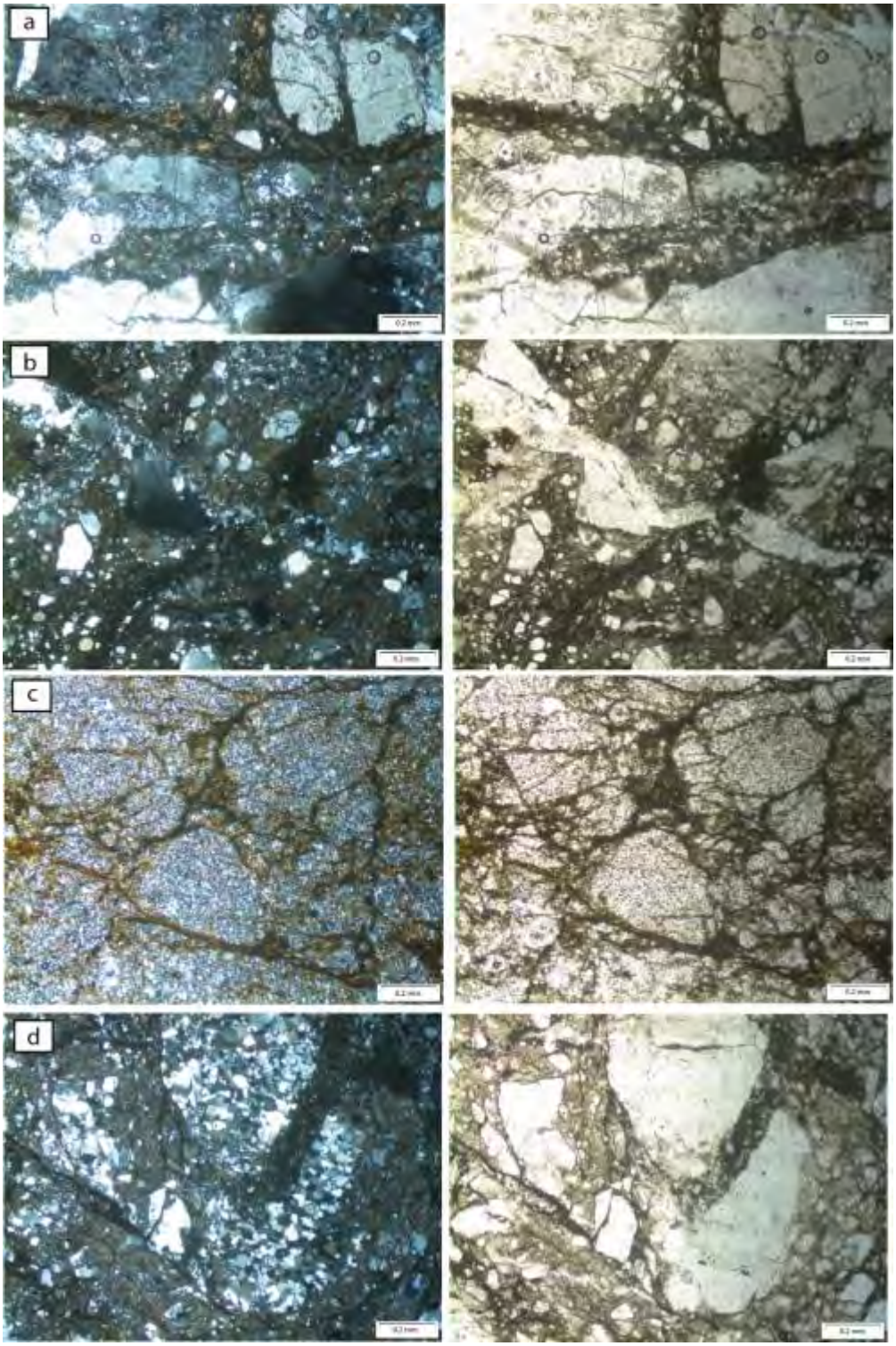

Figure 6.1: Photomicrographs of the large cataclasites a) fine-grained ground mass of qtz with clasts of plag within it in sample C1 b) phyllosilicates matrix of the cataclasite with the qtz dominated matrix in contact with the bt dominated matrix in sample C1 c) network fractures of bt and clusters of chl, bt, musc and opaques in sample S3.2 d) photomicrograph at a higher magnification of recrystallised qtz grains cut by cataclasite in sample S3.2.

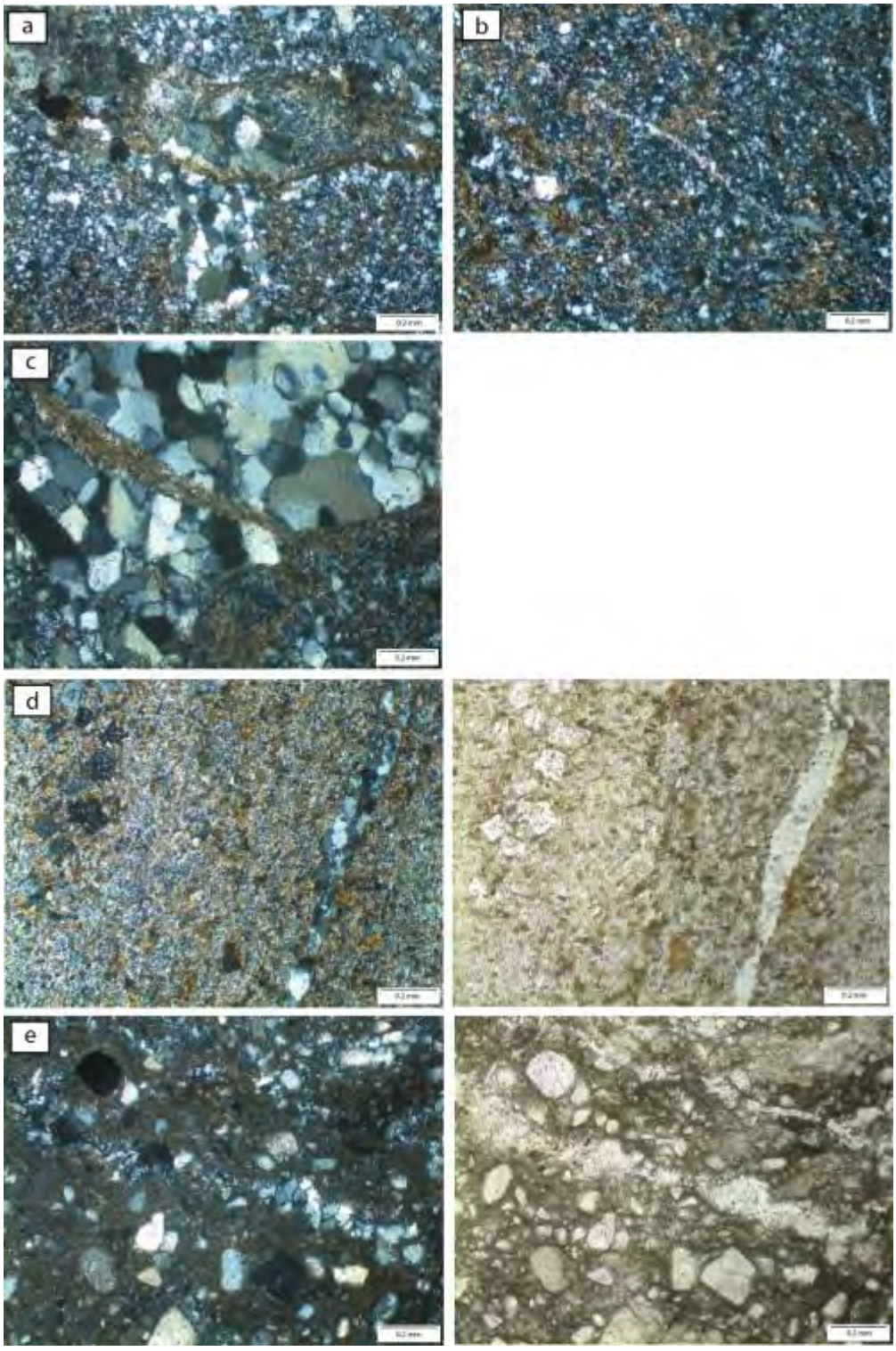

Figure 6.2: Photomicrographs of the large cataclastites a) fine-grained texture of the cataclasite where deformation is not so predominant in sample S3.2 b) foliation defined by musc, bt, chl in sample S3.2 c) in sample C3 foliation defined by bt cross cutting recrystallised (due to dislocation creep) qtz grain that show evidence for sub-grain rotation with laths of chl, with d) blocky qtz grains in sample S3.2 e) Vein networks of bt, chl, opaques and musc in sample S3.3.

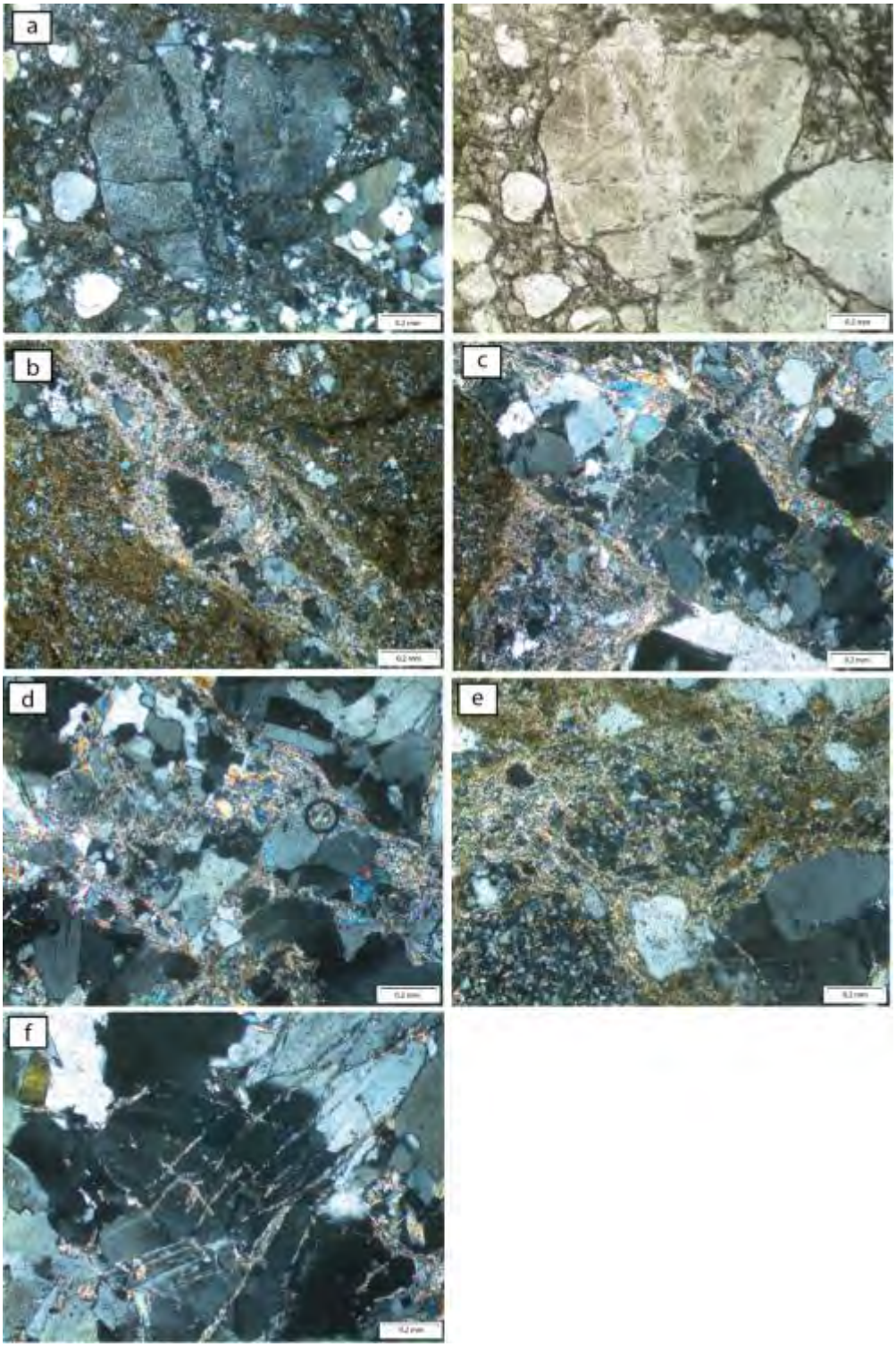

Figure 6.3: Photomicrographs of the large cataclasites a) qtz veins cutting through qtz grains b) phyllosilicate-rich breccia anastomoses across cataclasite c) Breccia can be traced further into the un-deformed granite and then tapers out d) the same breccia broadens at the contact between the un-deformed granite and the cataclasite e) in the lower left corner there is a relict grain of qtz that has been completely recrystallised f) in the area of the un-deformed granite some grains of plag and qtz have cross-cutting fractures that are filled with chl and musc.

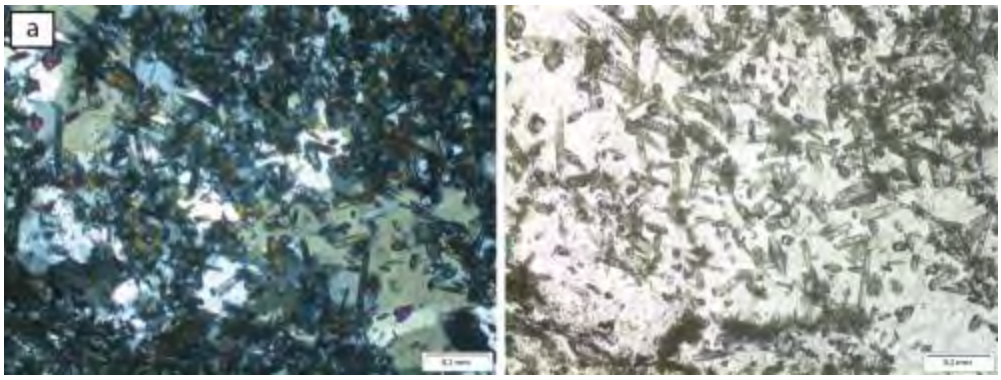

Figure 6.4: Photomicrographs of the large cataclastites a) Qtz grain with undulose extinction with laths of musc and zircons within it.

6.1.2 Small cataclasites 10 cm – 80 cm

The smaller cataclasites are very similar to the larger ones in terms of style of deformation and composition. The small cataclastic zones have a typical texture described previously; with angular clasts of a range of sizes in a fine-grained matrix (Figure 6.6a). The cataclasites have a typical network of anastomising fractures that are in-filled with biotite and muscovite and surrounded by a damage zone of cataclastic quartz grains (Figure 6.5a). Within areas of the cataclasite there are brecciated coarse-grained clasts, indicated by the sheared plagioclase twins (Figure 6.5b). The matrix are again phyllosilicates as within the larger cataclasites and are in areas quartz dominated and the other type biotite dominated and associated with the biotite are opaques and muscovite (Figure 6.6b). These fractured quartz grains have a biotite hydrothermal alteration within the matrix around the impermeable quartz grain (Figure 6.5c). Plagioclase grains exhibit a high intensity of deformation, the grains are brittlely deformed and the alteration of the plagioclase is to white mica (Figure 6.5d).

There are two generations of deformation within the cataclasites in the G1 granite, the first, generation of fracturing of quartz grains is truncated by a second generation of fractures, 90° from the first that contain a phyllosilicate foliation.

The small cataclasites of the G2 granite are different from other cataclasites in that there is not a very clear foliation within the rock as for example in Figure 6.5a, however there is the start of the development of the foliation as there is the clustering of biotite. Most of the quartz grains are ground up not to the usual fine-grained grains but rather have a more rounded texture

(Figure 6.6c). In some areas of the cataclasite there is a breccia, which is more muscovite rich than other areas (Figure 6.6d).

The cataclasite within the G3 granites of the Cape Granite Suite are similar to the large cataclasites although this is a unique sample as has 3 very different areas within it: A, B and C. Area B appears to be a small band within the Areas A and C. Area B is about half a centimetre wide. Areas A and C are representative of the primary G3 granite in the study area but are however slightly different to one another due to the difference in deformation as it is a asymmetric damage zone around the cataclasite. In between these primary textured granites is a cataclasite deformation. To follow is a definition of these 3 Areas.

Area A:

A very coarse-grained primary granitic material with primary quartz, perthite, plagioclase, muscovite, opaques, biotite with alteration of these minerals in some places to chlorite (Figure 6.7a). Throughout the sample there are fractures that run right across it, these fractures are in-filled with quartz, muscovite, biotite and opaques, for example in Figure 6.7b there is a quartz in-filled fracture through a quartz grain.

Area B:

The cataclastically deformed granitic material has been dynamically recrystallised and shows crystal plastic deformation in the biotite (Figure 6.7c). In Figure 6.7d is the boundary of the cataclasite and the primary granitic material. Within the cataclasite there are also prominent networks of anastomosing fractures that are in-filled with biotite and these fractures tend to run ~ 15 ° from the main fracture (Figure 6.7e)

Area C:

This area within the G3 granite represents a slightly different granitic material and is a medium-grained granite, with the same composition as Area A, however the modal proportions of the biotite is increased and there is less muscovite. The biotite clusters as ‘cusps’ with an interstitial texture. These bitotite clusters show recrystallisation due to fracturing through them. This tends to be a highly fractured granite in comparison to Area A (Figure 6.7f).

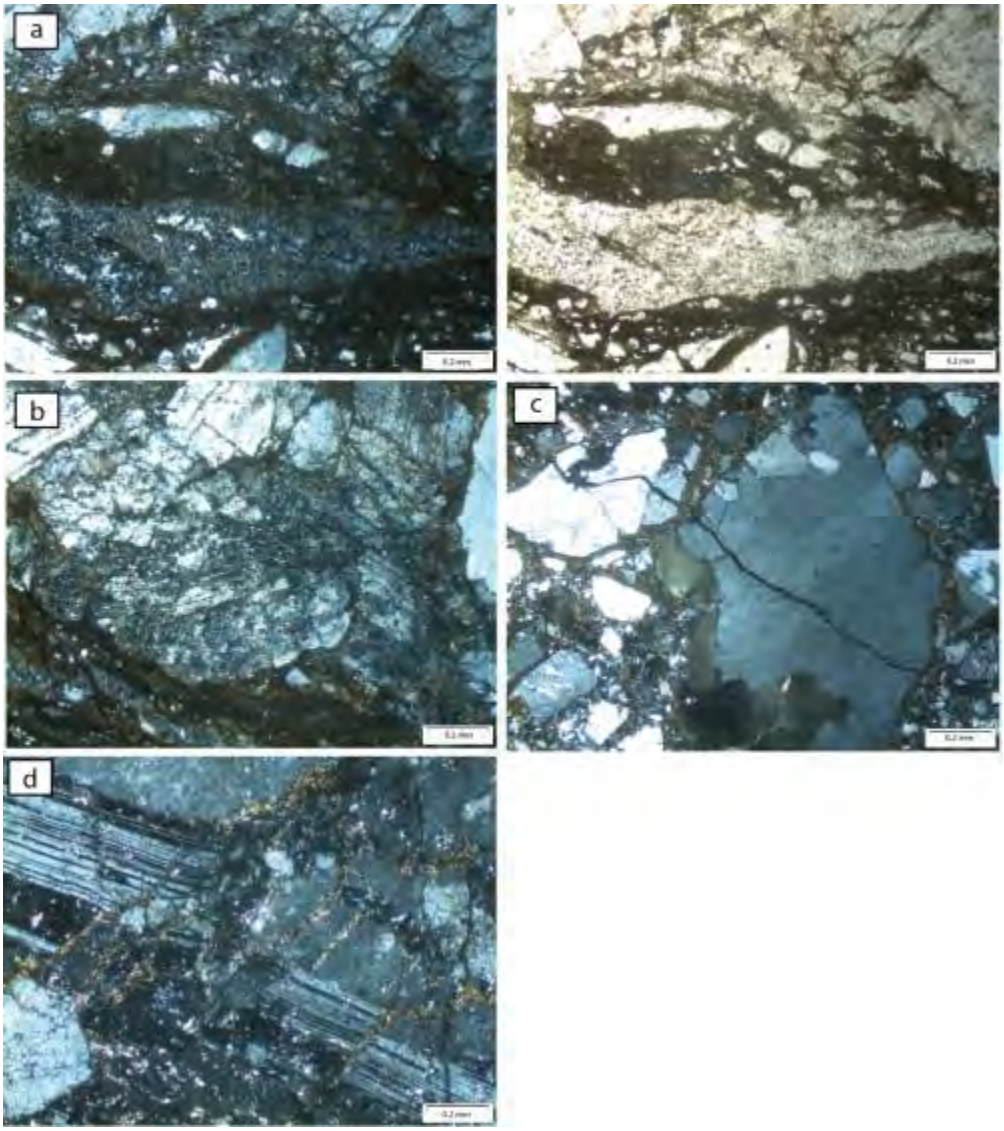

Figure 6.5: Photomicrographs of cataclasite in G1 granite a) anastomosing vein of foliated bt with recrystallised qtz around it, with fractured grains inside the cataclasite b) deformed plag twins c) fracture through qtz grain which is cross-cut by bt dominated cataclasite d) plag fractures filled by chl, bt and opaques, dextral sense of shear seen from the deformed plag twins.

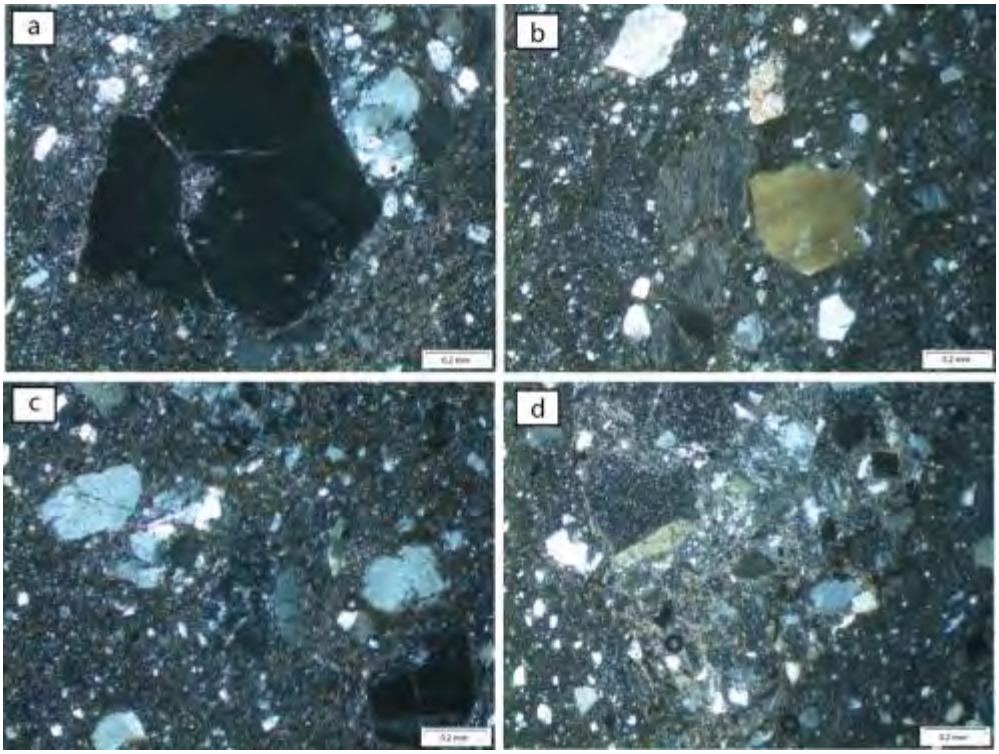

Figure 6.6: Photomicrographs of the cataclasite in the G2 granite a) porphyritic cataclasite with grains of plag and qtz which are often fractured b) the texture of the cataclasite is slightly bt rich within qtz porphyry c) recrystallised qtz with a more rounded texture d) brecciated area with a greater proportion of musc than other samples.

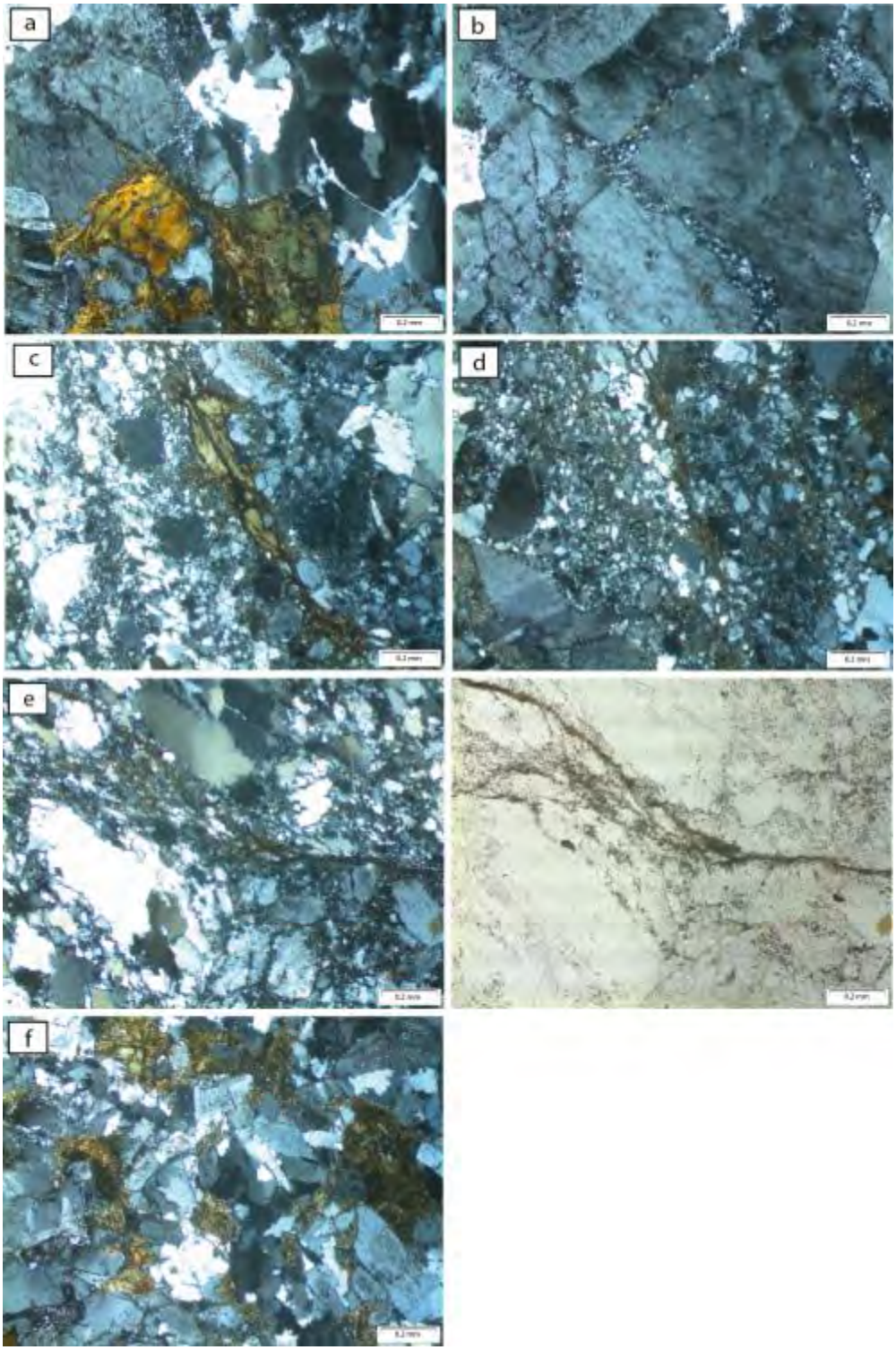

Figure 6.7: Photomicrographs of cataclasite in the G3 granite a) very coarse-grained granitic material of qtz, peth, plag, opaques, bt and chl b) cross cutting qtz vein through a qtz grain c) recrystallised granitic material with bt that is crystally deformed d) boundary between un-deformed granite and the cataclasite e) prominent bt fractured that anastomose and are ~15° from main contact f) higher intensity of fracturing than rest of the sample with cusps of bt.

6.1.2.1 Mylonite in the G3 granite

The only shear in the area that is deformed through ductile deformation and is a mylonite (sample KHS12), occurs in the G3 granite of the CGS to the north of the Colenso Fault Zone. It is a fine-grained rock and is banded with a quartz dominated matrix and the other band being biotite dominated (Figure 6.8a and 6.8b respectively). Sigma and delta clasts that show strain shadows and/or grain rotation of predominantly quartz grains show dextral sense of shear (Figure 6.8c, 6.8d and 6.9a). The quartz bands that are deformed are affected by the rotation of these delta clasts (figure 6.9b). A fracture that is in-filled by biotite cuts across the mylonite (Figure 6.9c). The quartz bands are primary grains that have flattened and are now in preferential flow directions as some bands still associated to their recrystallising grains.

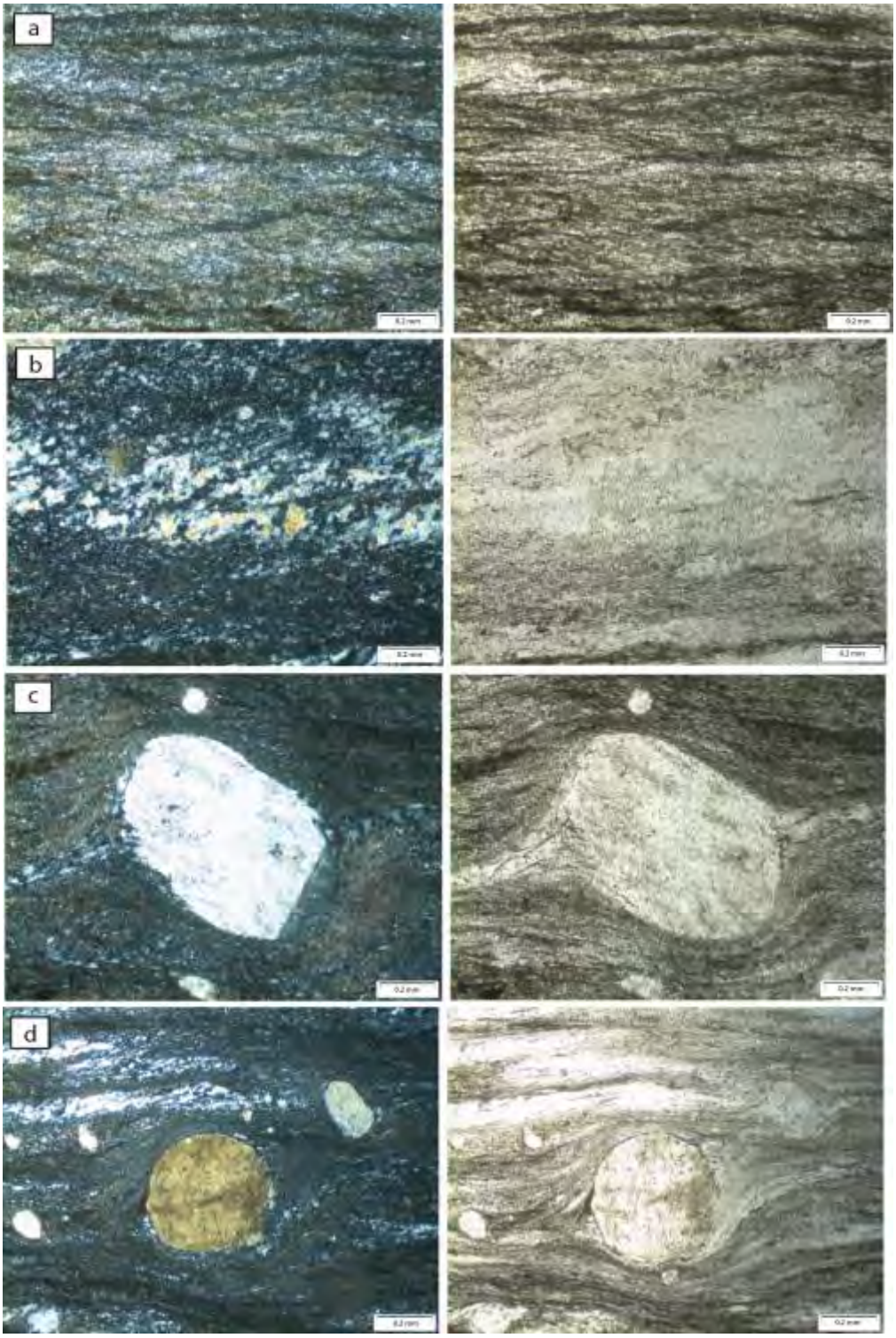

Figure 6.8: Photomicrographs of mylonite through G3 granite a) bt dominated matrix b) Qtz dominated matrix c) text book delta clast showing dextral sense of motion d) rounded sigma clast showing dextral sense of shear.

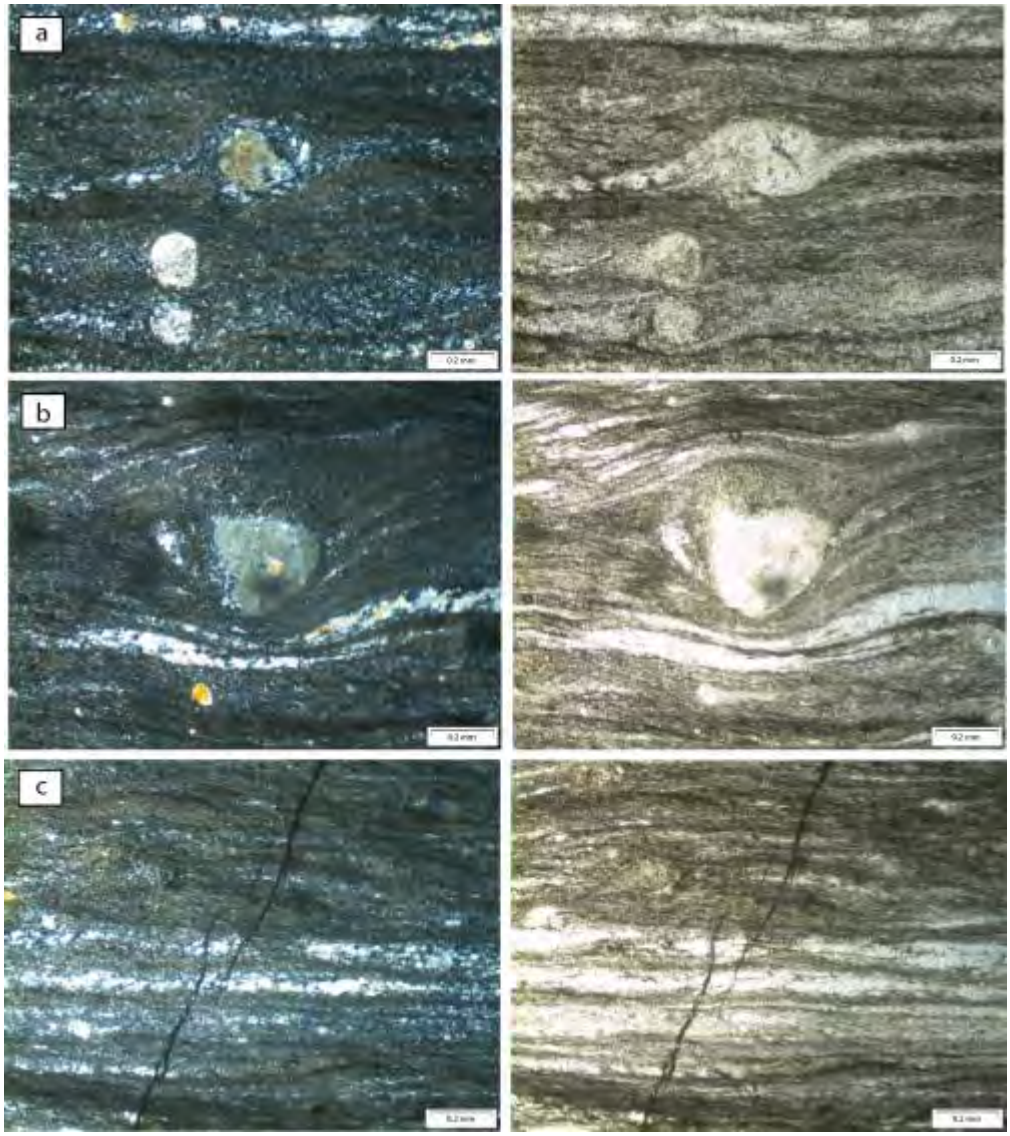

Figure 6.9: Photomicrographs of a mylonite through G3 granite a) multiple rotated delta clasts b) qtz band which is deformed below the delta clast c) fracture in-filled with bt must be late stage after shearing.

6.2 Summary

In summary cataclasites are areas of deformation that are represented by angular clasts in a range of sizes, these angular clasts occur within a fine-grained matrix. The matrix is composed of phyllosilicates that are predominantly sericite and biotite. The cataclasites contain little to no feldspar clasts, they are majority full of phyllosilicates. This implies that the feldspar has been altered to phyllosilicates by hydration due to the fluid-rock interaction as shown by the isotopes. Quartz in the cataclasites are recrystallized in places and the biotite a product from the deformation of the granites with opaques present in the parent material that is being strained and deformed as well. All the cataclasites contain networks of fractures that are infilled with

biotite, chlorite and muscovite. The cataclasites have a foliation defined by biotite, muscovite and chlorite often the foliation is cross cut by veins. They range in size from large cataclasite zones between 3 – 7 m wide down to 10 – 80 cm wide. The cataclasites show 2 generations of deformation the first; fracturing of quartz veins that are truncated by the second phase of deformation; the generation of biotite foliation 90 ° from fractures. In the study area the cataclasites occur in the G1, G2 and G3 granites.

The only mylonite found in the study area is to the north of the Colenso Fault Zone in the G3 granites. The mylonite was formed due to ductile deformation of the G3 granite and is a fine-grained rock. It is banded with a quartz dominated matrix and a biotite dominated matrix. The mylonite area contains sigma and delta clasts that show a dextral sense of shear.

7. Geochemistry Results

In the following chapter the geochemistry results will be discussed as well as what is currently in literature for the area around the Colenso Fault Zone. It highlights the results of the major element and trace element composition, as well as the oxygen isotope work done in the area. The results are then used for understanding the composition of the cataclasites in the area of study at the outcrop of the Colenso Fault Zone. The chapter aims to identify what fluids were involved in the deformation of the granites and to highlight the fluid flow pathways through the Fault Damage Zone.

7.1 Major element and trace element composition

XRF whole rock major element analysis of samples collected throughout the study area were analysed for major elements. Analysis was completed on fusion discs at the Geology Department, University of Cape Town, using the Norrish and Hutton (1969) fusion technique.

The average major element composition and trace element composition can be found in Table 7.1 with (all data composition can be found in Appendix 3). Looking at the major discriminating elements between the granites of the CGS the G1, G2 and G3 granites contain 0.17, 0.14 and 0.05 wt % respectively in P_2O_5. Other discrimating elements such as Th, Na_2O, K_2O, Zr and Nb do indeed show major differences as seen in table 7.1 below.

Table 7.1: Major and minor element composition of the different granites, xenoliths, large and small cataclasites as well as aplite veins in the study area.

Ganite Type	G1 Granite	G2 Granite	G3 Granite	Xenolith	Large Cataclasite	Aplite Vein	Small cataclasite shears
Sample	**Average**	**Average**	**Average**	**Average**	**Average**	**Average**	**Average**
Majors in wt%							
SiO_2	70.88	72.43	73.53	71.89	72.61	75.47	69.98
TiO_2	0.43	0.30	0.19	0.33	0.27	0.10	0.44
Al_2O_3	13.79	13.70	13.11	13.72	13.51	12.82	14.25
Fe_2O_3	2.95	2.14	2.08	2.49	2.24	1.07	3.16
MnO	0.04	0.02	0.03	0.02	0.02	0.02	0.04
MgO	0.77	0.36	0.24	0.35	0.32	0.16	0.97
CaO	1.36	1.23	1.52	1.19	1.32	0.44	1.64
Na_2O	2.51	2.74	3.22	2.68	2.88	2.84	3.07
K_2O	5.31	5.45	4.55	5.65	5.22	5.56	4.63
P_2O_5	0.17	0.14	0.05	0.14	0.11	0.12	0.15
SO_3	0.01	0.01	0.01	0.01	0.01	0.02	0.01
Cr_2O_3	0.01	0.01	0.01	0.01	0.01	0.01	0.01

NiO	0.01	0.01	0.01	0.01	0.01	0.01	0.01
H_2O-	0.11	0.08	0.08	0.07	0.08	0.10	0.16
LOI	0.92	0.59	0.46	0.65	0.57	0.58	0.84
Total	99.34	99.26	99.13	99.24	99.21	99.36	99.40
Traces in ppm							
Mo	2.84	0.2	0.2	0.2	0.20	3.60	0.50
Nb	31.66	16.59	12.85	20.0	16.48	14.95	18.35
Zr	396.82	170.18	235.8	218.6	208.19	95.11	214.43
Y	75.29	33.37	51.41	45.4	43.39	28.64	42.65
Sr	205.54	94.03	87.41	91.9	91.11	55.64	125.73
U	7.14	0.45	0.45	0.5	0.45	3.25	0.71
Th	36.88	20.26	23.96	22.2	22.13	20.43	21.48
Rb	544.93	224.52	210.3	234.4	223.08	430.53	279.17
Pb	65.95	34.53	36.82	34.9	35.41	41.35	36.75
Ba	508.71	612.80	380.98	691.4	561.71	115.41	506.49
Sc	7.03	5.36	14.31	7.4	9.02	4.18	10.04
Co	4.57	1.1	1.1	1.1	1.10	1.12	3.28
Mn	345.75	255.65	369.44	289.5	304.87	209.49	449.64
Cr	19.24	13.99	12.33	11.7	12.68	10.80	32.34
V	34.35	22.23	16.12	22.2	20.17	10.24	47.99
Zn	54.62	41.68	39.80	46.5	42.65	20.02	63.55
Cu	8.44	7.56	29.39	7.5	14.82	5.96	11.22
Ni	4.433	0.55	0.55	0.6	0.55	0.69	7.86
S	166.91	107.79	376.05	155.8	213.20	87.29	115.84

Figure 7.1 plots major element oxides vs SiO_2 for the granites, cataclasites, smaller cataclasite shears (shears), aplite veins and xenoliths of the study area. In general across all plots the granites, cataclasites, shears and xenoliths tend to cluster even if linearly along a trend. The aplite veins tend to cluster away from the other rocks (with little to no overlap with other rock types). The SiO_2 vs P_2O_5 graph shows a wide range of P_2O_5 values for the aplites as well as across all other rock types. Here there is a large overlap of the aplites and other rock types, the main discriminant would be the aplites high SiO_2 content. The cataclasites and shears are compositionally the same as that of the granites and xenoliths. They are only compositionally different to the aplite veins with which the cataclasites do not cluster (Appendix 3).

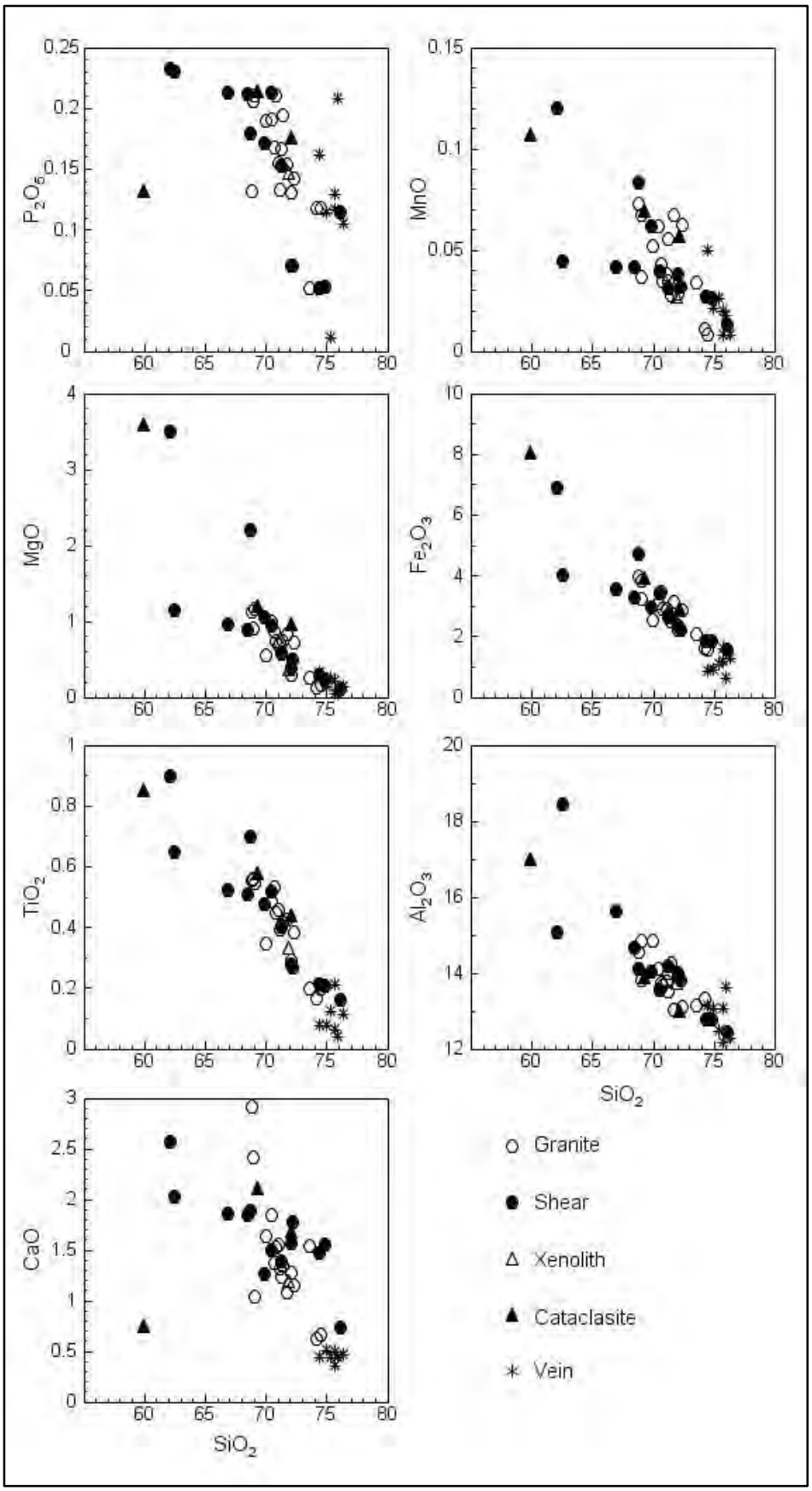

Figure 7.1: SiO_2 vs major element values for the rock types sampled in study area during this research.

Other diagrams that equally show the compositional relation between that of the cataclasites and shears to that of the granites are below in Figure 7.2. The plots of Y vs Nb, Zr vs Zr/Y and P_2O_5 vs Th again show the clustering and important compositional similarity of the cataclasites to the granites. The small cataclasites (shears) are also compositionally the same as the granites. Again as in the SiO_2 vs P_2O_5 plot above the P_2O_5 vs Th plot below show the aplites that have such a varying range in P_2O_5.

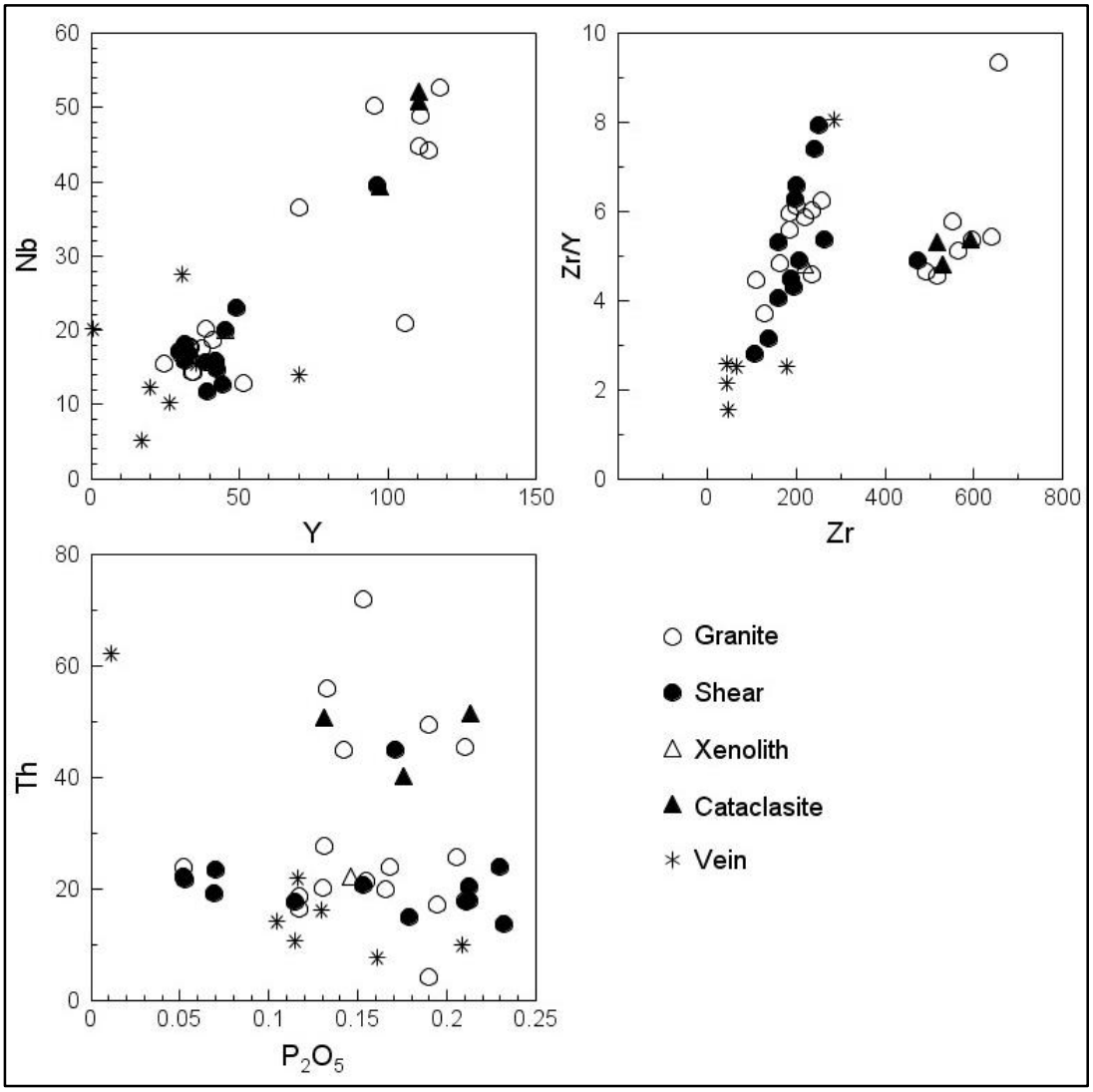

Figure 7.2: a) Y vs Nb b) Zr vs Zr/Y and c) P_2O_5 vs Th plots for the values of the rock types sampled in study area. They represent the elemental compositions for the granites, cataclasites, shears, aplite veins (vein) and xenoliths.

In Summary the XRF analyses show that the cataclasites are compositionally the same as the undeformed granites. The cataclasites are produced from deformation and grinding of the G1

granite and G2 Saldanha quartz porphyry. The composition of the cataclasites did not change significantly during formation.

7.2 Oxygen Isotopes

The measured Qtz $\delta^{18}O$ and WR $\delta^{18}O$ values for the Cape Granite Suite rocks studied in the area (G1, G2 and G3) as well as the cataclasites appear in Table 7.2 below. The average Qtz $\delta^{18}O$ values are 9.5, 9.8 and 12.1 ‰ for the G1, G2 and G3 granites respectively. The average WR $\delta^{18}O$ values are 7.8, 7.7 and 10.3 ‰ for the G1, G2 and G3 granites respectively. It is important to note that these average values include the $\delta^{18}O$ of deformed granites and not just that of the un-deformed units. The WR $\delta^{18}O$ values across the study area are lower than their corresponding Qtz $\delta^{18}O$ (Figure 7.4). The two exceptions to the above are samples KHG8 and KHG9 where the WR $\delta^{18}O$ is higher than that of the Qtz $\delta^{18}O$. The cataclasites WR $\delta^{18}O$ are lower than WR $\delta^{18}O$ of the granite directly next to them. The WR δ18O as well as the Qtz $\delta^{18}O$ value of the granites and cataclasites increases away from the fault zone thus the fluid rock interaction decreases away from the fault zone. The $\delta^{18}O$ WR and Qtz trends generally increase away from the fault zone (Figure 7.4) from ~6.3 to ~10.9 ‰ and ~7.75 to ~11.58 ‰ respectively. Along the trend the $\delta^{18}O$ values vary significantly, and the pattern of change in the $\delta^{18}O$ values can be attributed the samples proximity to:

1. The fault zone (temperature and fluid-rock ratio)
2. Nearby large shear zones (temperature and fluid-rock ratio)

The low $\delta^{18}O$ values in the Colenso Fault Zone cataclasite are attributed to exchange with external fluid. This is to be expected as the granites would have had a low permeability whereas the cataclasites are highly fractured with well-developed cleavage. Near the cataclasite fault strain the $\delta^{18}O$ values depart from the general trend and the difference between whole-rock and quartz values increases (Figure 7.3).

The difference between the higher Qtz $\delta^{18}O$ and relatively lower WR $\delta^{18}O$ (Table 7.3) is largest at the cataclasites but is not limited to the area of cataclasis. The largest differences in WR and Qtz $\delta^{18}O$ values can be found in table 7.3 below as well as Figure 7.4. The highest fluid rock interaction occurs in both the G1 and G2 granites (Figure 7.4). The cataclasites thus acted as fluid pathways through the area with decreasing fluid rock interaction away from these pathways.

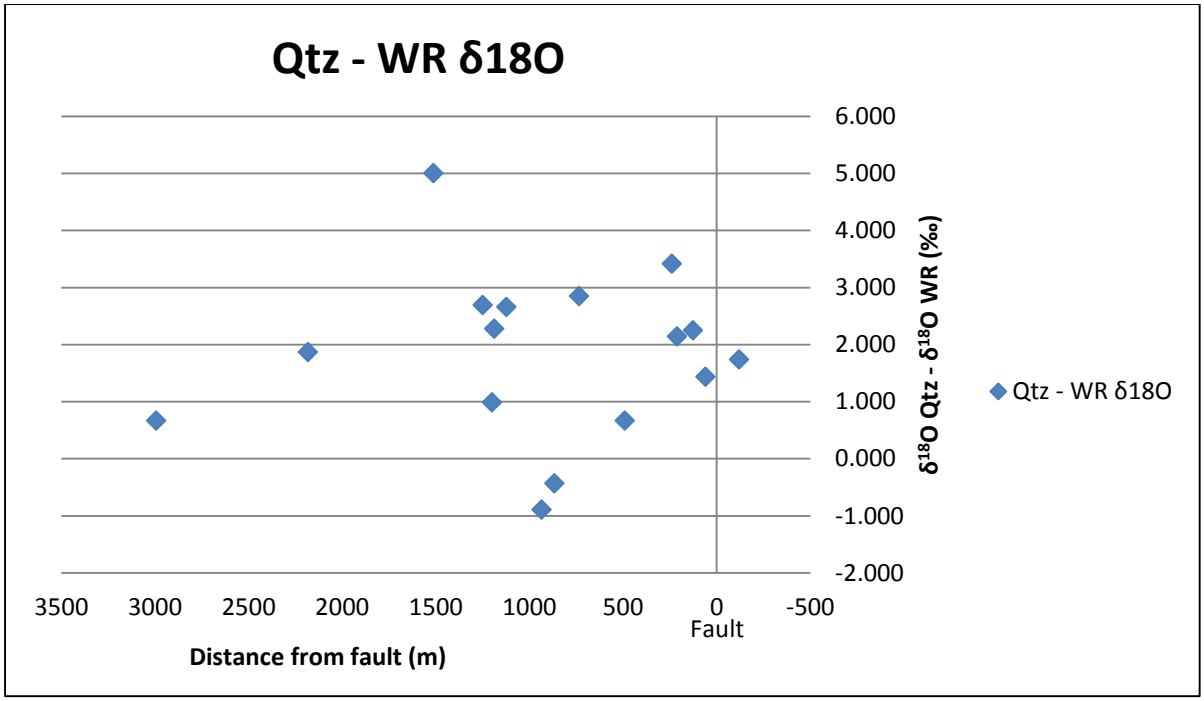

Figure 7.3: Plot of $\delta^{18}O$ of qz – $\delta^{18}O$ of whole rock (WR) versus the distance from the fault Core of the Colenso Fault Zone.

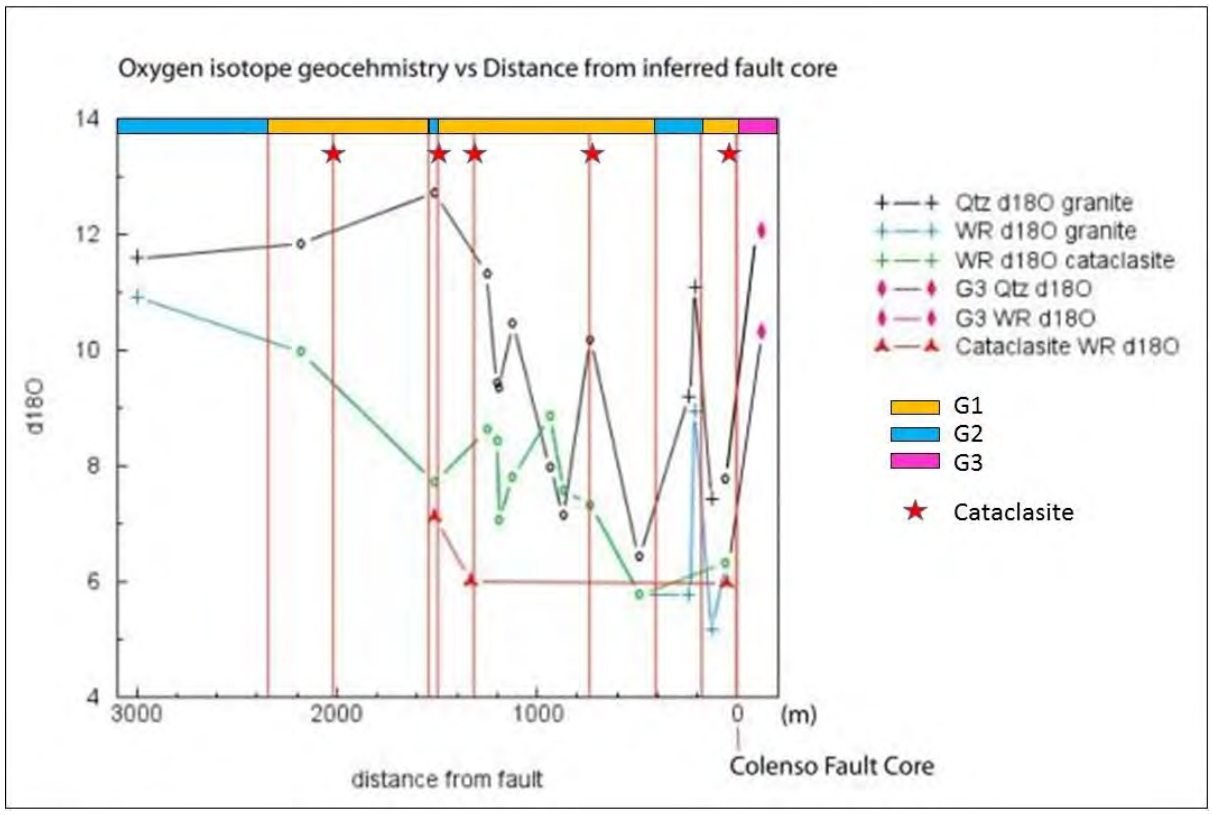

Figure 7.4: $\delta^{18}O$ vs distance from fault graph illustrating the Qtz and WR $\delta^{18}O$ values of the granites and cataclasites in the area. Includes the locality of the Colenso Fault Zone as well as changes in geology (red vertical lines).

Table 7.2: Table of Qtz and WR $\delta^{18}O$ values for the granites and cataclasites in the study area with corresponding distance from the fault as well as the corresponding Cape Granite Suite granite type.

Sample	distance from fault (m)	Qtz $\delta^{18}O$ (‰)	WR $\delta^{18}O$ (‰)	Qt-Wr (‰)	δD	Wt. % water	CGS Granite
KHG17	-120	12.1	10.3	1.8			G3
KHC3	49		6		-124	1.07	
KHG6	61	7.8	6.3	1.5			G1
KHG13	127	7.4	5.2	2.2			G2
KHG16	213	11.1	8.9	2.2			G2
KHG12	239	9.2	5.8	3.4			G2
KHG11	491	6.4	5.8	0.6			G1
KHG10	735	10.2	7.3	2.9			G1
KHG9	867	7.1	7.6	-0.4			G1
KHG8	935	8.0	8.8	-0.8			G1
KHG5	1123	10.4	7.8	2.6			G1
KHG3	1189	9.3	7.1	2.2			G1
KHG4	1201	9.4	8.4	1.0			G1
KHG2	1251	11.3	8.6	2.7			G1
KHC2	1329		6.0		-116	1.78	
KHG1	1513	12.7	7.7	5.0			G1
KHC1	1514		7.1		-113	0.90	
KHG15	2183	11.8	10	1.8			G1
KHG14	2995	11.6	10.9	0.7			G2

Table 7.3: table of Qtz and WR $\delta^{18}O$ values for the granites and cataclasites with the highest difference in Qtz-WR $\delta^{18}O$.

Sample	distance from fault (m)	Qtz $\delta^{18}O$	WR $\delta^{18}O$	Qt-Wr	CGS Granite type
KHG16	213	11.1	8.9	2.2	G2
KHG13	127	7.4	5.2	2.2	G2
KHG3	1189	9.3	7.1	2.2	G1
KHG5	1123	10.4	7.8	2.6	G1
KHG2	1251	11.3	8.6	2.7	G1
KHG10	735	10.2	7.3	2.9	G1
KHG12	239	9.2	5.8	3.4	G2
KHG1	1513	12.7	7.7	5.0	G1
KHC3	49		6		
KHC2	1329		6.0		
KHC1	1514		7.1		

7.2.1 Proximity to shear zones

The WR $\delta^{18}O$ and the qtz $\delta^{18}O$ trends closely match and follow one another; however, variations away from one another closely relate to the above three factors; their proximity to the fault zone that acts as a passageway and their proximity to large shear zones with increased permeability. However, in general the qtz $\delta^{18}O$ profile has higher values that of the WR $\delta^{18}O$ profile. The closer the sample sites are to large shears the more the profiles separate from one another and larger variations are found. The WR $\delta^{18}O$ decrease well below that of the increased qtz $\delta^{18}O$ profile when the sample site is situated alongside that of a large shear, also the greater the distance between the granite and that of the shear the less the effect of the fluctuation from the qtz $\delta^{18}O$ profile.

The area around the granite sample sites KHG8 and KHG9 is the only area on the plot where the trends cross one another and where the WR $\delta^{18}O$ plots above that of the qtz $\delta^{18}O$ the reasoning for this is the low temperature alteration has affected the feldspar values and hence the WR $\delta^{18}O$.

The lowest point on the plot corresponds with KHG13 and is presumed to be associated with the sample's proximity to the actual fault that is concealed by the large bay dune sands and calcrete. This area is expected to have received the largest fluid volume flowing through the area during faulting. The large decrease in the $\delta^{18}O$ value immediately to the contact with the fault zone is due to the large fluid-rock interaction that had occured WR- and qtz- $\delta^{18}O$ values.

7.2.2 Cataclasites

The $\delta^{18}O$ values for the 3 cataclasite zones have a very interesting profile as KHC3 the zone closest to the Colenso Fault itself and has a WR $\delta^{18}O$ value of 5.9 ‰ and the value only slightly increases for the very next cataclasite zone KHC2 with a WR $\delta^{18}O$ value of 6.0 ‰. The most distant cataclasite zone KHC1 has a slightly higher WR $\delta^{18}O$ isotope value of 7.1 ‰. The increase in the isotopic value of the cataclasite zones may be attributed to their increase in their distance away from the main fault zone. An alternative reason for this may include that KHC1 is surrounded at either of its sides by two large shear zones and the slight increase at KHC2 may be due to a nearby large shear within the granite.

7.2.3 WR vs Qtz $\delta^{18}O$

The plot of Qtz vs WR $\delta^{18}O$ for the G2 and G1 granites of the CGS (Figure 7.5) shows the migration from the general correlation between the WR and Qtz $\delta^{18}O$ values for fresh rock. The effect of low versus high temperature (>400 °C) alterations to normal good correlation between the two in fresh rock is shown by the migration of the points either upwards or downwards respectively. Expected differences would be the Qtz $\delta^{18}O$ being roughly 1 ‰ higher than its corresponding WR $\delta^{18}O$ for the same un-deformed fresh granite. A couple of the granites sampled in the area both G1 and G2 granites have a good correlation. Two G1 granites show evidence of low temperature alteration and the other 10 G1 and G2 granites show evidence of high temperature alteration and thus lowering of the points on the WR vs Qtz $\delta^{18}O$ plot to below the line of good correlation.

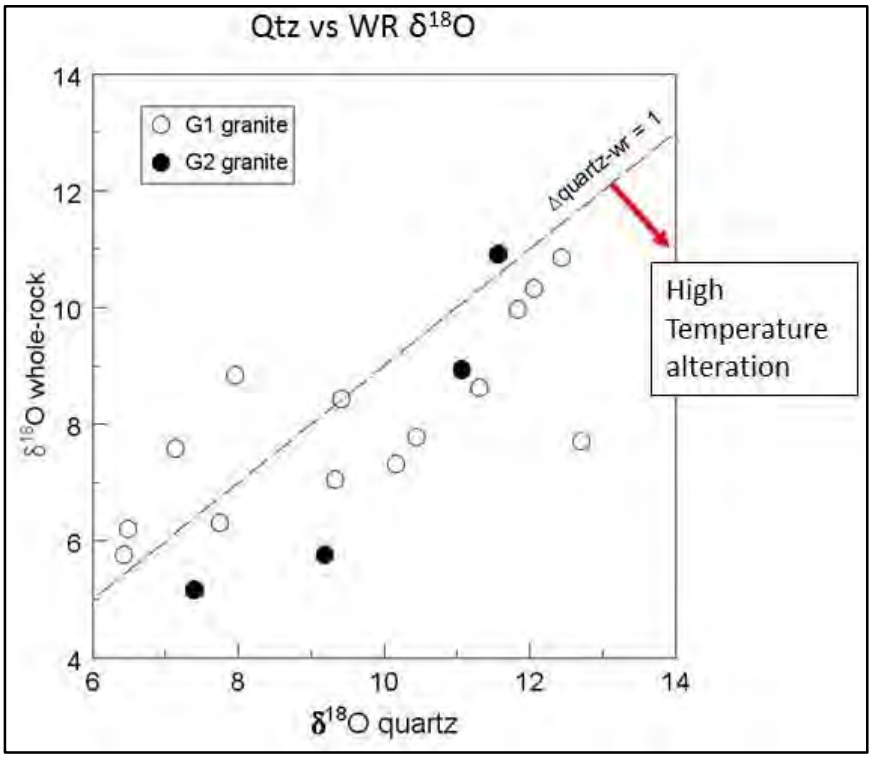

Figure 7.5: Plot of the WR $\delta^{18}O$ vs Qtz $\delta^{18}O$ for the granites in proximity to the Colenso Fault Zone.

7.2.4 δD vs $\Delta^{18}O$

All the points examined for both hydrogen and oxygen isotopes lie outside any field of waters involved during deformation because of the large fluid-rock alteration that is related to deformation (primarily at the cataclasites) and that meteoric water perculates down the fault and alters the fault rock (Figure 7.6). The rocks of the area have very little water and hence H

and the H-isotope composition would have equilibrated rapidly with fluids. The mineral-water fractionation factor for hydrogen isotopes for chlorite at greenschist facies temperatures of about 300 °C is about -30 ‰ (O'Neil, 1986). This allows fluid $\delta^{18}O$ values to be estimated with respect to the global meteoric water line (Figure 7.7). The δD value of the average fluid in Figure 7.7 is about -75, this corresponds with the water having a $\delta^{18}O$ value around -11 ‰. If this fluid was meteoric, it would have been on the Global Meteoric Water Line of Craig (1961) and had a value of -10.6 ‰; which is typical of high latitudes. Palaeomagnetic reconstructions (eg Tohver *et al*, 2006) show that the latitude of the Kalahari Craton varied from 60° and 20° between 600 and 525 Ma. Perhaps of more significance is that a global glaciation is thought to have occurred during the late Precambrian (eg Maruyama and Santosh, 2008). This would have been associated with very negative meteoric water. Estimates of the water/rock ratio (in atoms/atom) required the decrease the $\delta^{18}O$ value from 10.9 to 6 ‰ range from 0.35 (400°C) to 0.41 (300°C) assuming the closed-system model of Taylor (1977).

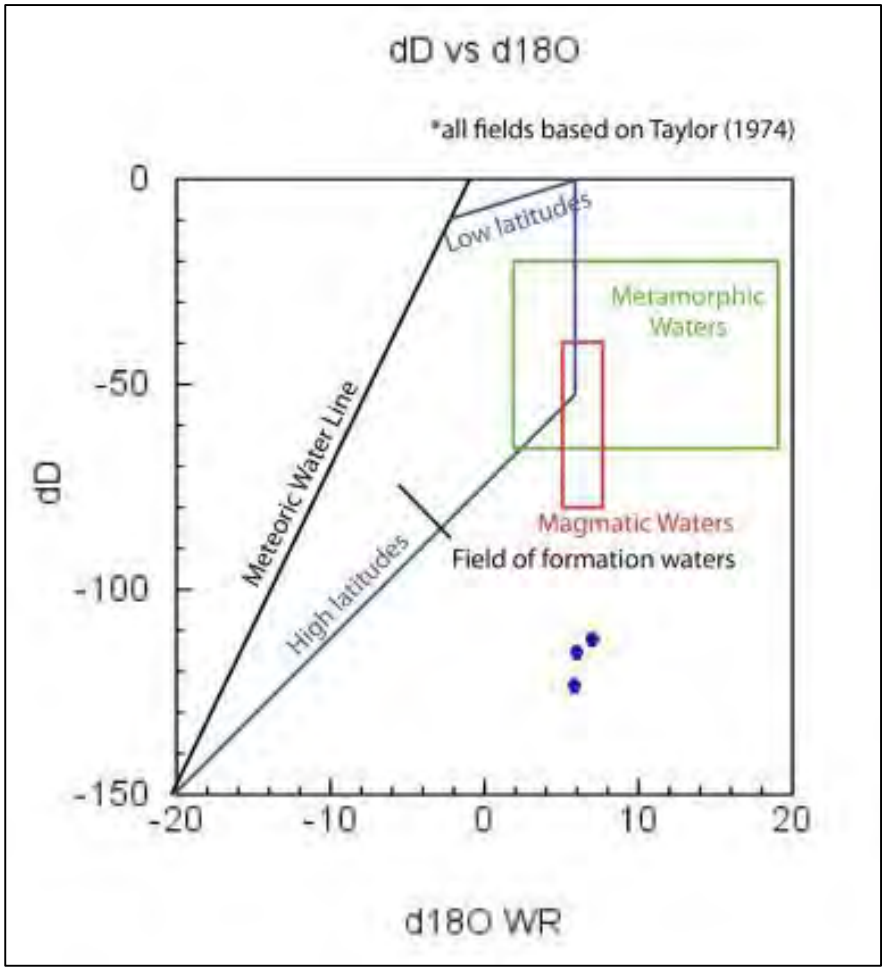

Figure 7.6: Plot of the large cataclasite WR $\delta^{18}O$ vs δD in relation to the formation water fields after Taylor (1974). The values of the cataclasites falls outside any field of formation water.

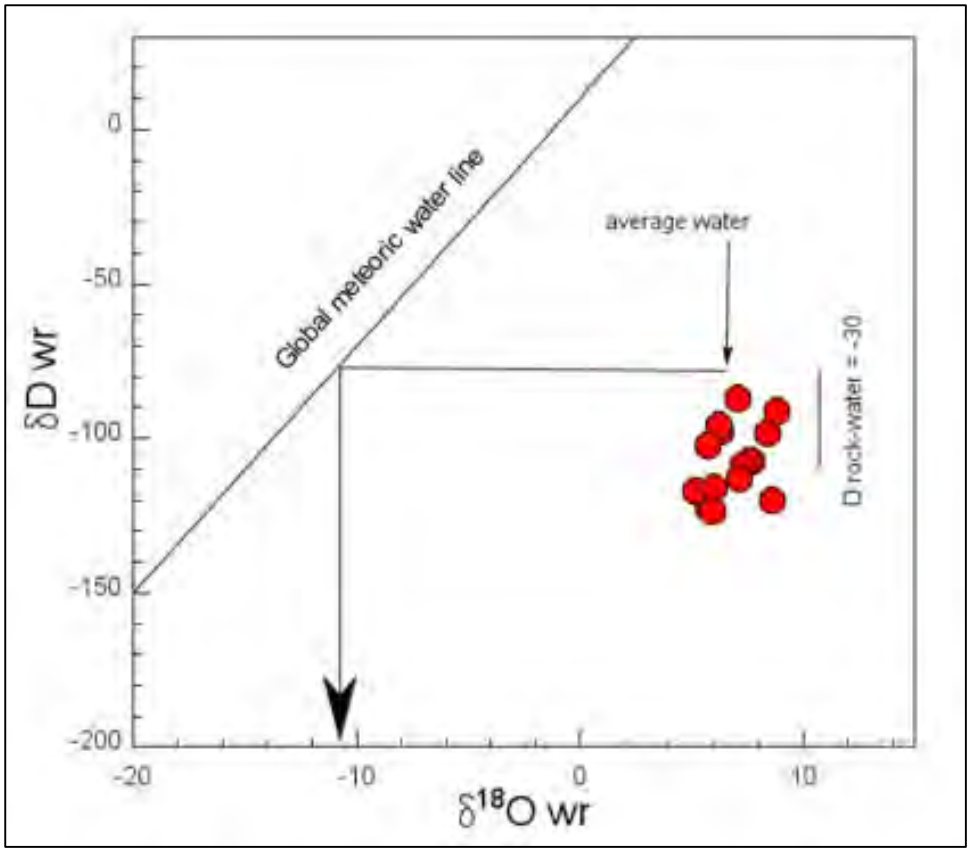

Figure 7.7: Plot of samples (large cataclasite as well as smaller cataclasite shears) from area with WR $\delta^{18}O$ vs δD in relation to the Global Meteoric Water Line of Craig (1961).

7.4 Summary

In Summary the whole-rock major and trace element composition of the cataclasites are very similar to that of the undeformed granites. The cataclasites are produced from deformation and grinding of the G1 granite and G2 Saldanha quartz porphyry. The composition of the cataclasites did not change significantly during formation. The average quartz $\delta^{18}O$ values for the G1, G2 and G3 granites are 9.5, 9.81 and 12.05 ‰ respectively. The average Whole Rock $\delta^{18}O$ values for the G1, G2 and G3 granites are 7.76, 7.69 and 10.31 ‰ respectively. The WR and Quartz $\delta^{18}O$ values of the granites and cataclasite increase away from the fault zone and thus the fluid-rock interaction decreases away from the fault. Decreases and increases along the increasing $\delta^{18}O$ profile away from the fault zone can be related to proximity to the fault with its heat and decreased permeability as well as being related to proximity to shear zones. The WR $\delta^{18}O$ value of the cataclasites are lower than the granites in which they formed. The difference in WR and Quartz $\delta^{18}O$ is greatest at the cataclasites but is not limited to these areas. The cataclasites acted as fluid pathways through the area with decreasing fluid-rock interaction away from the pathways due to decreasing permeability. The lowest WR and Quartz $\delta^{18}O$ is

directly to the south of the Colenso Fault Zone and received the largest quantity of fluids flowing through the area during faulting. The cataclasites have an increasing WR $\delta^{18}O$ value from closest to the fault away, 5.9 to 6.0 to 7.1 ‰ respectively. The fluid interacting with the fault rocks during deformation was meteoric in origin.

8. Conclusions

The Colenso Fault Zone comprises several discrete shear discontinuities cross-cutting relatively undeformed granites of the Cape Granite Suite. It is the terrane-boundary fault between the Tygerberg Terrane and the Swartland Terrane of the Malmesbury Group of the Pan-African Saldania orogenic belt. It extends from the town of Saldanha to Stellenbosch. The Colenso Fault separates the older S-type granites in the Tygerberg Terrane in the SW from the younger I-Type granites of the Swartland Terrane in the NE. It can be traced for ~150 km and is ~7km wide. Due to poor exposure along the length of the fault, the area under study in this work was along the western coastline at which the fault is visible along the coast.

1. The kinematics of the Colenso Fault Zone was initially sinistral strike-slip motion starting at 547 ± 6 Ma and changed at ~540 Ma to a dextral strike-slip motion (Kisters *et al*., 2002). The change in strike-slip motion has been attributed to the closure of the Adamastor Ocean. Dextral strike-slip sense of motion was said to end with the emplacement of the Cape Columbine granite at ~520 Ma. The relative age of deformation sequence from the study can be divided into 2 sequences as I could not find any relational features between the G3 granites to the north of the Colenso Fault Zone to the deformation to the features to the south of the Colenso Fault in the G1 and G2 granites of the area. The oldest deformation was the emplacement of the G1 and G2 granites of the Cape Granite Suite. The intrusive G2 granites are younger than the G1 granites as they contain xenoliths of the G1 granites. This was followed by syn-tectonic formation of aplite veins and cataclasites. The initial strike-slip sense of movement along the fault was sinistral and created shearing of the granites, followed by dextral strike-slip shearing. The above was followed by dextral strike slip faulting associated jointing and another phase of shearing and late stage jointing. The second deformation sequence was the emplacement of the G3 granite of the Cape Granite Suite to the north of the Colenso Fault Zone. The relative deformation sequence follows from the emplacement of the G3 granites with xenoliths of granitic material and Malmesbury Group sedimentary rocks to the syn-tectonic development of aplite veins. Then there was the sinistral shearing, followed by dextral shearing and finally late stage jointing.

2. Cataclasites are areas of strain represented by angular clasts in a range of sizes in a fine-grained matrix. Along the coastline around the Colenso Fault Zone there are 3 large

areas of cataclasis ranging from 36.8 – 126.3 m and 121 – 315.7 m in width and strike extent respectively. The clasts are composed of quartz and plagioclase, in either quartz dominated matrix or a biotite dominated matrix. The quartz dominated matrix is from the dynamic recrystallization of primary quartz grains of the granite. The biotite dominated matrix is associated with the deformation of the biotites with the presence of opaques in the granites. The cataclasites are commonly highly fractured with fractures filled with white mica, biotite and quartz. In the G1 granites the cataclasites show two generations of deformation, the first being the fracturing of quartz grains that is truncated by the generation of a biotite foliation at 90 ° from fractures in the cataclasites. The cataclasites that cut the G2 granite are porphyroblastic with primary grains of plagioclase and quartz still present in section. These biotite and quartz grains are in a fine-grained matrix of biotite, muscovite, quartz and plagioclase. The cataclasites formed from the G3 granites are of the smaller fraction 10 cm – 80 cm shears and are in section similar to the G1 cataclasites. In general whether the cataclasites are large (several metres wide) or small (tens of centimeters wide) in size the shear intensity decreases away from the Colenso Fault Zone Core, they are all very fine-grained and composed of the same minerals as that of the granites of the CGS in which they occure. The cataclasites have the same composition as the granites and are produced from the deformation and grinding of the G1 granite and G2 Saldanha Quartz porphyry. The cataclasites composition did not change from the granitic composition during formation.

3. Across the CGS the $\delta^{18}O$ values of quartz ranges from 8.6 – 13.4 ‰. In the study area the average Quartz $\delta^{18}O$ for the G1, G2 and G3 granites are 9.5, 9.8 and 12.1 ‰ respectively. The average Whole Rock $\delta^{18}O$ for the G1, G2 and G3 granites associated with the fault zone are 7.8, 7.7 and 10.3 ‰ respectively.

4. The WR and Quartz $\delta^{18}O$ values of the granites and cataclasite increase away from the fault zone towards the normal value for fresh granites and thus the fluid-rock interaction decreases away from the fault. Variation along the increasing $\delta^{18}O$ profile away from the fault zone can be related to proximity to the fault with its decreased permeability as well as being related to proximity to shear zones. The WR $\delta^{18}O$ values of the cataclasites are lower than the granites in which they formed. The difference in WR and Quartz $\delta^{18}O$ is greatest at the cataclasites but is not limited to these areas. The highest

fluid-rock interaction is in both the G1 and G2 granites with the cataclasites acting as fluid pathways through the area with decreasing fluid-rock interaction away from the pathways due to decreasing permeability. The cataclasites have the highest fluid-rock interaction due to the high Qtz – WR $\delta^{18}O$ differences in the granites at or near to the shear zones. The phyllosolicates within the cataclasites imply fluid-related alteration of the granites during deformation and thus also relate back to the cataclasites having a large fluid-rock interaction. The lowest WR and Quartz $\delta^{18}O$ is directly to the south of the Colenso Fault Zone and received the largest quantity and hottest fluids flowing through the area during faulting. The cataclasites have an increasing WR $\delta^{18}O$ value from closest to the fault away, 5.9 to 6.0 to 7.1 ‰ respectively.

5. The fluid interacting with the fault rocks during deformation was meteoric in origin as the rocks of the area have very little water in them. Hence the H and H-isotope composition would have re-equilibrated rapidly with fluids in the system. The mineral-water fractionation at greenschist facies temperatures is about -30 ‰. This allows the fluid $\delta^{18}O$ to be estimated with respect to the global meteoric water line, with a value of -10.6 ‰. This value is typical of areas at high latitudes, which at the time of deformation the area was at. Also at the time of deformation there was a global glaciation that is also associated with very negative meteoric water values.

References

Barnett, W., Armstrong, R.A., De Wit, M.J., (1997). Stratigraphy of the upper Neoproterozoic Kango and Lower Palaeozoic Table Mountain Groups of the cape Fold Belt, revisited. *South African Journal of Geology,* 100, pg 237-250.

Best, M.G., and Christiansen, E.H., (2001). *Igneous Petrology*, Blackwell Science Inc., Chapter 11: Generation of Magma (pg 283-315), 458 pg.

Borthwick, J., and Harmon, R.S., (1982). A note regarding ClF_3 as an alternative to BrF_5 for oxygen isotope analysis, *Geochimica et Cosmochimica Acta,* 46(9), pg 1665-1668.

Cawood, P.A., and Buchan, C., (2007). Linking accretionary orogenesis with supercontinent assembly, *Earth Science Review,* 82, pg 217-256.

Coplen, T.B., (1988). Normalization of oxygen and hydrogen isotope data, *Chemical Geology: Isotope Geoscience Section,* 72(4), pg 293-297.

Coplen, T., Kendall, C., and Hopple, J., (1983). Comparison of stable isotope reference samples, *Nature,* 302, pg 236-239.

Craig, H., (1961). Isotopic variations in meteoric waters, *Science,* 133, pg 1702-1703.

Da Silva, L.C., Gresse, P.G., Scheepers, R., McNaughton, N.J., Hartmann, L.A., and Fletcher, I.R, (2000). U-Pb and Sm-Nd age constraints on the timing and sources of the Pan-African Cape Granite Suite, South Africa, *Journal of African Earth Sciences,* 30, pg 795-815.

Dalziel, I.W.D., Dalla Salda, L.H., Gahagan, L.M., (1994). Palaeozoic Laurentia-Gondwana interaction and the origin of the Appalachian-Andean mountain system, *geological Society of America Bulletin,* 106, pg 243-252.

Da Silva, L.C., Mcaughton, N.J., Hartmann, L.A., Fletcher, I.R., Gresse, P.G., and Scheepers, R., (1997). U-Pb (SHRIMP) isotopic constraints for the evolution of Southern Brazilian

granitic province, and some correlated South African, Pan-African plutons, *2nd International symposiumon granites and associated mineralization, Salvador, Bahia, Brazil,* pg 276-277.

Duncan, A.R., Erlank, A.J., and Betton, P.J., (1984). Appendix 1: Analytical techniques and data base descriptions, *Special Publication, Geological Society of South Africa,* 13, pg 389-395.

Faure, K., (1993). Mineralogy and geochemistry of the carbonaceous mudstones and coal petrogenesis of the Grootegeluk Formation in the Waterberg Coalfield, South Africa, *unpublished PhD thesis, University of Cape Town,* pg 208.

Faure, K., Harris, C., and Willis, J.P., (1995). A profound meteoric water influence on genesis in the Permian Waterberg Coalfield, South Africa: Evidence from stable isotopes, *Journal of Sedimentary Research,* A65.4, pg 605-613.

Frimmel, H.E., Zartman, R.E., Späth, A., (2001). The Richtersveld Igneous Complex, South Africa: U-Pb zircon and geochemical evidence for the beginning of Neoproterozoic continental breakup, *Journal of Geology,* 109, 493-508.

Frimmel, H.E., and Folling, P.G., (2004). Late Vendian closure of the Adamaster Ocean: Timing of tectonic inversion and syn-orogenic sedimentation in the Gariep Basin. *Gondwana Research* 7 3, pg 685–699.

Frimmel, H.E., and Frank, W., (1998). Neoproterozoic tectono-thermal evolution of the Gariep Belt and its basement, Namibia/ South Africa, *Precambrian Research,* 90, pg 1-28.

Frimmel, H.E., Klotzli, U.S., and Siegfried, P.R., (1996). New Pb-Pb single zircon age constraints on the timing of Neoproterozoic glaciation and continental break-up in Namibia, *Journal of Geology,* 104, pg 459-469.

Goscombe, B., and Gray, D.R., (2008). Structure and strain variation at mid-crustal levels in a transpressional orogen: A review of Kaoko Belt structure and the character of West Gondwana amalgamation and dispersal. *Gondwana Research,* 13, pg 45–85.

Gresse, P.G., (1995). Transpression and transection in the late Pan-African Vanrhynsdorp foreland thrust-fold belt, South Africa, *Journal of African Earth Science,* 21, pg 91-105.

Gresse, P.G., Theron, J.N., Fitch, F.J., Miller, J.A., (1992). Tectonic inversion and radiometric resetting of the basement in the Cape fold Belt, in De Wit, M.J. (ed), *Inversion Tectonics in the Cape Fold Belt*, Balkema, Rotterdam, pg 217-228.

Gresse, P.G., and Scheepers, R. (1993). Neoproterozoic to Cambrian (Namibian) rocks of South Africa: a geochronological and geotectonic review, *Journal of African Earth Sciences,* 16, pg 375-393.

Gresse P.G., von Veh, M.W., and Frimmel, H.E., (2006). Namibian (Neoproterozoic) to Early Cambrian Successions, in M.R. Johnson, C.R. Anhaeusser and R.J. Thomas (eds), *The Geology of South Africa,* pg 395-421.

Grunow, A., Hanson, R., and Wilson, T., (1996). Were aspects of Pan-African deformation linked to lapetus opening? *Geology.* 24, pg 1063-1066.

Harris, C., and Erlank, A.J., (1992). The production of large-volume, low-$\delta^{18}O$ rhyolites during the rifting of Africa and Antarctica: The Lebombo Monocline, southern Africa, *Geochemica et Cosmochimica Acta,* 56(9), pg 3561-3570.

Harris, C., Faure, K., Diamond, R.E., Scheepers, R., (1997). Oxygen and hydrogen isotope geochemistry of S- and I-type granitoids: the Cape Granite suite, South Africa, *Chemical Geology,* 143, pg 95-114.

Harris, C., Smith, H.S., and le Roex, A.P., (2000). Oxygen isotope composition of phenocrysts from Tristan da Cunha and Gough Island lavas: variation with fractional crystallization and evidence for assimilation, *Contributions to Mineralogy and Petrology,* 138, pg 164-175.

Hartnady, C.J.H., (1969). Structural analysis of some pre-Cape formations in the Western Province, *Bull. Precambrian Research Unit*, University of Cape Town, 6, pg 1-70.

Hartnady, C.J.H., Newton, A.R., and Theron, J.N., (1974). The stratigraphy and structure of the Malmesbury Group in the southwestern Cape. *Bulletin of the Precambrian Research Unit,* University of Cape Town, South Africa, 15, pg 193-213.

Hartnady, C.J.H., Joubert, P., and Stowe, C.W., (1985). Proterozoic crustal evolution of southwestern Africa, *Episodes,* 8, pg 236-244.

Hickman, S., Sibson, R., and Bruhn, R., (1995). Introduction to special section: Mechanical involvement of fluids in faulting, *Journal of Geophysical Research,* 100, pg 12831-12840.

Hutton, D.H.W., (1982). A tectonic model for the emplacement of the Main Donegal Granite, N.W. Ireland, *Journal of Geology Society London,* 139, pg 615-631.

Jordaan, L.J., Scheepers, R., and Barton, E.S., (1995). The geochemistry and isotopic composition of the mafic and intermediate igneous components of the Cape Granite Suite, South Africa, *Journal African Earth Sciences,*21, pg 59-70.

Kerrich, R., La Tour, T.E., and Willmore, L., (1984). Fluid participation in deep fault zones: Evidence from geological, geochemical, and $^{18}O/^{16}O$ relations, *Journal of Geophysical Research: Solid Earth,* 89, pg 4331-4343.

Kisters, A.F.M., Belcher, R.W., Armstrong, R.A., Scheepers, R., Rozendaal, A., and Smith Jordaan, L., (2002). Timing and kinematics of the Colenso Fault: The Early Paleozoic shift from collisional to extensional tectonics in the Pan-African Saldania Belt, South Africa, *South African Journal of Geology,* 105, pg 257-270.

le Roex, A.P., (1985). Geochemistry, mineralogy and magmatic evolution of the basaltic and trchytic lavas from Gough Island, South Atlantic, *Journal of Petrology,* 21(1), pg 149.

le Roex, A.P., Erlank, A.J., and Needham, H.D., (1981). Geochemical and mineralogical evidence for the occurrence of at least three distince magma types in the 'Famous' region, *Coantributions to Mineralogy and Petrology,* 77(1), pg 24-37.

Maruyama, S., and Santosh, M., (2008). Snowball Earth to Cambrian explosion, *Gondwana Research,* 14, pg 1-4.

Middlemost, E.A.K., (1991). Towards a comprehensive classification of igneous rocks and magmas, *Earth Science Reviews,* 31, pg 73-87.

Miller, R.McG., (1983). The Pan-African Damara orogen of South-West Africa/ Namibia, *Special Publication Geological Society of South Africa,* 11, pg 431–515.

Norrish, K., and Hutton, J.T., (1969). An accurate X-ray spectroscopic method for the analysis of a wide range of geological samples, *Geochemica Cosmochimica Acta,* 33, pg 431-453.

O'Neil, J.R., (1986). Theoretical and experimental aspects of isotopic fractionation. In Valley, J.W., Taylor H.P., Jr & O'Neil, J.R., (eds) *Stable Irotopes in High temperature Geological Processes.* Mineralological Society of America, Reviews in nMineralogy, 16, pg 1-40.

Rowe, C.D., Backeberg, N.R., van Rensburg, T., Maclennan, S.A., Faber, C., Curtis, C., and Viglietti, P.A., (2010). Structural geology of Robben Island: Implications for the tectonic environment of Saldanian Deformation, *South African Journal of Geology,* 118, pg 57-72.

Rozendaal, A., Gresse, P.G., Scheepers, R., and De Beer, C.H., (1994). Structural setting of the Riviera W-Mo deposit, Western Cape, South Africa, *South African Journal of Geology*, 97, pg 184-195

Rozendaal, A., Gresse, P.G., Scheepers, R., and Le Roux, J.P., (1999). Neoproterozoic to Early Cambrian crustal evolution of the Pan-African Saldania Belt, South Africa, *Precambrian Research,* 97, pg 303-323.

Scheepers, R., (1995). Geology, geochemistry and petrogenesis of Late Precambrian S-, I- and A-type granitoids in the Saldania Belt, Western Cape Province, South Africa, *Journal of African Earth Sciences,* 21, pg 35-38.

Scheepers, R., and Nortje, A.N., (2000). Rhyolitic ignimbrites of the Cape Granite Suite, southwestern Cape Province, South Africa, *Journal of African Earth Sciences*, 31, pg 647-656.

Scheepers, R., and Poujol, M., (2002). Single zircon age of Cape Granite Suite ignimbrites: characteristics of the last phase of the Saldania magmatism, *South African Journal of Geology*, 105, pg 201-222.

Scheepers, R., and Rozendaal, A., (1992). Relationship of the Riviera W-(Mo-Cu) deposit to magmatism in the southwestern Cape Province, South Africa, *Abstracts Geocongress 1992*, Geological Society of South Africa, Johannesburg.

Schoch, A.E., (1975). The Darling Granite Batholith, *Annals of the University of Stellenbosch* (A1), 1, pg 1-104.

Slabber, N., (1995). The geology and geochemistry of the Bridgetown Formation of the Malmesbury Group, Western Cape Province, Unpublished M.Sc. Thesis, University of Stellenbosch, 98 pg.

Slabber, N., and Scheepers, R., (1994). Geology and geochemistry of the Bridgetown Formation, southwestern Cape Province, South Africa, Abstract Volume, *Proterozoic Crustal and Metallogenic Evolution*, Windhoek, 61.

Taylor, H.P., (1977). Water / rock interactions and the origin of H_2O in granite batholiths, *Journal of the Geological Society of London,* 133, pg 509-558.

Theron, J.N., (1970). A stratigraphical study of the Bokkeveld Group (Series), *I.U.G.S., Commission on Stratigraphy, 2nd Gondwana Symposium, South Africa,* Proceedings and Papers, pg 197-204.

Theron, J.N., Gresse, P.G., Siegfried, H.P., and Rogers, J., (1992). The Geology of the Cape Town Area, *Geological Survey of South Africa. Explanation of sheet 3318,* 140 pg.

Tohver, E., Cawood, P.A., Rossello, E.A. and Jourdan, F., (2006). Paleomagnetic record of Africa and South America for the 1200-500 Ma interval, and evolution of Rodinia and Gondwana assemblies, *Precambrian Research,* 147, pg 193-222.

Valley J.W., Kitchen, N., Kohn, M.J., Niendorf, C.R., and Spicuzza, M.J., (1995). UWG-2, a garnet standard for oxygen isotope ratios: strategies for high precision and accuracy with laser heating, *Geochemica et Cosmochimica Acta*, 59, pg 5223-5231.

Veevers, J.J., (2007). Pan-Gondwanaland post-collisional extension marked by 650-500 Ma alkaline rocks and carbonatites and related detrital zircons: A review, *Earth Science Reviews*, 83, pg 1-47.

Vennemann, T.W., and O'Neil, J.R., (1993). A simple and inexpensive method of hydrogen isotope and water analyses of minerals and rocks based on zinc reagent, *Chemical Geology,* 103, pg 227-234.

Vennemann, T.W., and Smith, H.S., (1990). The rate and temperature of reaction of ClF_3 with silicate minerals, and their relevance to oxygen isotope analysis, *Chemical Geology: Isotope Geoscience section,* 86(1), pg 83-88.

Vigneresse, J.L., (1995). Control of granite emplacement by regional deformation, *Tectonophysics,* 249, pg 173-186.

Villaros, A., Stevens, G., and Buick, I.S., (2006). *Goldschmidt Conference Abstracts*, pg A673.

Von Veh, M.W., (1983). Aspects of sedimentation, structure and evolution in the Tygerberg terrane, southwestern Cape province, *Bulletin of the Precambrian Research Unit,* University of Cape Town, South Africa, 32, pg 1-88.

Von Veh, M.W., (1992). Origin of the Gariep Arc, Abstracts Geocongress 1992, *Geological Soaciety of South Africa*, Johannesburg.

Von Veh, M.W., (1993). The stratigraphy and structural evolution of the Late Proterozoic Gariep Belt in the Sendelingsdrif- Anisfontein area, northwestern Cape Province, *Bulletin of the Precambrian Research Unit*, University of Cape Town, 38, 174 pg.

Acknowledgements

I would like to thank the National Research Foundation (NRF) for the funding received during my two years at the University of Cape Town. Without which I would not have been able to complete this study nor even have started with it. A very big thank you to Professor Chris Harris and Åke Fagareng for their undivided attention and help throughout. It has been trying and a long process and their patience and help has been greatly appreciated. To the staff at the Department of Geological Sciences at the University of Cape Town thank you for all your help from sample preparation to helping me in the labs to just a general chat always happy and willing to provide services and help. To my mom thank you for your support throughout and eventually it is done. To Allen thank you for everything and your patience and understanding.